

# Assessment of Current Understanding of Mechanisms of Initiation, Arrest, and Reinitiation of Stress Corrosion Cracks in PWR Steam Generator Tubing

Argonne National Laboratory

U.S. Nuclear Regulatory Commission  
Office of Nuclear Regulatory Research  
Washington, DC 20555-0001



## AVAILABILITY NOTICE

### Availability of Reference Materials Cited in NRC Publications

NRC publications in the NUREG series, NRC regulations, and *Title 10, Energy, of the Code of Federal Regulations*, may be purchased from one of the following sources:

1. The Superintendent of Documents  
U.S. Government Printing Office  
P.O. Box 37082  
Washington, DC 20402-9328  
<[http://www.access.gpo.gov/su\\_docs](http://www.access.gpo.gov/su_docs)>  
202-512-1800
2. The National Technical Information Service  
Springfield, VA 22161-0002  
<<http://www.ntis.gov>>  
1-800-553-6847 or locally 703-605-6000

The NUREG series comprises (1) brochures (NUREG/BR-XXXX), (2) proceedings of conferences (NUREG/CP-XXXX), (3) reports resulting from international agreements (NUREG/IA-XXXX), (4) technical and administrative reports and books [(NUREG-XXXX) or (NUREG/CR-XXXX)], and (5) compilations of legal decisions and orders of the Commission and Atomic and Safety Licensing Boards and of Office Directors' decisions under Section 2.206 of NRC's regulations (NUREG-XXXX).

A single copy of each NRC draft report for comment is available free, to the extent of supply, upon written request as follows:

Address: Office of the Chief Information Officer  
Reproduction and Distribution  
Services Section  
U.S. Nuclear Regulatory Commission  
Washington, DC 20555-0001  
E-mail: <[DISTRIBUTION@nrc.gov](mailto:DISTRIBUTION@nrc.gov)>  
Facsimile: 301-415-2289

A portion of NRC regulatory and technical information is available at NRC's World Wide Web site:

<<http://www.nrc.gov>>

After January 1, 2000, the public may electronically access NUREG-series publications and other NRC records in NRC's Agencywide Document Access and Management System (ADAMS), through the Public Electronic Reading Room (PERR), link <<http://www.nrc.gov/NRC/ADAMS/index.html>>.

Publicly released documents include, to name a few, NUREG-series reports; *Federal Register* notices; applicant, licensee, and vendor documents and correspondence; NRC correspondence and internal memoranda; bulletins and information notices; inspection and investigation reports; licensee event reports; and Commission papers and their attachments.

Documents available from public and special technical libraries include all open literature items, such as books, journal articles, and transactions, *Federal Register* notices, Federal and State legislation, and congressional reports. Such documents as theses, dissertations, foreign reports and translations, and non-NRC conference proceedings may be purchased from their sponsoring organization.

Copies of industry codes and standards used in a substantive manner in the NRC regulatory process are maintained at the NRC Library, Two White Flint North, 11545 Rockville Pike, Rockville, MD 20852-2738. These standards are available in the library for reference use by the public. Codes and standards are usually copyrighted and may be purchased from the originating organization or, if they are American National Standards, from—

American National Standards Institute  
11 West 42nd Street  
New York, NY 10036-8002  
<<http://www.ansi.org>>  
212-642-4900

---

### DISCLAIMER

This report was prepared as an account of work sponsored by an agency of the United States Government. Neither the United States Government nor any agency thereof, nor any of their employees, makes any warranty, expressed or implied, or assumes

any legal liability or responsibility for any third party's use, or the results of such use, of any information, apparatus, product, or process disclosed in this report, or represents that its use by such third party would not infringe privately owned rights.

# Assessment of Current Understanding of Mechanisms of Initiation, Arrest, and Reinitiation of Stress Corrosion Cracks in PWR Steam Generator Tubing

---

---

Manuscript Completed: January 2000  
Date Published: February 2000

Prepared by  
S. Majumdar

Argonne National Laboratory  
9700 South Cass Avenue  
Argonne, IL 60439

J. Muscara, NRC Project Manager

Prepared for  
Division of Engineering Technology  
Office of Nuclear Regulatory Research  
U.S. Nuclear Regulatory Commission  
Washington, DC 20555-0001  
NRC Job Code W6487



**Assessment of Current Understanding of Mechanisms  
of Initiation, Arrest, and Reinitiation of Stress Corrosion Cracks  
in PWR Steam Generator Tubing**

**by**

S. Majumdar

**Abstract**

This report summarizes the status of our current understanding on mechanisms of stress corrosion crack initiation and propagation in Alloy 600 PWR steam generator tubes. More than 200 publications from the literature were reviewed for this purpose. Factors influencing stress corrosion cracking and various mechanistic and empirical models available for predicting stress corrosion cracking behavior are critically reviewed. Tests are recommended for enhancing our understanding and predictive capability on stress corrosion cracking in Alloy 600 steam generator tubes.

# Contents

---

Abstract.....	iii
Executive Summary.....	xi
Acknowledgment.....	xiv
List of Acronyms.....	xv
List of Symbols.....	xvii
1 Introduction.....	1
2 Historical Background.....	2
2.1 Field Experience.....	2
2.2 Laboratory Testing.....	4
2.2.1 Specimens for crack initiation studies.....	4
2.2.2 Specimens for crack propagation studies.....	6
2.2.3 Control of solution chemistry.....	6
3 Factors that Influence IGSCC of Alloy 600.....	8
3.1 Metallurgical State or Microstructure.....	9
3.1.1 Primary water IGSCC/PWSCC.....	11
3.1.2 Secondary water IGA/IGSCC/ODSCC.....	14
3.2 Alloying Elements.....	15
3.2.1 Primary water IGSCC/PWSCC.....	15
3.2.2 Secondary water IGA/IGSCC/ODSCC.....	16
3.3 Coolant Chemistry, Inhibitors, and Impurities.....	17
3.3.1 Primary water IGSCC/PWSCC.....	17
3.3.2 Secondary water IGA/IGSCC/ODSCC.....	19
3.4 Temperature.....	24
3.4.1 Primary water IGSCC/PWSCC.....	24
3.4.2 Secondary water IGA/IGSCC/ODSCC.....	25
3.5 Stress and Strain Rate.....	26
3.5.1 Primary water IGSCC/PWSCC.....	27
3.5.2 Secondary water IGA/IGSCC/ODSCC.....	29
4 Models for IGA/IGSCC of Alloy 600.....	32
4.1 Influence of Fundamental Variables on IGA/IGSCC.....	32
4.1.1 Oxide films.....	32
4.1.2 Hydrogen ion activity (pH) and potential.....	34
4.1.3 Composition, structure, and creep of grain boundaries.....	37

4.2	Mechanistic Models.....	40
4.2.1	Film rupture/dissolution/repassivation model.....	41
4.2.2	Enhanced surface mobility theory.....	43
4.2.3	Hydrogen-assisted-cracking model.....	45
4.2.4	Internal-oxidation model.....	47
4.2.5	Corrosion deformation interaction model.....	50
4.2.6	Selective dissolution-vacancy-creep model for IGSCC.....	51
4.3	Empirical Models.....	52
4.3.1	Scott model for PWSCC.....	52
4.3.2	Strain rate damage model of Garud for PWSCC.....	53
4.3.3	Numerical model of Rebak and Smialowska.....	55
4.3.4	Gorman model for PWSCC.....	56
4.3.5	Hernalsteen model for PWSCC.....	57
4.3.6	EPRI model for caustic SCC.....	59
5	Discussion and Conclusions.....	61
5.1	Deaerated Hydrogenated Pure Water.....	62
5.2	Deaerated Caustic Solution.....	62
5.3	Deaerated Acidic Solution.....	63
5.4	PWSCC Mechanisms.....	63
5.5	IGA/ODSCC Mechanisms.....	65
6	Recommended Future Tests.....	68
6.1	PWSCC.....	68
6.2	IGA/ODSCC.....	68
6.3	Crack Arrest and Reinitiation.....	68
	References.....	70

## Figures

---

1. Causes of steam generator tube plugging in U.S. by year.....	92
2. Crack growth rate of mill-annealed Alloy 600 tubes: schematic representation of crack depth vs. time and CERT in primary water at 360°C.....	93
3. Regions of poor, uncertain, and good resistance to IGSCC of mill-annealed Alloy 600 in pure hydrogenated water at 350°C.....	93
4. Influence of final annealing temperature on the crack initiation time as determined from RUB tests in high-purity water with hydrogen for 19.1-mm-diam Alloy 600 tube at 365°C..	94
5. Variation of stress corrosion crack initiation time in Alloy 600 with grain size and room temperature yield strength.....	94
6. Regions of poor and good resistance to IGSCC of Alloy 600, thermally treated at 700°C, in pure hydrogenated water at 350°C.....	95
7. Average CGRs in CERTs vs. cold work in bending for low-temperature mill-annealed Alloy 600 tubes.....	95
8. Relationship between stress threshold for IGSCC of mill-annealed Alloy 600 in NaOH at 350°C and yield stress at 350°C.....	96
9. Variation of time for initiation of SCC in Alloy 600 with amount of grain boundary carbides.....	96
10. Effect of chromium content on rupture time of solution-annealed Ni-base-Cr-Fe-alloys in lithiated water at 360°C.....	97
11. Effect of chromium and nickel contents on caustic SCC resistance of 0.02%C-x%Ni-y%Cr-bal.....	97
12. Effect of hydrogen partial pressure on crack initiation time in high-temperature water, and 400°C steam.....	98
13. Effect of concentration of sodium thiosulfate and sodium tetrathionate on time to failure of SAS U-bends and plot of nominal stress vs. time to failure for SAS tensile specimens in 1.3% boric acid with 0.7 ppm sulfur as thiosulfate and 0.7 ppm lithium as lithium hydroxide.....	99
14. Average IGA rates of Alloy 600, as influenced by caustic concentration and temperature.....	100
15. Effect of temperature on SCC crack initiation and crack propagation of mill-annealed Alloy 600 tube.....	100
16. Effect of temperature on CGRs in as received and 5% cold-worked mill-annealed Alloy 600 tubes in primary water with a hydrogen partial pressure of 0.03 MPa and $20 < K_I < 30 \text{ MPa}\sqrt{\text{m}}$ .....	101
17. Temperature effect on the corrosion of mill-annealed Alloy 600 C-rings in 240-h tests in 9% NaOH + 1% KOH + 1% Na <sub>2</sub> SO <sub>4</sub> .....	101
18. Activation energy for 40-day IGA tests on mill-annealed Alloy 600.....	102
19. Relationship between square root of time and IGA depth.....	102

20. Failure time vs. normalized stress for constant load tests of as-received and cold-worked Alloy 600 tubes in distilled demineralized water at 345 and 365°C.....	103
21. Crack initiation time vs. normalized true stress for split-tube U-bend tests and C-ring tests on LTMA Alloy 600 tubes in deaerated, hydrogenated water at 338 and 360°C.....	103
22. Failure time vs. normalized stress for U-bend tests on mill-annealed and thermally treated Alloy 600 tubes in pure water at 343°C. ....	104
23. Effect of temperature on limiting strain rate below which SCC is observed in as-received Alloy 600 tested in primary water with hydrogen.....	104
24. Collected literature data on crack growth rate vs. stress intensity factor for Alloy 600 in simulated primary water.....	105
25. Failure time vs. normalized stress for U-bend tests on mill-annealed and thermally treated Alloy 600 tubes in 10% NaOH solution at 289°C, and pressurized tube tests on Alloy 600 tubes in 10% NaOH at 315°C.....	106
26. Crack depth vs. normalized stress for C-ring tests on mill-annealed and thermally treated Alloy 600 tubes in 10% NaOH solution at 315°C for 2000 h.....	107
27. Minimum time to initiate a 500- $\mu$ m crack at 350°C in C-ring tests of mill-annealed and thermally treated tubes at approximately yield stress vs. NaOH concentration. ....	107
28. Crack growth rate vs. stress intensity factor for tubular specimen in 360°C AVT water with hydrogen and WOL mill-annealed and thermally treated specimens of Alloy 600 in deaerated dilute NaOH solutions at 350°C, and precracked mill-annealed tubing in 10% caustic at 315°C.....	108
29. Main domains of IGA and IGSCC of Alloy 600 in aqueous solutions at 290-360°C.....	109
30. Anodic polarization curve of as-received Alloy 600, $M_{23}C_6$ carbide, and graphite in 108 ppm B + 7 ppm Li solution at pH = 7, deaerated with hydrogen at 350°C. ....	109
31. Superimposition of potential areas for IGA and SCC on the polarization curve of Alloy 600 in 10% NaOH + 1% $Na_2CO_3$ at 300°C at a scan rate of 20 mV/min.....	110
32. Effect of grain boundary chromium concentration that is a result of chromium carbide precipitation on intergranular cracking of high-purity Alloy 600 in deaerated high-temperature water and in argon.....	110
33. Schematic diagram of oxidation charge density/time relationships of a strained crack tip and unstrained crack sides. ....	111
34. Collected literature data on crack growth rate vs. stress intensity factor for Alloy 600 in simulated primary water together with that predicted by the Ford and Andresen model.....	112
35. Collected literature data on crack growth rate vs. stress intensity factor for Alloy 600 in simulated primary water together with that predicted by Scott's internal-oxidation model.....	112

36. Collected literature data on crack growth rate vs. stress intensity factor for Alloy 600 in simulated primary water together with those predicted by Scott's empirical and internal-oxidation models ..... 113

37. Typical frequency histograms for crack length and crack length increments for 186 cracked tubes from Belgian steam generators during 1986 and 1987..... 113

## Tables

---

1. Threshold stress, normalized by yield stress, for crack initiation in Alloy 600 tubes in 10% NaOH solution. .... 30
2. Garud's model parameters for as-received and mill-annealed Alloy 600..... 55

## **Executive Summary**

This report contains the results of a literature survey on mechanisms of stress corrosion cracking (SCC) in Alloy 600 steam generator tubes. An historical study of corrosion problems in pressurized water reactor (PWR) steam generator tubing shows that a succession of failure processes have afflicted steam generators in the U.S. and around the world since the early 1960s. Current steam generators face three main types of intergranular corrosion problems. They are, on the primary side, intergranular stress corrosion cracking (IGSCC), also referred to as primary water SCC (PWSCC), mainly in the transition zone of expanded tubes at the tube sheet; and, on the secondary side, intergranular attack (IGA) and intergranular SCC (IGSCC), also referred to as outer-diameter SCC (ODSCC), in crevices and under sludge piles at the tube/tube sheet (TS) and tube support plate (TSP).

A large experimental data base currently exists on initiation and propagation of stress corrosion cracks in Alloy 600 steam generator tubing. The data in the data base were primarily generated with autoclave systems that simulate either the primary side or the secondary side chemical environment, although limited data from model boiler tests have also been reported. A complicating factor in planning autoclave tests has been our incomplete knowledge of the chemical and electrochemical state within the crevices of operating steam generators. Despite a large body of empirical evidence that links various chemical, electrochemical, metallurgical, and environmental factors with PWSCC and IGA/ODSCC, exact mechanisms that are responsible for these phenomena remain elusive.

Among the empirical facts that are common to both primary and secondary side SCC are the following:

- A high-temperature mill-annealed or thermally treated Alloy 600 with continuous or semicontinuous grain boundary carbide is generally more resistant to IGA/IGSCC than low-temperature-mill-annealed material.
- A key to understanding IGA/IGSCC mechanisms is the effect of the environment on the nature, properties, and stability of the surface oxide film that is present on the surface of the tubes.
- Increase in temperature leads to shorter IGA/IGSCC life, both for crack initiation and crack propagation. The relatively high apparent activation energy of 30-40 kcal/mole, with a large scatter band, indicates that the rate-limiting step cannot be liquid diffusion.
- Resistance to IGSCC is high at neutral pH and decreases with increasing or decreasing pH. Lead is detrimental to transgranular SCC (TGSCC)/IGSCC under conditions of acidic to caustic pH.

- Grain boundary sliding rate (rather than total creep rate) appears to be important for IGSCC. Grain boundaries that are resistant to sliding are also resistant to IGSCC

### **Primary-water SCC**

The threshold stress for PWSCC is relatively high for mill-annealed Alloy 600. A high, close-to-yield stress is necessary for initiation of PWSCC cracks, with the crack initiation time varying approximately inversely with the fourth power of stress. Cold work decreases life by a factor of 3-4 and thermal treatment at 650-750°C increases life by a factor of 2-3. The smaller the grain size (i.e., the higher the yield stress), the more susceptible the alloy is to PWSCC.

PWSCC life decreases with hydrogen partial pressure up to 0.05 MPa, beyond which the effect saturates and life actually increases. Laboratory tests have shown that Alloy 600 cracks more readily in lithiated borated water than in pure water. Experimental data fail to show any consistent influence of trace impurities, such as sulfur, phosphorous, and silicon, on PWSCC life.

Various sources show that scatter in the data on crack growth rate (CGR) as a function of stress intensity factor is approximately a factor of 100. The threshold stress intensity factor is  $\approx 10 \text{ MPa}\sqrt{\text{m}}$ .

PWSCC is observed over a limited range of potential, centered on the Ni/NiO equilibrium in neutral to slightly alkaline solutions. The composition of the spinel oxide surface film changes rapidly within this region, and the film rupture/dissolution/repassivation mechanism suggests itself as a natural candidate. It has been suggested that transport of ions into the oxide or oxygen transport into the metal may be the rate-controlling process, which would account for the high apparent activation energy. However, other experimental evidence links hydrogen with PWSCC, although, currently, no quantitative model is based on hydrogen-assisted cracking for predicting PWSCC life.

Although the mechanisms are uncertain, an extensive data base exists on crack initiation and propagation of relatively long cracks in Alloy 600 in hydrogenated deaerated water at high temperature. Future tests should be directed toward measuring CGRs of relatively short, axial and circumferential cracks, with systems that are used to monitor crack length during the tests.

### IGA/ODSCC

Although the bulk water in both the primary and secondary sides is pure and deaerated with dilute additives, much of the cracking in the secondary side occurs in crevices and under sludge piles at the TTS and TSP junctions, where the local chemical and electrochemical environments differ significantly from those in the bulk water. The exact environment in these inaccessible regions is still largely unknown because direct measurements are almost impossible. Data from model boilers may not be representative of plant conditions because, in the model studies, bulk water

concentration of impurities is increased to accelerate the tests. Traditionally, it was posited that local boiling and poor circulation would tend to concentrate caustic impurities in superheated crevices and under sludge piles, a position that was backed up by calculations performed by codes like MULTEQ with inputs from hideout return data. Therefore, a large quantity of experimental data has been generated on the IGA/IGSCC behavior of Alloy 600 in highly caustic solutions and a large data base on and some mechanistic understanding of Alloy 600 IGA/IGSCC in caustic solutions is available. However, OD-initiated SCC is not restricted to crevice corrosion; it has also been observed to initiate from surface scratches in free spans of recirculating steam generators and in superheated steam space of once-through steam generators (OTSGs).

Recent analyses of the deposits on pulled tubes suggest that the environment in the crevices is neither highly caustic nor highly acidic, but is nearly neutral to slightly alkaline. The presence of plugged crevices increases the potential for local dryouts and the crevice environment may approach that of laboratory tests with doped steam. It is hard to explain some of the secondary-side cracking observed in plants as occurring in a liquid environment, because not enough impurities enter the steam generators to fill the crevice volumes in which cracking occurs. A possible explanation for the cracking over the full height of a crevice, even though the crevice is not filled by liquid, is that much of the cracking occurred in a contaminated steam environment.

It is clear that apart from OD-initiated SCC in free spans, the greatest uncertainty in predicting IGA/IGSCC life of steam generator tubing is in predicting the local environment within the crevice or under the sludge pile where crack initiation occurs. Furthermore, the crack initiation data that are generated in autoclave systems are not directly applicable to predicting crack initiation life of steam generator tube bundles because most of the time needed to nucleate cracks in a steam generator is spent in developing the local chemistry that is necessary for cracking within the crevices. This process is, of course, dependent on the operational details of individual steam generators. Model boiler data are not very helpful for this purpose either because the concentration of bulk impurities is usually increased to accelerate the tests. From laboratory data on caustic or acidic SCC one could argue that, once the appropriate chemistry is established within the crevices or under sludge piles, crack initiation should occur relatively quickly.

Because direct measurement of crevice chemistry in steam generators is extremely difficult, deposits from TSP and TS crevices of retired steam generators should be chemically analyzed to shed more light on the crevice chemistry. Model boiler testing, accelerated by chemical or thermal means, should be conducted in parallel to refine, improve, and validate models for predicting crevice chemistry. Future autoclave testing should concentrate on generating crack initiation and crack propagation data in near-neutral high-temperature water with controlled ionic conductivity (by introducing additives such as sulfates) and "doped" steam environments.

## **Acknowledgment**

---

The author thanks Dr. A. P. L. Turner of Dominion Engineering, Inc., for reviewing the report and suggesting many additions or alterations, which have been acknowledged by footnotes throughout the report. Helpful discussions with Drs. D. R. Diercks and W. J. Shack of ANL and J. Muscara of USNRC are also acknowledged.

## List of Acronyms

---

AES	Auger electron spectroscopy
ANL	Argonne National Laboratory
ASME	American Society of Mechanical Engineers
AVT	All volatile (water) treatment
BNL	Brookhaven National Laboratory
B & W	Babcock & Wilcox
BWR	Boiling water reactor
CDI	Corrosion deformation interaction
CEA	Commissariat a l'Energie Atomique, France
CERT	Constant-extension-rate test
CGR	Crack growth rate
CIEMAT	Center for Energy and Environment Technology Research, Spain
CP	Coordinated phosphate
CSL	Coincident site lattice
CWA	Cold work and annealed
DCB	Double cantilevered beam
ECP	Electrochemical potential
EDF	Electricité de France
EDS	Energy dispersive spectroscopy
EPRI	Electric Power Research Institute
GE	General Electric Co.
GHAB	General high-angle boundary
HTMA	High-temperature-mill-annealed
ID	Inside diameter
IDSCC	Inner diameter (primary water) stress corrosion cracking
IG	Intergranular
IGA	Intergranular attack
IGSCC	Intergranular stress corrosion cracking
LAB	Low angle boundary
LTMA	Low-temperature mill-annealed
MEA	Materials Engineering Associates, Inc.
NRC	(U.S.) Nuclear Regulatory Commission
OD	Outside diameter
ODSCC	Outer diameter (secondary water) stress corrosion cracking
OTSG	Once-through steam generator
PWR	Pressurized water reactor
PWSCC	Primary-water (inner diameter) stress corrosion cracking
RHE	Reference hydrogen electrode
RSG	Recirculating steam generator
RTZ	Roll transition zone
RUB	Reverse U-bend

SAS	Solution-annealed sensitized
SC	Stress corrosion
SCC	Stress corrosion cracking
SDVC	Selective dissolution vacancy creep
SEM	Scanning electron microscopy
SHE	Standard hydrogen electrode
SIMS	Secondary ion mass spectroscopy
SS	Stainless steel
SSRT	Slow strain rate tensile test
TEM	Transmission electron microscopy
TGSCC	Transgranular stress corrosion cracking
TS	Tube sheet
TSP	Tube support plate
TTS	Top of tube sheet
TW	Through wall
WOL	Wedge opening load

## List of Symbols

---

$a$	atomic diameter, crack length
$a_c$	size of critical defeat
$da/dt$	crack growth rate
$D_o$	grain boundary diffusion coefficient
$D_s$	surface diffusion coefficient
$E$	Young's modulus
$E_{corr}$	corrosion potential
$f$	function
$F$	Faraday constant
$i_o$	bare surface dissolution rate parameter
$k$	Boltzmann's constant
$K$	stress intensity factor
$K_I$	mode I stress intensity factor
$L$	diffusion path length
$M$	atomic weight
$n$	exponent
$N_s$	surface solubility
$Q$	activation energy
$Q_f$	oxidation charge density between rupture events
$t_1$	incubation period
$t_f$	periodicity of rupture event
$t_o$	passivation parameter
$T$	absolute temperature
$T_m$	absolute melting temperature
$V_f$	period of rapid propagation
$V_s$	period of slow propagation
$V_T$	average CGR
$x, x_p$	diffusion distance
$z$	oxidation number, number of sites explored per jump
$\epsilon$	strain
$\dot{\epsilon}$	strain rate
$\epsilon_f$	fracture strain
$\delta$	grain boundary width
$\gamma$	surface energy
$\rho$	mass density
$\sigma$	stress
$\bar{\sigma}$	"fracture" stress
$\sigma_y$	yield stress

# 1 Introduction

---

Corrosion in steam generators has been a problem since the very introduction of pressurized water reactor (PWR) technology. The first recorded instance of stress corrosion cracking (SCC) of Alloy 600 was reported<sup>1</sup> in 1957 as intergranular SCC (IGSCC) of a single tube from the water side near the tube sheet (TS) of a heat exchanger that was operating at 550°F. Shippingport, the first commercial PWR operated in the United States, developed leaking cracks in two Type 304 stainless steel (SS) steam generator tubes as early as 1957, after only 150 h of operation.<sup>2,3,4</sup> The cracks were attributed to SCC that was produced by free caustic in the secondary water and steam that blanketed the tubes at the top inlet portion of the steam generator, leading to concentration of the caustic. The leaking tubes were plugged, and the addition of sodium phosphate was instituted to control the pH of the secondary water. Other early incidents of SCC in austenitic SS steam generator tubes occurred at the Savannah River Heavy Water Plutonium Production Reactor in 1960,<sup>5</sup> the USS Nautilus reactor (no date given),<sup>6</sup> the Hanford New Production Reactor in 1963,<sup>7</sup> the Yankee Rowe PWR in 1966–69,<sup>8,9</sup> and the Indian Point Unit 1 PWR in 1968.<sup>9</sup> The first three failures were attributed to halide-induced SCC and the latter two to free caustic.

Because austenitic SS steam generator tubes were found to be susceptible to SCC by both chlorides and free caustic, the decision was made in the late 1950s to use Alloy 600 tubes in the United States and most of Europe, and Alloy 800 tubes in Germany.<sup>10</sup> However, these changes did not eliminate corrosion-related tubing degradation in steam generator tubing. As shown in Fig. 1,<sup>11</sup> a succession of failure processes has continued to afflict steam generators in the United States since the widespread use of Alloy 600 tubing in the late 1960s.<sup>12</sup> Essentially similar failure processes have also been experienced around the world.<sup>11</sup> The remainder of this report will deal with a review of the possible mechanisms and available correlations for various forms of SCC as they relate to initiation, propagation, arrest, and reinitiation of cracks that affect Alloy 600 steam generator tubing. However, to this date, the exact mechanisms for SCC of Alloy 600 in deaerated high-temperature water remain elusive.

## 2 Historical Background

---

### 2.1 Field Experience

Before the publication of a seminal paper by Coriou et al.<sup>13</sup> in 1959, the general belief in the PWR steam generator community, based on hundreds of laboratory tests,<sup>14</sup> was that Alloy 600 tubing was immune to IGSCC when exposed to high-purity deaerated water at high temperature. The occasional SCC failures of PWR steam generator tubes during these early years were attributed to impurities such as caustic, lead compounds, etc. The results of Coriou et al. were not confirmed by other investigators for almost 10 years. Later, however, many other laboratory tests have confirmed that depending on microstructure and processing history, Alloy 600 can and does experience IGSCC when exposed to aerated or deaerated high-temperature high-purity water.

The evolution of IGSCC-related problems in the steam generator tubes in the primary and the secondary sides differs because, although the bulk water in both the primary and the secondary sides of PWR's is pure and deaerated with dilute additives to control pH, concentration processes can significantly alter the local chemical environment in the top of the tube sheet (TTS) and in tube support plate (TSP) crevices, and under sludge piles on the secondary side, where IGSCC occurs. Hence, the IGSCC mechanisms that operate in these two types of environments differ substantially. The primary environment consists of lithium hydroxide-buffered borated water, with hydrogen overpressure to remove oxygen that is formed by radiolysis. Concentration of boric acid is set by the requirements for reactivity control and ranges from 1800 ppm boron at the beginning of a cycle for high-burnup fuel to essentially 0 ppm boron at the end of the cycle. Lithium hydroxide is added to establish slight alkalinity. The pH in typical primary water ranges between 6.9 and 7.4.<sup>15</sup> During normal operation, the reactor coolant is 305-330°C when it enters the primary side of a recirculating PWR steam generator and 288-293°C during normal operation when it exits.

The chemistry of the secondary water is more complex and has evolved over the years as the industry experienced various types of corrosion on the secondary side. An early secondary-side corrosion problem for steam generators with Alloy 600 tubes was wastage, as indicated in Fig. 1. This problem was associated with the widely used coordinated sodium phosphate water chemistry (trisodium and disodium phosphate plus an oxygen scavenger such as sodium sulfite or hydrazine). The wastage was attributed to the development of corrosive phosphate solutions in regions of dryout, and the problem was controlled when almost all plants converted to an all-volatile ammonia-hydrazine secondary water treatment (AVT). This changeover was essentially completed in 1974, and wastage problems declined dramatically over the next two years (Fig. 1). However, tube denting at TSPs then became a significant problem, primarily in units with copper alloy condensers cooled by sea or brackish water. Unlike the phosphate water chemistry, AVT provides no buffering against the local formation of highly acidic or alkaline conditions associated with impurity intrusion. The denting problem, caused by corrosion of the TSPs and the associated volume expansion of the corrosion products, was eventually alleviated by the addition of boric acid and better controls on impurity ingress.

With time, however, more and more steam generator tubes began to exhibit IGSCC that was reminiscent of the earlier experience when AVT was used. This spurred R&D activities worldwide to investigate the causes and evaluate potential remedies for IGSCC. Historically, secondary water chemistry has been maintained within purity limits established by individual operating utilities. The purity levels that are maintained are functions of cooling water composition, secondary plant material and design, availability of full-flow condensate polishers, blowdown system capacity, and various other factors. Until recently, typical composition of recirculating steam generator (RSG) secondary water was chloride, ( $\leq 30$  ppb); phosphate, 2-3 ppm; Na/PO<sub>4</sub> molar ratio, 2.0; dissolved oxygen,  $\approx 10$  ppb; hydrazine  $\approx 20$  ppb; copper,  $\approx 2$  ppb; iron,  $\approx 20$  ppb; conductivity,  $\leq 50$   $\mu$ S-cm; and pH, 8.8 to 9.5.<sup>16</sup> On-line addition of boric acid has sometimes been recommended to alleviate intergranular attack (IGA)/SCC at TSPs by possibly partially neutralizing caustics and providing a thicker, and more tightly adherent borate-containing film on the alloy.<sup>17</sup> Because operation of plants at these very low feedwater and/or blowdown impurity concentrations did not ensure the absence of steam generator tubing corrosion, Revision 3 of Electric Power Research Institute (EPRI) water chemistry guidelines<sup>18</sup> recommended an increase in feedwater hydrazine to  $>100$  ppb, a decrease in feedwater iron concentration to 5 ppb, addition of boric acid, and consideration of controlling molar (cation to anion) ratio to establish a less aggressive (neutral to slightly acidic) crevice chemistry.

Historically, the earliest SCC cases in Alloy 600 steam generator tubing worldwide occurred somewhat rapidly on the secondary side. The degradation process involved the concentration of corrosive chemicals (e.g., NaOH, acid sulfates, etc.) in areas of limited coolant flow (crevices), e.g., tube/TS junctions. Incidences of outer-diameter (OD)-initiated SCC unrelated to crevice corrosion have been observed at the upper TS of a once-through steam generator (OTSG).<sup>19</sup> Secondary side cracking has also been observed along scratches or lines of abrasion in free spans (e.g., SGs in McGuire, Oconee, and Farley). Secondary side SCC occurs in many forms and has always been responsible for a significant fraction of tubes that are plugged annually both in France<sup>10</sup> and in the U.S.<sup>20</sup> In the U.S., the first steam generator replacement was at Surry 2 in 1980 and was the result of denting. The first replacement of a steam generator due to secondary side IGA occurred in 1984.<sup>20</sup>

Beginning in the early 1970s, Alloy 600 tubing was affected by another form of the IGSCC phenomenon, this time occurring on the primary side in highly stressed areas such as the roll transition zones (RTZs), inner-row U-bends, and subsequently at TSPs. This phenomenon was responsible for the greatest number of pluggings during mid to late 1970s (denting) and 1980s (primary-water SCC [PWSCC]) in the U.S.<sup>20</sup> and during the 1980s (PWSCC) in France; it also was the cause of the first replacement of a steam generator in France in 1990.<sup>10</sup> Similar replacements have also been carried out in Belgium, Spain, Sweden and Japan.

In recent years, denting-related cracking has been controlled by improved secondary water chemistry, and inner-row U-bend cracking has been controlled by improved in-situ stress relief or by preventive plugging of susceptible tubes. Currently, SCC/IGA (OD) at the TSPs and TTS, where chemical concentration can occur, and PWSCC in expansion

zones continue to be the major cause of IGSCC-related damage in steam generator tubing. Also, transgranular SCC (TGSCC) has been found on the secondary side because of lead contamination.<sup>21</sup>

To summarize, most of the cracking currently suffered by Alloy 600 tubes of PWR steam generators is intergranular and three main types of intergranular attacks have been identified. Intergranular stress corrosion cracking/PWSCC occurs in the primary side mainly in the RTZs of the expanded tubes. On the secondary side, IGSCC, known as outer-diameter SCC (ODSCC), occurs typically in the crevices at the junctions of tubes with TS's and TSPs and under sludge piles, and IGA has been observed under sludge piles as well as at the tube to TSP junctions. Outer-diameter-initiated cracking can also occur from scratches or lines of abrasion in free spans.

## 2.2 Laboratory Testing

Numerous laboratory studies have been conducted worldwide to investigate the IGSCC behavior of Alloy 600 in PWR primary and secondary water environments. Of particular interest are those reported by INCO,<sup>14,21-24</sup> Babcock & Wilcox (B & W),<sup>25-34</sup> Westinghouse Corp.,<sup>35-42</sup> Brookhaven National Laboratory (BNL),<sup>43-51</sup> and Ohio State University<sup>52-55</sup> in the U.S., Studsvik,<sup>56-59</sup> Commissariat a l'Energie Atomique, France (CEA),<sup>13,60-63</sup> Electricité de France (EDF),<sup>10,64-71</sup> Framatome,<sup>72-78</sup> and Laborelec<sup>79</sup> in Europe, and Mitsubishi and Sumitomo<sup>80-83</sup> in Japan.

### 2.2.1 Specimens for crack initiation studies

Several specimen geometries (unflawed) have been used for IGSCC tests in various laboratories all over the world. One must be careful when comparing results of IGSCC tests conducted at various laboratories and also by the same laboratory at various times, because test specimens and loading evolved over the years. In the early tests at Inco, rectangular specimens 127 x 11.1 x 1.5 mm (5 x 0.438 x 0.06 in.), were stressed in a jig by three-point bend loading (displacement control) to  $\approx 90\%$  of the room-temperature yield strength. Sometimes, a second piece was mated against the first and a step, 0.127 mm (0.005 in.) deep, that covered the middle 89 mm (3.5 in.) of the samples was machined in one of the samples to create a crevice that varied from 0.127 mm (0.005 in.) at the edge of the step to 0 mm at the load point. At CEA, test specimens 50 x 5 x 1 mm (2 x 0.2 x 0.4 in.) (without crevice), were loaded in four-point bending (displacement control) to a maximum plastic strain of  $\approx 0.5\%$ . Later, similar four-point bend tests were also conducted at Inco in an effort to duplicate the CEA tests (most showed IGSCC after 3600 h at 350°C) and the specimens were loaded to a maximum displacement of 2.5 mm (0.1 in.), which corresponded to an elastically calculated maximum bending stress of 1380 MPa (200,000 psi) (cf. yield strength = 276 MPa [40,000 psi]). In one series of tests, CEA supplied to Inco both the specimens (mounted in a four point bend loading fixture) and the high-purity water; none of the specimens cracked in 4000 h at 350°C. The discrepancy between the CEA and the Inco tests was not satisfactorily explained.

Later, for convenience of testing, Inco used both single and double U-bend specimens made from polished 152 x 12.7 x 3.2 mm (6 x 0.5 x 0.125 in.) or 82.6 x 12.7 x

3.0 mm (3.25 x 0.5 x 0.12-in.) blanks. The double U-bend specimens were made by grinding a slot, 0.127 mm (0.005 in.) deep and 19.1 or 25.4 mm (0.75 or 1 in.) long, in the center of a U-bend blank. A second U-bend blank was placed against the groove side of the first and the composite was bent around a 19.1- or 38.1-mm (0.75- or 1.5-in.)-diameter mandrel, with the grooved specimen against the mandrel. Both the single and double U-bend specimens were stressed (constant displacement) by an Alloy 600 bolt, nut, and washers. The double U-bend specimen contained a crevice that varied from line contact at the apex to 0.127 mm (0.005 in.) at the edges of the slot. Because of the complexity of the bending of the specimens around the mandrel, the stress distribution in the specimens was not known and not analyzed. To complicate matters, the U-bend shaping procedure was improved over the years to reduce the scatter in the data. All of these specimens were fabricated from Alloy 600 plates (or ingots).

The tests at BNL were conducted on several types of specimens. First, single U-bend specimens were made from 88.9 x 12.7 x 3.8 mm (3.5 x 0.5 x 0.15-in.) blanks; a 19.1-mm (0.75 in.)-diameter mandrel was used as before. A second tube type, called the reversed U-bend (RUB) specimen, was also used. These specimens were prepared from tubing that was split longitudinally and then bent by a tube bender. This formed a U-bend, with the original inside surface of the tube in tension and a 12.7 mm (0.5 in.) inside radius of bend. Standard C-ring specimens were also machined from the tubing and used after expanding to stresses that correspond to 95 and 110% of the yield strength at the inside diameter (ID) surface of the tube. All of the tests discussed so far were of the constant deflection type and the experimental setup did not permit the measurement of load at the start or during the tests.

Constant extension rate tests (CERT) were also conducted at BNL with a CERT apparatus originally designed at General Electric (GE). The extension rate range of this apparatus was  $10^{-4}$  to  $10^{-9}$  cm/s. Tensile specimens were obtained from tubing that was split in half and then flattened it (estimated cold work = 3%). Later, instead of flattening the split tubes, curved tensile specimens were tested. A load cell connected in series measured the load on the specimen. Constant stress experiments were also conducted at BNL with five C-ring specimens in series with a long Alloy 600 spring that fit between two flat plates on the underside of the autoclave head. This procedure eliminated the need for opening the autoclave for interim inspections before failure. Later, tensile specimens (with or without flattening) were loaded in constant stress by a lever arm (ratio of 10:1) via a 10-mm (0.39 in.) pull rod that passed through a Teflon seal into the autoclave; this was later replaced by a Materials Testing System, Inc. (MTS) machine (to measure strain) with dead weight loading that could test three plate-type tensile specimens at a time. Some investigators also used pressurized sealed capsules to conduct IGSCC tests.

Most other laboratories have used some variations of the specimen geometries discussed above. Two critical problems that face all investigators have been determination of stress and determination of strain or time to crack initiation. Although initial estimates for stresses in RUB or C-ring specimens during setup are calculated, significant ( $\approx 20\%$  for initial stresses that are close to yield stress) relaxation of stress can occur during heat up from room temperature to test temperature. Additional relaxation of stress during testing at temperature is small ( $\approx 3\%$ ). In this

respect, the CERT tests are superior to RUB or C-ring tests because loads are monitored during the tests. Most crack initiation specimens are loaded into the plastic regime so that stresses in samples with higher yield strength are higher than stresses in samples with lower yield strength. Therefore, it is difficult to separate the effects of stress from those of yield strength.

The determination of time or strain to crack initiation poses a different kind of problem. Usually, in a relatively inert environment, like PWR primary water, the incubation period is much longer than the time needed to obtain significant crack propagation. Therefore, in most cases, the specimens are examined at regular intervals ( $\approx 2$  weeks) and crack initiation time or strain is defined by whenever a crack is first detected by visual examination. Crack initiation for a loading condition is then described by a Weibull plot of cracking data that are obtained from multiple specimens. However, it is emphasized that, because of the large number of variables involved, very few studies contain a sufficient number of tests under the same conditions to produce statistically valid results.

### **2.2.2 Specimens for crack propagation studies**

Although most of the laboratory studies have been limited to crack initiation, some of researchers have reported crack growth rates (CGRs). However, in-situ crack length measurements are rare. In many cases, an initial flaw is machined into the specimen, which is then loaded either by constant-extension rate or at constant load until failure or significant crack propagation has occurred. The average CGR is then calculated by dividing the final crack extension by the test time. Crack initiation time in these specimens can be substantial often requiring a plastic strain of several percent. Hence, the reported CGRs are not precise because of uncertainties in crack initiation time. In a few cases, in-situ crack lengths (both axial and circumferential) have been measured by a DC potential drop method. However, typically, these fracture-mechanics-type (compact-tension) specimens are made from Alloy 600 plates rather than tube material. Recently, tubular-fracture-mechanics specimens (bending type) with longitudinal cracks have been used at Framatome to measure CGRs by using a reverse DC potential drop to measure crack lengths. Although these specimens remove the uncertainties of using specimens from plate, they are subject to the drawback that the crack front stress intensity factor  $K_I$  is not constant but decreases substantially from the ID to the OD surface.

### **2.2.3 Control of solution chemistry**

A critical factor in any laboratory test that involves SCC is the proper control of solution chemistry, with respect to such components as oxygen, hydrogen, LiOH, NaOH, boric acid, etc. during the entire test. First and foremost, the autoclave material is either Alloy 600 or Type 316 SS (or Alloy 800) with an Alloy 600 jacket that is electrically insulated from the autoclave. Most reputable laboratories perform elaborate procedures to control the solution chemistry. These procedures begin with cleaning the autoclaves or pressure vessels (made of Type 316 SS or Alloy 600) repeatedly with distilled, demineralized water until the conductance is reduced to a small value

(typically < 0.5  $\mu\text{S-cm}$ ). Next, various additives are added, depending on what is being simulated.

To simulate primary water, the oxygen concentration is reduced to 0-5 ppb by evacuation and repeated pressure-vent cycles with a high-purity gas such as  $\text{N}_2$ . During the tests, oxygen is continually removed from the reservoir by sparging. Additives include  $\text{LiOH}$  and boric acid with hydrogen overpressurization of the makeup water. Simulated secondary water that corresponds to water subjected to AVT is achieved by first degassing the water-filled vessel, then cooling and injecting hydrazine and morpholine or ammonia. Decomposition of these compounds at high temperature is a concern. The heat up rate of the vessel should be sufficiently slow so that hydrazine can complete its gettering action of removing residual  $\text{O}_2$  before the test temperature is reached. Morpholine ( $\text{C}_4\text{H}_9\text{ON}$ ), which is used to control the test solution at basic pH, requires a much longer time to decompose.

Secondary-side cracking in a real steam generator generally occurs in crevices formed by tube/TSP or tube/TS intersections. The local chemistry in crevices that promotes IGSCC/IGA consists of concentrated nonvolatile impurities that are a result of boiling and restricted mass transport. The exact chemistry of the solution in the crevices during steam generator operation is unknown. To complicate matters, ionic impurities such as  $\text{NaCl}$  and sulfates have recently been shown to hide out within thin deposits on steam generator tubes by a process called wick boiling.<sup>84</sup> These deposits should be partially removed by hide out return during shutdown. Results from computer codes like MULTEQ-REDOX, which use hideout return data from secondary-side steam generator as input, indicate that, in most cases, the crevice chemistry is caustic.<sup>85</sup> Therefore, in the past, the simulated secondary water in the laboratory has often included 10-50% caustics (e.g.,  $\text{NaOH}$ ).

In recent years, based on chemical analyses of crevice deposits from steam generators, a consensus is developing that the crevice chemistry may in fact, be near-neutral to slightly alkaline, which, if true, makes much of the laboratory-generated SCC data irrelevant. Sometimes, MULTEQ analyses based on blowdown water and presence of lead compounds or sulfate as input predict the crevice condition to be acidic.<sup>86</sup> Therefore, impurities, such as, sulfates, lead, phosphate, magnetite, etc. are also often added.

After the test is completed, the solution is chemically analyzed for dissolved impurities. Sometimes a vapor phase sample is extracted at higher temperature and analyzed. Clearly, poor control of the solution chemistry during the tests can lead to excessive data scatter. This is a concern particularly for tests conducted in static autoclaves in which the chemistry (especially hydrogen but also impurities such as sulfates) may not be constant during the test. However, in many publications, the experimental details of how the solution chemistry is controlled during the tests are not provided. Also, it is important to note that most laboratory testing is conducted in either static or recirculating autoclaves that have limited flow rate capability when compared with real steam generators.

### 3 Factors that Influence IGSCC of Alloy 600

---

Stress corrosion cracking of any type requires that three elements be present simultaneously; if any one is absent, SCC will not occur. These elements are

- an aggressive environment,
- a tensile stress greater than some threshold value, and
- a susceptible metallurgical condition or microstructure.

It is important to distinguish between the presence or absence of oxygen when discussing SCC of Alloy 600 in high-temperature water, because the electrochemical potential (ECP) of the alloy is considerably higher in aerated water than in deoxygenated water. Like the austenitic SSs in oxygenated water, Alloy 600 is prone to IGSCC in the sensitized condition (heated between 500 and 800°C) but resistant to IGSCC in the mill-annealed condition.<sup>22</sup> In deoxygenated (or caustic) water, the reverse is found, i.e., mill-annealed Alloy 600 is prone to IGSCC and sensitization makes it more resistant to cracking.<sup>87-89</sup> The exact reasons for this striking difference in the behavior of Alloy 600 in oxygenated and deoxygenated water is not yet fully understood. Inasmuch as the subject of our review is IGSCC in PWRs, we will concentrate primarily on SCC in deoxygenated water.

In most laboratory corrosion tests that are interrupted to measure crack depths, three stages of cracking can be observed, as shown schematically in Fig. 2a.<sup>10</sup> Tests begin with an incubation period  $t_1$ , which is the time required to set up the local physico-chemical and mechanical conditions for enhanced crack initiation. The initiation time is followed by a period of slow propagation ( $V_s$ ) that is characterized by formation of short cracks, the depth of which does not exceed a few tens of micrometers until they reach the size of a critical defect  $a_c$ . The last period of the test is one of rapid propagation ( $V_f$ ), leading to macroscopic cracks and to rupture. Tests on C-rings with cracks  $<500 \mu\text{m}$  can generally be associated with  $V_s$ , tests on capsules lead to both  $V_s$  and  $V_f$ , and wedge opening load (WOL) specimens provide data on rapid CGR  $V_f$ . Thus, differing specimen geometries, tested with the same material and in the same environment can give differing CGRs. The test results shown in Figs. 2a and 2b<sup>62</sup> were obtained from Alloy 600 tubes that were highly susceptible to IGSCC. In general, the parameters  $t_1$ ,  $V_s$ , and  $a_c$  vary with the tube material. Tubes that are resistant to IGSCC show a large value of  $t_1$  and/or low value of  $V_s$ , and/or a high value of  $a_c$ .

Generally, PWSCC is associated with high stress, high temperature, and susceptible microstructure, whereas secondary-side IGSCC or IGA (also influenced by susceptible microstructure) is usually observed in crevices where impurities (such as caustics) are concentrated by elevated local temperature and restricted water flow. However, many factors influence IGSCC in primary and secondary water in the same way. For example, the beneficial effects of a continuous or semicontinuous network of fine intergranular carbide and the lack of a significant effect of chromium depletion in deaerated environments are the main microstructural effects that are common to both

types of IGSCC. However, it is not clear whether the beneficial effect of high-temperature solution annealing and/or a low yield strength, observed for PWSCC, is also valid for caustic cracking. A most important difference between the two is in the incubation period: for caustic cracking, it is very short whereas, for PWSCC, it is usually much longer and dependent on temperature, material, and environment. As a result, in most laboratory studies on Alloy 600, the stress levels are much higher for PWSCC than for caustic cracking. Thus, it is difficult to compare the threshold stresses for caustic cracking and PWSCC on an experimental basis.

By and large, the same set of factors influences both primary and secondary side corrosion. The main differences between the primary and secondary sides are as follows:

- The temperature in the secondary side is slightly lower than that in the primary side.
- Design-dependent crevices, where impurities can concentrate, are present only in the secondary side.
- Boiling occurs in the secondary side but not in the primary side.
- Hydrazine, not gaseous hydrogen, is purposely added in the secondary side (however, the corrosion potential corresponds to the hydrogen electrode). Although the hydrogen concentration in the bulk secondary water is very low, it continuously diffuses from the primary side through the tubes so that the hydrogen concentration on the primary and secondary metal surfaces may not differ as much as the hydrogen concentration in the environments.

### 3.1 Metallurgical State or Microstructure

Microstructure, which is one of the most important factors that control IGSCC of Alloy 600, depends upon the thermomechanical history and the carbon content of the alloy. As mentioned earlier, Coriou et al.<sup>13</sup> were the first to relate the IGSCC behavior of Alloy 600 to its microstructure. Correlations between metallurgical variables and the IGSCC behavior of Alloy 600 is now well established.<sup>27,34,90</sup> A critical microstructural parameter that determines the IGSCC behavior of Alloy 600 is the nature of the grain boundary carbide precipitates.

Based on RUB tests and transmission electron microscopy (TEM) studies on mill-annealed and thermally treated Alloy 600 tubes, EDF has classified the carbide precipitates in Alloy 600 into three types.<sup>10</sup> In Type I precipitates, which are most resistant to IGSCC, the grain boundaries are covered continuously by the carbide precipitates. In Types II and III, most of the carbide precipitate is intragranular, with Type II showing more intergranular precipitates (and higher resistance to IGSCC) than Type III. The importance of carbide distribution has been clearly demonstrated in the examination of hot-leg tubes that were removed from the Ringhals 2 reactor.<sup>91</sup> The severe secondary side IGSCC was restricted to tubes without intergranular carbides, while tubes with intergranular carbides were almost free of cracks. In a similar fashion,

primary side cracks at RTZs were exclusively found in tubes without intergranular carbides, while tubes with intergranular carbides were crack free.

The main fabrication variable that affects these material characteristics is the heat treatment applied after the tubing is cold worked to final size. Carbides exist at intergranular and intragranular sites before final tube forming as a result of prior fabrication history. After reduction to final size, the tubes are given a final heat treatment (mill annealing) that recrystallizes the cold-worked grains. The final grain size, yield strength, carbon content, intergranular/intragranular carbide densities of the alloy and the mill-annealing temperature are all interrelated in a complicated way.<sup>92</sup>

The annealing temperature that must be achieved to dissolve all of the carbides in Alloy 600 depends on the carbon content. When the intragranular carbides are all dissolved, grains grow rapidly. If the annealing temperature is not sufficiently high, it will not dissolve all of the carbides that are inside the grains. The undissolved carbides prevent significant grain growth and thus lead to fine grains and high yield strength. Also, the remaining undissolved carbides change the kinetics of the carbide precipitation, particularly the split between intra and intergranular precipitates, during subsequent cooling. With enough undissolved carbides, the carbon can precipitate on the existing carbides and thus avoid a nucleation step in the grain interiors. This can prevent the supersaturation of carbon from becoming sufficiently high during cooling to nucleate the desired density of grain boundary carbides. Because a higher annealing temperature is required to dissolve all of the carbides in a high-carbon material, it is possible for high-carbon materials to contain fewer grain boundary carbides than low carbon materials that were annealed at the same temperature.

Alloy 600 tubes subjected to mill annealing at low temperatures ( $\leq 925^{\circ}\text{C}$ ) generally exhibit a fine-grained microstructure, with Type II or III precipitates, i.e., heavy intragranular carbide precipitates with little or no carbide precipitates on the grain boundaries. Such microstructures are susceptible to IGSCC in both primary and secondary waters.<sup>10</sup> In contrast, a high-temperature ( $>1000^{\circ}\text{C}$ ) mill annealing of the alloy with the same carbon content tends to put more carbon into solution, increases grain size, and produces continuous or semicontinuous grain boundary chromium carbide precipitates (Type I) during controlled cooling, all of which tend to increase the resistance of Alloy 600 to IGSCC, but do not make the alloy immune to IGSCC. However, the work of Owens<sup>92</sup> shows that not only the final anneal but also the penultimate anneal are important in determining the final carbide distribution.

As-processed Alloy 600 has a tendency to develop "bands" that consist of fine-grained regions that contain many intragranular carbides. Banding is a concern because the microstructure within the dark bands contains little of the intergranular chromium-rich carbide precipitates that are necessary for resistance to SCC.<sup>42</sup> Banding can be minimized by employing high-temperature ( $\geq 982^{\circ}\text{C}$ ) as opposed to low-temperature processing ( $\leq 928^{\circ}\text{C}$ ). However, once formed, the dark bands, which are rich in chromium and titanium and depleted in iron, are persistent even after high-temperature annealing because of the sluggish diffusion rates of chromium and titanium.

An alternative way to increase the resistance of Alloy 600 to IGSCC in high temperature water is by thermal treatment,<sup>27,46,87</sup> i.e., heating the alloy at 650-750°C for a sufficiently long time, e.g., 1-15 h. Cattant et al.<sup>69</sup> reported that tubes removed from two steam generators in a 900 MWe plant after 48,000 h in service showed that 40% of the nontreated mill-annealed tubes experienced primary side cracking whereas very few of the thermally treated tubes showed any cracking at all. Thermal treatments can potentially affect three aspects of the grain boundary microstructure: grain boundary carbide precipitation (Type I), grain boundary chromium depletion associated with carbide precipitation, and segregation of impurities to the grain boundaries. Although the net effect of thermal treatment is beneficial in most cases, it cannot be concluded that chromium depletion or segregation of impurities alone have a beneficial effect on IGSCC of Alloy 600 in deoxygenated water.

Steam generator tubes are usually given a pickling treatment (HNO<sub>3</sub> and HF) to clean the surfaces before service. It has been observed experimentally that the IGSCC failure times of pickled specimens are consistently shorter than the failure times of unpickled companion specimens.<sup>43</sup> Hydrogen introduced in the specimens by pickling may be responsible for this observation, although this has not been established.

### 3.1.1 Primary water IGSCC/PWSCC

Gorman<sup>93</sup> and Owens,<sup>94</sup> who reviewed the PWSCC behavior of Alloy 600 in operating PWR steam generators, reported that Alloy 600 tubings that are highly susceptible to PWSCC exhibit two properties in common: first, a high yield strength (>425 MPa) that is a result of a fine-grained microstructure (ASTM 9-11), and second, carbides that are predominantly intragranular and contain relatively few intergranular carbides. On the other hand, having tubes with large grains and low strength does not necessarily make the generator immune to PWSCC. For example, a low-susceptibility Alloy 600 tube that was used in the Main Yankee steam generator experienced circumferential cracking due to PWSCC at the TTS after 14 effective full power years of service even though it had a semicontinuous to continuous network of intergranular carbides, a relatively coarse grain size (ASTM 5-8), and a low yield strength (330 MPa).<sup>95</sup>

The importance of grain size was highlighted by Tas et al.,<sup>96</sup> who examined steam generator tubes removed from Doel Unit 2, which had experienced PWSCC. Of the nine removed steam generator tubes, only one showed no evidence of PWSCC. This particular steam generator tube, like those of Unit 1 (which experienced no steam generator problem), exhibited a significantly larger grain size (ASTM 6-7) than the other steam generator tubes (ASTM 9-10), all of which experienced PWSCC. In laboratory tests, Norring et al.<sup>57</sup> exposed RUB specimens of Alloy 600 to hydrogenated water at 365°C and observed that crack initiation time decreased from 15,000 h for an ASTM grain size of 5, to 5000 h for an ASTM grain size of 9.5. In a similar fashion, Totsuka et al.<sup>52</sup> performed CERTs at 350°C and RUB tests at 363 and 400°C in hydrogenated 0.01 m boric acid plus 0.001 m LiOH to show that a fine-grained microstructure was more susceptible to SCC than a coarse-grained microstructure. However, in both of these studies, how much of the change in susceptibility to SCC could be attributed to change in carbide distribution as opposed to change in grain size was not determined.

Tests at EDF have shown that both the mill-annealing temperature and the carbon content of the alloy determine its susceptibility to IGSCC in hydrogenated pure water at 350°C (Fig. 3).<sup>10</sup> Fairly convincing evidence for the importance of annealing temperature in IGSCC was also provided by Norring et al.,<sup>56</sup> who used RUB tests to demonstrate that a reasonably good correlation (Fig. 4) existed between crack initiation time and the final mill-annealing temperature of Alloy 600. Increasing the annealing temperature from 925 to 1025°C increases the crack initiation time from 1200 to 10,000 h at 365°C. This corresponds to an increase from 3 to 23 years at 320°C.

Because the grain size and room temperature yield strengths of Alloy 600 are functions of the annealing temperature, Norring et al.<sup>56</sup> found good correlation between crack initiation time and grain size (Fig. 5a) and room-temperature yield strength (Fig. 5 b). However, as discussed earlier, correlations of IGSCC resistance with yield strength are usually complicated by correlated differences in grain boundary carbide structure and carbon content. From correlations of cracked tubes with heat numbers of generators that contain a mix of tubes from two different vendors, it has been noted that susceptibility decreases with increasing yield strength within the group of tubes of one vendor, but that the correlation is reversed when the two vendors are compared.\* That is, the tubes from Vendor A exhibit greater yield strength and are more susceptible than those of Vendor B. However, the stronger Vendor-B tubes are slightly less susceptible than the weaker Vendor-B tubes. Thus, the reasons for the increased yield strength are different when comparing vendor to vendor than when comparing various heats from the same vendor.

Thermal treatment at 600-700°C has been shown to increase the crack initiation time in primary water by at least a factor of 2.5, compared with that of mill-annealed material.<sup>97</sup> Tests at EDF have also shown that susceptibility to IGSCC of Alloy 600, thermally treated at 700°C, depends on the carbon content and the mill-annealing temperature (Fig. 6).<sup>10</sup> Heating at  $\approx$ 700°C has a double beneficial effect on the resistance of Alloy 600 to IGSCC. In addition to making the microstructure less susceptible to localized attack, it relaxes the residual stresses in cold-deformed tubes. However, the effect of the thermal treatment on PWSCC can be detrimental if the carbon content of the alloy is  $>0.032\%$ .<sup>69</sup> Thermal treatment is ineffective in very-low-carbon heats of Alloy 600 and may be ineffective in higher carbon heats if essentially all of the carbon is tied up in intragranular carbides. This probably reflects the fact that thermal treatment has more to do with changing the grain boundary carbide distribution (i.e., increasing the grain boundary carbide decoration to a near-continuous distribution) than with replenishing chromium.

Cold work enhances the susceptibility of Alloy 600 to IGSCC in high-temperature hydrogenated water. Field evidence for this comes from the observation that PWSCC in operating steam generators has mainly occurred at three locations: tight-radius U-bends, dented tubes at tube/TSP intersections, and in the RTZ above the TS. In all of these locations, the alloy was plastically deformed, i.e., cold worked.

---

\* A. P. L. Turner, Dominion Engineering, Inc., personal communication, 1998.

Laboratory evidence of the effects of cold work is the observed increase in the susceptibility of Alloy 600 to IGSCC by 5% cold work.<sup>47,74</sup> Cassagne and Gelpi<sup>74</sup> reported an order-of-magnitude increase in CGR at 360°C due to 5% cold work, although the increase was less at 315°C. It has been suggested that a small amount of cold work ( $\approx 5\%$ ) is more detrimental to IGSCC than a large amount of cold work ( $\approx 20\%$ ).<sup>98,99</sup>

Also, the way the cold work is introduced appears to be important. For example, prestraining seems to be more detrimental than cold rolling.<sup>100</sup> Cold work introduced by bending appears to be one of the most detrimental types of cold work for IGSCC in Alloy 600. For example, Totsuka et al.<sup>52</sup> did not find cracking at 350°C during CERTs on smooth mill-annealed specimens in hydrogenated water at initial strain rates of  $5 \times 10^{-7}/s$  and  $2 \times 10^{-7}/s$  after 343 h and 408 h of straining, respectively. However, when a 35% bending strain was produced at the middle of the gage by cold pressing, the fracture surface was 65% intergranular after 60 h of straining. Rebak et al.<sup>101</sup> reported that CGR in simulated primary water followed a power law relationship with prior cold work in bending (Fig. 7).

Some of the confusion about the effects of cold work on susceptibility may be related to loading. Most field experience with steam generator tubes, vessel head penetrations, and pressurizer heater sleeves indicates that cold work is detrimental if residual stresses or additional deformation raises the stress to the cold-worked flow stress. This means that if the stress in the tube is close to the flow stress and the flow stress is high, the tube is susceptible to IGSCC. The best example of this is the pressurizer heater sleeves that were abusively reamed and then strained into the plastic regime by weld shrinkage during installation.\* These sleeves were much more susceptible to IGSCC than sleeves that were not reamed.

In other cases where the applied stress is fixed or load-controlled (i.e., not dependent on material flow strength), some cold work can be beneficial because the applied stress is a lower fraction of the material strength. The effects of applied stress and material strength are not satisfactorily separated in either field experience or laboratory tests. As mentioned earlier, most laboratory tests have been conducted on samples that were loaded into the plastic regime, where stress is controlled by strength.

Testing in deaerated high-temperature water with dissolved hydrogen has also shown that susceptibility of Alloy 600 to IGSCC is dependent on material processing, i.e., whether by cold work and annealing (CWA) or by hot work and annealing (HWA), and the hot working temperature.<sup>42</sup> Cold work and annealed tubing material is more susceptible to IGSCC than HWA ring forging material with similar microstructure. Even when corrected for differences in stress and strength levels, HWA materials have failure times that are five times longer than the failure times for CWA tubing material.

Two factors may have contributed to the poor performance of the CWA tubing material. First, the tubing material, with a very thin wall (1.2 mm), may exhibit cooling

---

\* A. P. L. Turner, Dominion Engineering, Inc., personal communication, 1998.

rates that are too fast for carbide precipitation. The HWA ring-forged material, which is more massive, exhibits a slower cooling rate and allows more carbides to precipitate during cooling from final annealing. The second factor is the final annealing atmosphere. The final anneal of the tubing is performed in a dry hydrogen environment, whereas the final anneal of the forging is performed in an inert environment.

Recently, the importance of grain boundary structure on IGSCC has received some attention. Crawford and Was<sup>102</sup> performed CERTs on high-temperature-mill-annealed (HTMA) Alloy 600 in argon and in deaerated, high-purity water at 360°C to show that coarse-grained samples of Alloy 600 with increased proportions of coincident site lattice (CSL) boundaries are more resistant to cracking than similar samples with low proportions of CSL boundaries. They also conducted scanning electron microscopy (SEM) studies to show that CSL boundaries were more crack resistant than high-angle random boundaries, irrespective of the environment, although the resistance was higher in argon than in water.

### 3.1.2 Secondary water IGA/IGSCC/ODSCC

On the basis of statistical analyses of secondary side SCC data obtained from French generators, Fournel<sup>103</sup> concluded that the parameter with the greatest influence on ODSCC at the TSP level of mill-annealed Alloy 600 tubes was yield strength. From more than 80,000 tubes and 30 investigated variables, it was found that the lower the yield strength, the higher the sensitivity to SCC for tubes made by some (but not all) manufacturers. The main second finding from the studies on the French generators was that mill-annealed Alloy 600 was much more susceptible to cracking than thermally treated Alloy 600.<sup>104</sup> However, this result should be accepted with caution because mill-annealed Alloy 600 is used in older plants with drilled carbon steel TSPs, whereas the thermally treated Alloy 600 is used in more recent plants with 12%Cr-steel TSPs. Moreover, it must be remembered that the operating chemistry of the plants has been steadily improving over the years.

Domian et al.<sup>27</sup> reported that IGSCC of Alloy 600 in 343°C water (AVT-treated) of pH 9.3-9.5 was reduced by heat treatment that produced grain boundary carbide precipitation. Thermal treatment of Alloy 600 has been shown to produce a microstructure that is resistant to IGSCC in caustic environments,<sup>65,105,106</sup> although no obvious effect of grain size on crack severity was observed.<sup>106</sup> Also, according to Airey,<sup>87</sup> semicontinuous grain boundary precipitates are very beneficial in caustic environments. A similar observation for IGSCC in a caustic environment was also recorded by Vaillant et al.<sup>71</sup> who tested Alloy 600 tubes whose carbon varied from 0.016% to 0.045% and whose yield stress varied from 125 to 300 MPa (obtained by varying the mill-annealing temperature from 1150°C to 980°C), with and without thermal treatment at 700°C. Although tubes with low carbon and low-intergranular-carbide precipitates were very susceptible to cracking in NaOH solution, Vaillant et al.<sup>71</sup> were able to better correlate IGSCC of mill-annealed Alloy 600 with the yield stress at 350°C than with carbon content and microstructure.

In contrast to PWSCC, resistance to IGSCC in caustic improved with increasing yield stress (Fig. 8).<sup>71</sup> Jacko<sup>107</sup> conducted SCC tests on mill-annealed and thermally

treated Alloy 600 over a range of caustic concentration, temperature, and stress to confirm that thermal treatment produces superior resistance to IGSCC/IGA when compared with mill annealing. The magnitude of the improvement (in terms of maximum crack depth) varied from heat to heat and was primarily related to delayed crack initiation. Also, the improvement in resistance to IGA was less than that to IGSCC.

Vaillant et al.<sup>108</sup> summarized the results from French studies on the slow-crack-propagation stage ( $V_s$ ) with the CERT and C-ring tests and rapid-crack-propagation stage ( $V_f$ ) with WOL specimens in Alloy 600 (plates). C-ring tests in 10% NaOH at 350°C indicated only a small benefit of thermal treatment ( $V_s = 0.5 \mu\text{m/h}$  for mill annealing vs.  $0.4 \mu\text{m/h}$  for thermal treatment). However, a much greater beneficial effect of thermal treatment was observed at 320°C. Thermal treatment at 700°C produced a 100-fold reduction in  $V_s$  values. For the rapid-propagation stage at 350°C in 10% NaOH, thermal treatment at 700°C had a mildly beneficial effect on  $K_{ISCC}$  ( $9 \text{ MPa}\sqrt{\text{m}}$  for mill annealing vs.  $12 \text{ MPa}\sqrt{\text{m}}$  for thermal treatment) but a more pronounced beneficial effect on  $V_f$  ( $6 \mu\text{m/h}$  for mill annealing vs.  $0.85 \mu\text{m/h}$  for thermal treatment).

Under mill-annealing conditions, acidic and sulfate environments can promote IGSCC whatever the microstructure of Alloy 600: mill-annealing temperature and carbon content had little effect on susceptibility.<sup>109</sup> But thermal treatment at 700°C greatly improved the resistance to SCC, primarily by increasing the initiation time. However, later tests at Materials Engineering Associates, Inc. (MEA) failed to duplicate Newman's<sup>109</sup> results and concluded that his test environment was not adequately deaerated. The MEA tests showed that in deaerated acid sulfate solutions, sensitized HTMA (12 h at 621°C) material was much less susceptible to IGA/IGSCC than LTMA or HTMA materials.<sup>110</sup>

Airey<sup>87</sup> conducted C-ring tests at 150% yield stress to study the effect of thermal treatment on the stress corrosion behavior of Alloy 600 in water doped with lead oxide and in 10% caustic solution. When tested in lead-doped environment, the mill-annealed material cracked in an intergranular mode, whereas thermally treated material cracked in a transgranular mode. Some mixed cracking was also observed. Thermal treatment significantly improved the caustic SCC resistance of Alloy 600 tubing with carbon content between 0.006 and 0.046 wt.%.

## 3.2 Alloying Elements

### 3.2.1 Primary water IGSCC/PWSCC

It is difficult to separate the effects of alloying elements from other microstructural effects. Thus, the evidence for the effect of carbon content of the alloy on susceptibility to SCC is conflicting. For example, Theus<sup>111</sup> found low-carbon material to crack more rapidly than higher carbon material. On the other hand, accelerated (10% NaOH) C-ring tests showed that tubing with a lower carbon content was slightly more resistant to SCC than tubing with a higher carbon content.<sup>112</sup> Norring et al.<sup>56</sup> did not find any correlation between total carbon content ( $C_{\text{Tot}}$ ) and crack initiation time. On the other

hand, they found that crack initiation time generally increased with increased coverage of grain boundaries by carbides (Fig. 9).

Many studies have been conducted to determine the effect of chemical composition of Fe-Ni-Cr alloys on corrosion in primary water. It is now recognized that an increasing chromium content in Fe-Ni-Cr alloys exerts a beneficial effect on resistance to SCC in pure/primary water, as shown in Fig.10.<sup>113</sup> These findings have been the primary reason for the utility industry's current interest in Alloy 690, which is Alloy 600 that has been modified with 19% Cr, as a replacement steam generator tube material. However, no clear explanation is available for why Alloy 690 behaves better than Alloy 600 in a PWR environment regardless of heat treatment.

Segregation of minor alloying elements and impurities such as boron, sulfur, cobalt, niobium, silicon, titanium, nitrogen, and phosphorus to grain boundaries is often considered the reason for selective grain boundary dissolution and thus should influence IGSCC of Alloy 600. However, experimental results are inconclusive and more research is needed in this area. There is experimental evidence linking phosphorus and silicon<sup>114</sup> with susceptibility to intergranular attack in a highly oxidizing environment (boiling HNO<sub>3</sub>) and linking niobium with resistance to IGSCC in oxygenated water.<sup>115</sup> But there is no evidence that the same is true in deaerated primary water. McIlree et al.<sup>116</sup> found that, after 8000 h in deaerated water, Alloy 600, in the high-temperature mill-annealed condition with or without thermal treatment, did not experience grain boundary attack, regardless of the sulfur or phosphorous content of the alloy. Many researchers have reported results of Auger electron spectroscopy (AES) analyses of phosphorus and sulfur segregation in Alloy 600.<sup>117</sup> Based on their results and literature data, Guttman et al.<sup>117</sup> concluded that segregation of phosphorus did not appear to be the cause of IGSCC in Alloy 600 in pure or alkaline water. Results from EDF have never demonstrated a direct correlation between PWSCC and trace elements such as boron and sulfur in Alloy 600.<sup>10</sup>

### 3.2.2 Secondary water IGA/IGSCC/ODSCC

The role of alloying elements of Alloy 600 in IGSCC in secondary water environments has not been studied extensively in recent years. Some old results are available in the literature that show that increasing nickel content reduces SCC susceptibility of Cr-Ni-Fe alloys in a chloride environment.<sup>118</sup> From a thermodynamic viewpoint, the solubility of chromium in Alloy 600 is the greatest in caustic solutions when compared with nickel and iron, because of the difficulty in forming a chromium oxide film on the metal surface. However, it has been shown that chromium is beneficial for the IGA/IGSCC of Alloy 600 in caustic solutions. Wilson and Aspden<sup>119</sup> found that, in deaerated high-temperature caustic solutions (10-50%), a decrease of nickel content from 75% (Alloy 600) to 60% (Alloy 690) with a corresponding increase in chromium resulted in decreased cracking susceptibility. More recent work by Vaillant et al.<sup>71</sup> also shows that Alloy 690 is less susceptible to SCC than Alloy 600 in caustics. However, these investigators did not test alloys in which higher nickel was obtained by lowering iron. Increasing chromium content appears to increase the corrosion kinetics in caustic environments. As a result, increasing nickel does not appear to be beneficial at or beyond 20-25% chromium. Similar conclusions can also be drawn from single U-

bend test results (Fig. 11), which show the synergistic effects of chromium and nickel on IGSCC of nickel-base alloys in 10% NaOH at 325°C.<sup>120</sup>

Based on U-bend tests in which specimens were exposed to 50% NaOH solution, McIlree et al.<sup>116</sup> concluded that high carbon exerted a deleterious effect on the IGSCC behavior of high-temperature-annealed and thermally treated material. However, high sulfur (0.015%), together with high carbon (0.075%), appeared to be beneficial for the high-temperature-annealed material with or without thermal treatment. Yamanaka<sup>82</sup> has conjectured that the beneficial effect of intergranular carbide precipitates on resistance to caustic IGSCC is due to the incorporation of grain boundary segregants, such as carbon, boron, and phosphorus, into the chromium carbides. He ruled out alternative explanations, such as the insolubility of the carbide itself relative to the matrix, because he found similar dissolution rates of the carbides and the Alloy 600 matrix in deaerated 40% NaOH at 325°C. However, the high caustic solution he used may have masked the difference in the dissolution rates of the two materials, because the work of Rebak et al.<sup>121</sup> showed that in hydrogenated high-temperature water, the carbides exhibited a lower passive current than the matrix. Generally, the results of experimental studies on the effect of impurities like phosphorus and sulfur on IGSCC of Alloy 600 are confusing and more research is needed in the future.

### 3.3 Coolant Chemistry, Inhibitors, and Impurities

#### 3.3.1 Primary water IGSCC/PWSCC

Among primary water elements (boric acid, LiOH, and hydrogen), hydrogen is the most influential, although it was long considered to be innocuous or even beneficial to the performance of Alloy 600 in primary water. Hydrogen is added to the primary side to maintain a minimum concentration of dissolved oxygen that is produced by radiolysis of the coolant, to minimize primary circuit material corrosion, and to maintain low redox potentials in the primary loop. Airey<sup>36</sup> and Bandy and van Rooyen<sup>48</sup> were the first to demonstrate that molecular hydrogen is detrimental for SCC of Alloy 600 in primary water.

Experiments<sup>36,38,48,52</sup> have shown that by increasing the partial pressure of hydrogen in contact with primary water or in a mixture with steam, the rate of IGSCC increases to a maximum and then decreases. Compiled data have shown that increasing the partial pressure of hydrogen decreases the crack initiation time in high-temperature water (Fig. 12a).<sup>58</sup> Similar behavior has also been found in steam at 400°C.<sup>38</sup> However, the so-called 400°C steam tests were conducted in supercritical water, in which ionic transport processes can work, whereas they cannot work in 7 MPa (1000 psi) steam. This is an important point to keep in mind because cracking and IGA have been observed in the superheated steam space in OTSGs at Oconee.\* But a decrease in susceptibility to IGSCC with further increase of hydrogen partial pressure has also been reported,<sup>122</sup> as shown in Fig. 12b. Tests at Center for Energy and Environment Technology Research, CIEMAT (Spain) have shown that, at 330°C, Alloy

\* A. P. L. Turner, Dominion Engineering, Inc., personal communication, 1998.

600 is more resistant to SCC in primary water with 45 cm<sup>3</sup>/kg of hydrogen than with 23 cm<sup>3</sup>/kg of hydrogen.<sup>123</sup> In dry hydrogen gas, no IGSCC has been found to occur in Alloy 600, even at a pressure of 35 MPa at 300-400°C.<sup>53</sup> However, it should be remembered that IGSCC does occur in Alloy 600 in high-temperature water without dissolved hydrogen.<sup>124</sup>

It is generally accepted that Alloy 600 cracks more readily in lithiated, borated water than in pure water, although the experimental results are not unequivocal on this point.<sup>10</sup> Tests conducted by EDF and CIEMAT have shown that increasing lithium content of the primary water from 0.7 to 5 ppm can reduce the crack initiation time by almost a factor of 2.<sup>123</sup> The current industry position, based on correlations of laboratory data, is that PWSCC susceptibility and rate change by less than a factor of 2 over the range of lithium and boron concentration currently used in the primary circuit.

A key parameter that controls SCC reactions in PWR primary system materials is the oxide film on the material. As long-term reliability and dose rate reduction during maintenance have become more important, PWR plant operators have begun to examine the modification of primary water chemistry that potentially offer more protective oxide films, limit corrosion release, and delay PWSCC initiation. Two approaches that have been considered are addition of zinc and controlled modification of lithium/boron primary water chemistry during a fuel cycle.<sup>125-128</sup>

Esposito et al.<sup>125</sup> compared the PWSCC in 50% of the sample population of RUB specimens in a hydrogenated solution that contained 1200 ppm boron plus 2.2 ppm lithium at 330°C and the same solution plus 20 ppb zinc as zinc borate. The time to crack initiation for mill-annealed material increased by a factor of 2.5 in the solution that contained zinc. They also reported that the oxide film thickness decreased by 50% in the presence of zinc.

Andresen and Angeliu<sup>128</sup> found that CGR was two times lower in sensitized Alloy 600 when 5-10 ppm zinc (as zinc oxide) was added to 288°C water that contained 200 ppb oxygen and 0.3 μM H<sub>2</sub>SO<sub>4</sub>. The higher beneficial effect of zinc was reported at lower potentials (low oxygen). The authors suggested that the beneficial effect of zinc was related to improving the ductility of the oxides and thereby reducing the frequency of oxide rupture, and controlling the pH inside the crack.

Byers and Jacko<sup>127</sup> postulated that the beneficial effect of zinc in reducing PWSCC of Alloy 600 tubing was related to the reduction of solubility of chromium and iron by changing the local pH on the oxide surface, thus leading to the rapid formation of a protective oxide after a slip event exposes bare metal at the crack tip. Property changes due to controlled modification of lithium/boron primary-water chemistry was also correlated with changes in the protective oxide films that form on Alloy 600.

In stress corrosion CGR tests ( $K_I = 22-56 \text{ MPa}\sqrt{\text{m}}$ ) on Alloy 600 in pH-buffered, deaerated, hydrogenated water at 316-360°C, soluble zinc did not mitigate CGRs.<sup>129</sup> It was speculated that the inability of zinc to incorporate into crack tip nickel oxides was the reason that a beneficial effect was not observed and that zinc mitigation is possible when the process-controlling oxide is spinel.

Mill-annealed Alloy 600 does not crack at 290°C in a deaerated 40 wt.% boric acid solution that contains 50 ppm chlorides. However, addition of 300 ppb oxygen in the presence of chloride can cause rapid cracking.<sup>109</sup> In simulated primary water (1000 ppm boron + 2 ppm lithium), the presence of oxygen alone is not detrimental in the absence of chlorides. Only the simultaneous presence of oxygen and chlorides causes cracking over the range of pH from 3 to 8.<sup>109</sup>

In 1981, widespread tube cracking was noticed on the primary coolant side of each of the two OTSGs of the Three Mile Island Unit 1 power plant. It was hypothesized that sulfur-bearing compounds, such as sulfuric acid and sodium thiosulfate (used in building containment spray) leaked into the primary system from time to time. The concentration of sulfur in the aqueous phase was estimated to be  $\approx 0.7$  ppm and boric acid was  $\approx 1.3\%$ . In a study at BNL to investigate the role of sensitization in the SCC of Alloy 600 steam generator tubes in dilute sulfur environment, it was noticed that U-bends of Alloy 600 material that was directly sensitized by the mill-annealed condition did not crack in sodium thiosulfate solutions (up to 0.1 M concentration and 80°C), but cracked readily in sodium tetrathionate.<sup>130</sup> However, specimens that were solution-annealed before sensitization (SAS) cracked in both environments.<sup>131</sup> The relationships between the time to throughwall cracking of SAS U-bend material and the log of the concentration of thiosulfate ( $\text{Na}_2\text{S}_2\text{O}_3$ ) and tetrathionate ( $\text{Na}_2\text{S}_4\text{O}_6$ ) in an air-saturated environment at room temperature are shown in Fig. 13a.<sup>56</sup> Clearly, cracking is very rapid, even at ppm concentration levels of thiosulfate and tetrathionate. Data on failure times for constant-load tests on SAS tensile specimens in dilute thiosulfate solution are shown in Fig. 13b,<sup>130</sup> which displays an apparent threshold stress of about  $\approx 207$  MPa (yield stress = 210 MPa). The mill-annealed material (without sensitization treatment, yield stress = 310 MPa), not shown in Fig. 13, was immune to cracking in both solutions.

### 3.3.2 Secondary water IGA/IGSCC/ODSCC

Secondary side SCC of steam generator tubing occurs mainly in zones where local boiling of feedwater in crevices can concentrate (concentration factors may reach as high as  $10^8$ ) liquid corrosives to a level limited only by the available superheat: tube/TSPs and tube/TS crevices and sludge pile regions. During operation of a steam generator, sludge (metal oxides) may accumulate in the annulus between the tube and TS and in the tube/TSP crevices. Determining the exact chemistry in these zones is still a subject of active research. However, sludge appears to be very important to the IGSCC/IGA mechanisms; it plays the dual role of controlling the ECP and forming restricted regions in crevices and in sludge piles where alkaline species can concentrate. Laboratory studies show that copper-bearing sludges that are oxidizing promote IGSCC, whereas sludges that are less oxidizing or inert, e.g.,  $\text{Cr}_2\text{O}_3$ , promote IGA.<sup>132</sup> Magnetite itself has no significant effect on IGA of Alloy 600 in caustic solution at high temperature, although impurities in magnetite, such as sulfate, may promote IGA.<sup>72</sup> Sludge also facilitates the concentration of contaminants. Restricted flow areas may be created as a result of sludge accumulation on the TTS. A sludge pile height of 1 cm (0.4 in.) or greater may permit sufficient available superheat to allow concentration of contaminants.<sup>133</sup>

The main sources of water impurities in the secondary side of steam generators are condenser in-leakages, resin particles or regenerants released by condensate polishers, corrosion products of secondary circuit and, possibly, chemicals used to condition the secondary water, e.g., hydrazine, morpholine or ammonia. In particular, it is now well established that plants with copper alloy condensers, which may release copper, zinc, arsenic, and lead into secondary water, are more prone to IGA/IGSCC than plants with titanium or stainless steel condensers. Various contaminants have been found in the crevice regions and the composition of the causative solutions is not unique but may consist of a complex mixture of alkaline materials, such as NaOH, KOH, Na<sub>2</sub>CO<sub>3</sub>, NaHCO<sub>3</sub>, Na<sub>2</sub>SO<sub>4</sub>, Na<sub>2</sub>PO<sub>4</sub>, Na<sub>2</sub>HPO<sub>4</sub>, and Na<sub>2</sub>O•SiO<sub>2</sub>. It is thought that these compounds, either individually or in combination, can cause IGSCC and that many chemical pathways can lead to the alkaline condition necessary for promoting IGSCC/IGA. The field observations of IGSCC/IGA in crevices have been replicated in the laboratory with single-tube model boilers.<sup>132</sup>

The chemical impurities generally cited as concentrating in superheated crevices are sodium (and to a lesser extent potassium), which leads to strongly caustic occluded solutions or, less frequently, chloride and sulfate, which lead to strongly acidic occluded solutions. The pH of concentrated crevice solutions has been estimated to range from highly basic (alkaline) if the bulk water cation/anion ratio is high, to slightly acidic if the cation/anion ratio is low.<sup>85</sup> A large body of experimental data shows that Alloy 600 is susceptible to IGA/IGSCC in these media; most of the data pertain to pH values >10 or <5 at 300°C. Sulfur compounds are known to enhance caustic cracking whereas thermal decomposition of ion exchange resins leads to aggressive acidic media. Only lead reproducibly provokes IGA/IGSCC in Alloy 600 over the entire pH range between 3 and 11. Although many PWR steam generator systems may have been damaged by hideout of such aggressive solutions, recent studies that involve analyses of surface deposits on pulled tubes from plants have shown the presence of species, e.g., silica, silicates, and alumino-silicates, that cannot be stable in very caustic or very acidic environments.<sup>75</sup> In fact, several recent studies of deposits from pulled tubes have led to the conclusion that the local crevice environment that leads to IGA/IGSCC can range from slightly acidic/near neutral<sup>134</sup> to slightly alkaline/near neutral.<sup>135,136</sup>

The chemistry of the corrosion products on the fracture surface and the OD surface of Alloy 600 steam generator tubes provides clues to the local environment in the crevice or free-span regions from which the tube sections are removed. As the pH and oxidizing conditions of the aqueous environment change, various corrosion products become thermodynamically stable. Surface analysis techniques, such as AES and X-ray photoelectron spectroscopy (XPS), combined with ion beam sputtering have been used to give the in-depth composition profiles of these films.<sup>137</sup> Reference films were formed in the laboratory by exposing samples to solutions and temperatures that are typical of those found in PWR steam generator crevices. Surface analysis techniques applied to these films showed a correlation between percent chromium in the films, relative to all alloy metals, and the pH at temperature.

The film composition methodology was also used by Lumsden et al.<sup>137</sup> to examine tubes from eleven plants. Most of the tubes were from TTS and TSP crevices and

contained regions of IGA/IGSCC. The results from three plants (Point Beach, Trojan, and Catawba) gave the most convincing evidence that the IGA/IGSCC occurred under highly alkaline or caustic conditions. The chromium concentrations from the fracture surfaces of other plants suggested alkaline to highly alkaline conditions. Tubes removed from a French plant, Saint Laurent, contained the most chromium, which suggested a mildly alkaline crevice chemistry.

To gain an insight into crevice chemistry, Lancha et al.<sup>138</sup> used AES to analyze the surface chemistry of a degraded pulled tube and compared it with surface analysis results from laboratory reference samples in caustic and acidic solutions. In the pulled tube from the ASCO Unit 2 reactor that showed OD circumferential cracking at the TTS and axial ODS/IGA at TSP's, there were sometimes clear differences in the composition of deposits on the outer surface of the tubes and in the fracture surface of the IGSCC cracks. For example, in TSP's 2 and 8, analysis of the outer surface indicated a high concentration of iron, depletion of nickel, and chromium enrichment. On the other hand, analysis of the intergranular fracture surface at TSP 12 showed the opposite, i.e., no high concentration of iron, nickel enrichment, and chromium depletion.

To understand this difference in behavior, Lancha et al.<sup>137</sup> compared the results from the pulled tube with surface analysis results on laboratory reference samples in caustic (10% NaOH, 500h) and acid solutions (0.75M Na<sub>2</sub>SO<sub>4</sub> + 0.25M FeSO<sub>4</sub>, 250h) with and without the addition of CuO and PbO. All of the results from the outer surfaces of samples tested in caustic solution showed no iron enrichment, nickel enrichment and chromium depletion, with even stronger enrichment of nickel and depletion of chromium when copper was added, and much smaller changes when lead was added. All of the results from the oxide scales on fracture surfaces also showed no iron enrichment, nickel enrichment and chromium depletion, regardless of whether or not copper or lead was added. In contrast, all of the outer-surface analysis results of samples tested in an acid environment (with or without PbO) showed iron enrichment, nickel depletion, and chromium enrichment. Based on their results, they concluded that the outer-surface environment at the degraded region of the pulled tube was acidic while, within the crack, the environment was caustic.

Björnkvist et al.<sup>139</sup> conducted SEM/energy dispersive spectroscopy (EDS) characterization of TSP crevice deposits and AES with depth profiling to reveal the OD oxide film on pulled steam generator tubes from Ringhals 3. The AES analyses showed an outer oxide depleted of chromium and enriched in iron (Fe<sub>3</sub>O<sub>4</sub>) and nickel. A 1-2- $\mu$ m-thick chromium-enriched oxide was found below the magnetite. Chromium-rich oxides were also found in the free-span region. For comparison, reference samples were tested in an autoclave with both an alkaline (pH<sub>320°C</sub> = 9.9) and an acidic (pH<sub>320°C</sub> = 4.3) solution that contained sodium, chloride, and sulfate. The typical chromium profile seen on the pulled tube samples was also found on the laboratory samples that were exposed to an alkaline environment. From this observation, it was concluded that the TSP crevice chemistry was alkaline (the exact pH was not determined). The local crevice chemistry agreed with that predicted by the MULTEQ code when hide-out return data (pH<sub>320°C</sub> = 10) were used.

It is emphasized that not all SCC in the secondary side is related to crevice corrosion. Incidences of OD-initiated SCC unrelated to crevice corrosion have been observed near the upper TS of an OTSG.<sup>19</sup> Secondary-side cracking has also been observed along scratches or lines of abrasion in free spans (e.g., SGs in McGuire and Farley) and in the superheated steam space of an OTSG (at Ocone) where chemical concentration is unlikely.

By far, the effect of caustics on IGSCC of Alloy 600 have been studied most extensively.<sup>17,23-25</sup> It has long been known that NaOH can enter the secondary side from three sources: decomposition of sodium carbonate as in the case of river water in-leakage through the condenser; decomposition of sodium phosphates by precipitation of a phosphate that is less rich in sodium, or by reaction of these phosphates with iron oxides; and when condensate polishing is used, it can be released by the resins. As mentioned earlier, although the concentration of caustics in the bulk water is low, it can be significantly increased in crevices by local boiling. In laboratory tests, IGSCC has been observed in NaOH solutions at concentrations above 1% by weight. Figure 14 shows average IGA rate as a function of caustic concentration and temperature for solutions that range from 5 to 50% NaOH + KOH.<sup>140</sup> From 1 to 10%, the rate of IGSCC increases, but above 10%, it remains relatively constant. Addition of 1% carbonates (calcium, sodium, and potassium) to 10-50% caustic solutions at 600°F led to enhanced IGA rates, whereas addition of 10% carbonates led to reduced IGA rates. Addition of 10% CaCO<sub>3</sub> to a 10% caustic solution led to no detectable rate of IGA in 270 days.<sup>140</sup>

Several studies in which C-ring tests were used to investigate IGA and IGSCC of Alloy 600 in acidic sulfate and chloride solutions have been undertaken by EPRI.<sup>110,141-143</sup> The results showed that in solutions with high sulfate (with or without chloride), IGA occurred quite uniformly and extensively at strain levels from 0.3 to 4%, and, although much nucleation of IGSCC was observed, the amount of wastage overwhelmed CGR and IGSCC initiation did not occur. However, some tests at pH<sub>315°C</sub> < 4.0 did show IGSCC. The amount of wastage at free corrosion potential generally increased with increasing proportion of sulfate ions and decreasing pH. As the sulfates were replaced by chlorides, the amount of wastage decreased for the same pH. The amount of wastage observed in acid sulfate solutions far exceeded that observed in pulled steam generator hot-leg tubes, a finding that led to the conclusion that crevice chemistry cannot be typified as high in sulfate. Chloride-based solutions that contained small amounts of or no sulfates produced more realistic amounts of wastage.

High-nickel austenitic alloys, like Alloy 600, are immune to SCC, as determined from standard boiling magnesium chloride tests. Numerous studies have shown that the resistance of Alloy 600 to SCC in chloride-containing media at low temperatures (<200°C) is good. However, tests have shown that Alloy 600 can exhibit cracking at high temperatures in pure water, where the accelerating effect of chloride ions increases with increasing oxygen content.<sup>109</sup> Boric acid and chlorides may concentrate to aggressive levels in steam generator crevices when they are at normal levels (10 ppm boric acid and 5 ppb chloride) in the bulk water.

Lead has recently been identified as a possible contaminant that causes mixed intergranular/transgranular cracking and IGA in steam generator tubes that have been removed from service in the U.S. (St. Lucie Unit 1),<sup>86</sup> Canada (Bruce A NGS),<sup>144</sup> and France (Bugey 3 and Dampierre 2).<sup>145</sup> In the case of St. Lucie Unit 1, the cracking location at a TTS junction was considered highly acidic because of seawater intrusion. Thus, the role of lead in promoting cracking was considered secondary, because the acidic sulfate environment by itself was considered sufficient to cause IGSCC. However, because of the presence of the transgranular SCC (TGSCC) component in the cracking, lead was considered to have contributed to the cracking process.

Potential sources for lead contamination in the secondary side include lead wires that are used for measuring turbine rotor-stator gap, lead mallets that are used in maintenance operations, and biological shields. The fact that lead contamination in near-neutral water can lead to SCC in steam generator tubes has been known for a long time.<sup>21</sup> Lead concentration of 100 ppm can cause SCC susceptibility in slow strain rate tensile (SSRT) tests of mill-annealed Alloy 600 (MA) in NaOH solution of pH 10 at 340°C.<sup>146</sup> The threshold concentration of dissolved lead for lead-induced corrosion in mill-annealed, thermally treated Alloy 600 was reported to be 0.1 ppm in AVT water.<sup>147</sup> Susceptibility of mill-annealed, thermally treated Alloy 600 to IGA in a caustic environment that contained lead was reported by Castano-Marin et al.,<sup>147</sup> who also found that mill-annealed, thermally treated Alloy 600 is more susceptible to cracking in AVT water with lead than in a caustic environment with the same concentration of lead.

Titanium and cerium inhibitors have proved ineffective for controlling this type of corrosion. Removing the source of dissolved lead was found to be the most effective remedy for cracking, even when lead remained within the simulated tube deposits.<sup>149</sup> Alloy 600 has also been observed to be susceptible to cracking in lead-contaminated acidic solutions.<sup>150</sup>

Recently, some contradictory claims have been made about the effect of silica deposits on ODSCC. Investigations of pulled tubes from French plants have showed that IGA and IGSCC generally occur under deposits of silica compounds (aluminosilicate).<sup>151</sup> It was concluded that these deposits contribute to the formation of nonprotective chromium-rich layer in the oxide film. On the other hand, Baum et al.<sup>152</sup> have noted that some plants with higher silica concentrations have experienced less ODSCC. Based on their limited study that correlated chemistry variables and ODSCC, Baum et al.<sup>152</sup> have suggested that plants should place more emphasis on maintaining a minimum silica concentration rather than maintaining a sodium-to-chloride molar ratio alone.

To mitigate SCC, inhibitors are being investigated for use in the secondary side. Boric acid was originally added to reduce denting.<sup>153</sup> However, laboratory evidence suggested that it is also an effective inhibitor for IGA/IGSCC; being more effective in TSP crevices than in deeper TS crevices.<sup>154</sup> It appears that, in addition to reducing pH, boric acid prevented IGA by incorporation of boron in the surface film (oxide borate).<sup>155</sup> Miglin and Paine<sup>156</sup> reported a beneficial effect of the addition of 2 g/L of TiO<sub>2</sub> to a 10% NaOH solution at 320°C. They speculated that the addition of TiO<sub>2</sub> helped form a more protective surface oxide film.

### 3.4 Temperature

Gorman et al.<sup>157</sup> analyzed degradation data from operating steam generators for three categories of degradation: PWSCC at standard roll transitions, IGA/SCC at TSPs or eggcrate supports (secondary side initiation), and IGA/SCC for all hot-leg locations, including tube supports, TS, and sludge pile crevice areas (secondary side initiation). Because of the lack of sufficient data they were unable to conclude definitively the effect of temperature on degradation of HTMA Alloy 600. However, the data for LTMA material indicated that the tendency toward increased levels of degradation increased with increasing hot leg temperature for both primary and secondary side corrosion. Correlations of rate of cracking with plant operating temperature and the differences in corrosion rates among various locations in the same plant are both consistent with a strong temperature dependence. However, several cases have been noted where cracking has occurred much more quickly at OD cold-leg locations (cold-leg TTS cracking) than to hot-leg cracking that is expected from the activation energy models. The usual explanation is that the environment is more severe (possibly acidic) in the cold leg.

#### 3.4.1 Primary water IGSCC/PWSCC

PWSCC cracking in Alloy 600 is strongly dependent on temperature. Gorman et al.<sup>157</sup> collected PWSCC tube degradation data from operating steam generators and concluded that degradation of LTMA tubes increases with increasing hot-leg temperature, in accordance with an Arrhenius type relationship and an apparent activation energy of 45-50 kcal/mole (190-210 kJ/mole). The PWSCC behavior of LTMA tubing (made by Huntington) of older plants did not show a strong temperature dependence and was not consistent with an activation energy model. Gorman et al.<sup>157</sup> ascribed this lack of temperature dependence on less precise inspection practices and different rolling practices used in earlier times. Also, the amounts of PWSCC in these plants was small when compared with secondary side IGA/SCC in the TS crevices that attracted most of the attention.

Laboratory data have shown that increasing temperature increases the susceptibility of mill-annealed Alloy 600 tubes to PWSCC. Van Rooyen et al.<sup>45-47</sup> initially reported that, in pure water at 325 and 365°C, the activation energy for crack initiation increased linearly with carbon content; from 30 kcal/mole (125 kJ/mole) at 0.01% carbon to 70 kcal/mole (290 kJ/mole) at 0.06% carbon. However, later, based on more data, the activation energy was revised to 50 kcal/mole (210 kJ/mole) for all heats, independent of carbon content.\* The revised value of activation energy agrees with that reported by Webb,<sup>41</sup> who derived it from a larger data base on split-tube U-bend and C-ring tests on LTMA Alloy 600 tubes. Available activation data on crack initiation have been summarized by McIlree et al.<sup>158</sup> and are plotted in Fig. 15a. A value of 43-44 kcal/mole (180-184 kJ/mole) is sometimes used as an average value, which implies an increase in life by a factor of  $\approx 2$  for every 10°C reduction in

---

\*U. C. Kim and D. Van Rooyen, *The stress corrosion cracking of Inconel 600 steam generator tubing in primary water and related conditions*, unpublished paper, Brookhaven National Laboratory (1985).

temperature. As pointed out by Garud and McIlree,<sup>159</sup> the observed range of the apparent activation energy is so wide that there is no clear way to associate the reported activation energy with any specific rate-controlling process. They suggest that the apparent activation energy represents some average value that reflects the integrated effect of several mechanisms operating simultaneously.

The apparent activation energy includes the initiation and slow propagation stages of SCC. A limited number of studies<sup>32,48,52,56,62</sup> have addressed the effect of temperature on crack propagation rates in mill annealed Alloy 600.

Assuming that crack propagation in CERTs between 290 and 365°C starts at yield stress, Bulischeck and van Rooyen<sup>46</sup> reported an activation energy of 43 kcal/mole (180 kJ/mole) for crack propagation. Later, on the basis of a more accurate metallographic estimation of crack initiation in the CERT on flattened tensile specimens, they<sup>47</sup> revised the activation energy down to 32 kcal/mole (134 kJ/mole). The lowering of the activation energy highlighted the importance of separating crack initiation and crack propagation phases. Crack propagation data have also been summarized by EDF<sup>10</sup> and are plotted in Fig. 15b. Although there is a large scatter, the data obtained by RUB, CERT, and C-ring tests are not inconsistent with each other. The activation energy for crack propagation is  $\approx$ 25-30 kcal/mole (110-125 kJ/mole).

Fracture mechanics tubular specimens (bending type for CGRs in simulated primary water) have been developed by Cassagne and Gelpi.<sup>74,160</sup> Crack growth data at various temperatures have been generated for midwall  $K_I$ , varying between 20 and 30 MPa $\sqrt{m}$  for as-received and 5% cold worked tubes.<sup>160</sup> The results, plotted in Fig. 16, show that, although the CGRs in 5% cold-worked specimens are an order of magnitude higher than those in as-received material, the activation energies for crack propagation are comparable, 20 kcal/mole (84 kJ/mole) for the as-received material and 28 kcal/mole (117 kJ/mole) for the 5% cold worked material.

### 3.4.2 Secondary water IGA/IGSCC/ODSCC

Gorman et al.<sup>157</sup> also reported that the apparent activation energy for IGA/SCC at TSPs in plants with LTMA tubing ranged from 43 to 73 kcal/mole (180-300 kJ/mole). However, the scatter in the data was significant, indicating that temperature was only one of many variables that affected IGA/SCC at TSPs. Very little IGA/SCC at TSPs was reported for plants with hot leg temperatures  $\leq$ 316°C. The activation energy for hot-leg IGA/SCC in plants with LTMA tubing varied between 22 and 60 kcal/mole (90 and 250 kJ/mole). As with the TSP data, the hot-leg data also showed a large scatter.

In laboratory tests, both IGA and IGSCC of Alloy 600 in caustic solutions have been found to be dependent on temperature;<sup>17</sup> Fig. 17 shows a plot of the IGA and IGSCC depth of attack as functions of temperature. Increasing the temperature above 300°C substantially accelerates intergranular corrosion. It is apparent that, at the same stress, IGSCC propagation rate is  $\approx$ 10 times faster than IGA propagation rate. Figure 18 shows the activation energy for IGA in 10% NaOH solution when the tube surfaces are held in compression.<sup>161</sup> The activation energy is 18 kcal/mole (75 kJ/mole), which is of the same order as other determinations, although higher

values, 19-46 kcal/mole (80-190 kJ/mole), have been reported, depending on test conditions.<sup>33</sup> On the basis of tests in a 25% NaOH, deaerated solution that contained magnetite, Malagola<sup>162</sup> reported an activation energy value of 31 kcal/mole (130 kJ/mole) for IGA. Connor et al.<sup>140</sup> reported a value of 40.8 kcal/mole (170 kJ/mole) for tests in 20% NaOH + 5% KOH solution at 600 and 650°F. The values of the activation energy for IGA are of the same order as those for IGSCC in dilute solutions, suggesting that the same mechanisms may operate in both cases.

Determination of rate of attack is difficult because of the variability of initiation times, test conditions, ID and OD surface conditions, heat-to-heat variation, etc. In an EPRI report<sup>163</sup> Bandy reported results from a series of capsule tests with caustic and sodium sulfate at 315°C (600°F). The depth of attack was found to be linear with time up to 6 months, but the depth of attack was more dependent on the square root of time in tests to one year, as shown in Fig. 19. Miglin reported a similar relationship in an EPRI report,<sup>164</sup> even though his corrosion rates were half of Bandy's, in 6000 h tests, in greater than 50% caustic at 343°C (650°F) (Fig. 19). The activation energy for average IGSCC CGR (assuming zero initiation time) of mill-annealed Alloy 600 in 10% NaOH was reported by Jacko<sup>107</sup> to be 25 kcal/mole (105 kJ/mole).

Sarver<sup>165</sup> conducted tests on C-rings of Alloy 600 that had been subjected to differing thermal processing in solutions that contained various concentrations of lead at 288 and 360°C. Very severe cracking was observed at 360°C and very little cracking was observed at 288°C. Because the calculated pH values and calculated lead species were similar at the two temperatures, the cracking severity was attributed to temperature. Helie et al.<sup>166</sup> performed CERTs on mill-annealed Alloy 600 tubing in water contaminated with lead oxide, and reported an activation energy of 30 kcal/mole (125 kJ/mole) in both primary and lead-contaminated water. However, the CGR was an order of magnitude higher in lead-contaminated water than in primary water.

### 3.5 Stress and Strain Rate

The presence of stress is always necessary for SCC to occur. However, with a susceptible microstructure in an aggressive environment, the application of stress seems to be a necessary but not a sufficient condition to obtain SCC in Alloy 600. It appears that a precise combination of stress, strain, and strain rate is needed. It is difficult to study the effect of strain rate on SCC by using constant-deformation tests, such as RUB, C-rings, WOL specimens, etc., or constant-load tests. On the other hand, CERTs can be used very effectively to study the effects of strain rate on the initiation of SCC.

For specimens with cracks loaded in Mode I, if CGR in the environment is plotted against the stress intensity factor  $K_I$ , three distinct regions are observed. In Regions I and III, the CGR is strongly dependent on  $K_I$ . In Region II, the crack growth rate is more or less independent of  $K_I$ . In Region I, there is a threshold stress intensity factor  $K_{I,SCC}$  below which crack growth should not be observed. However, because CGRs are small in Region I, it is difficult to establish  $K_{I,SCC}$  with certainty. Crack growth rate is generally reported as a power function of  $K_I$

$$\text{CGR} = \frac{da}{dt} = AK_I^n \quad (1)$$

where  $a$  is the crack length,  $t$  is time,  $A$  is a coefficient, and  $n$  ( $>0$ ) is an exponent.

### 3.5.1 Primary water IGSCC/PWSCC

Tensile stresses close to yield strength are necessary to cause PWSCC of Alloy 600.<sup>48</sup> Field experience may be the best evidence that the threshold stress for PWSCC initiation and growth is very close to yield. PWSCC in operating steam generators is only observed at locations where tubes have been deformed nonuniformly, giving rise to residual stresses that are close to the flow stress. These locations include expansion transitions, U-bends, and dents where the local constraints prevent the relaxation of stresses that produce the nonuniform deformation. Very few incidents of PWSCC are reported in uniformly expanded tubes in the TS except at anomalies such as roll overlaps. An exception is the case of a WEXTEx explosively expanded tube where the expansion apparently did not provide a tight joint and cracks occurred in the tube, 50-75 mm (2-3 in.) below the transition.\* In Europe, where tubes with throughwall cracks at roll transitions are often left in service, cracks generally do not grow beyond the boundaries of the transition where the residual stresses are reduced.

For stresses above yield, constant-load data on tensile specimens from BNL<sup>48</sup> showed that the time to crack initiation is inversely proportional to approximately the fourth power of stress ( $\sigma^{-4.3}$ ), as shown in Fig. 20. Because of lack of data at stresses below yield, no threshold stress for crack initiation was established. Note that the crack initiation time for cold-worked (flattened,  $\approx 1-3\%$  cold-worked) material is a factor of 3-4 less than that for as-received mill-annealed material.

A much higher stress exponent ( $\sigma^{-5.7}$ ) was observed in tests at Westinghouse,<sup>41</sup> where true stresses, as calculated from strains measured by photogrid on the split-tube U-bend specimens and by strain gages on the C-ring specimens were used for data correlation (Fig. 21). The exponent would have been even larger if engineering stress rather than true stress were used. The crack initiation lives at 360°C in Fig. 21 are approximately an order of magnitude greater than those in Fig. 20, even though the reported room-temperature yield strengths of the two tubes are 323 MPa for the BNL material (0.01 carbon) and 340 MPa for the Westinghouse material (0.04 carbon). Two factors may have contributed toward this observed difference. First, the BNL tests were run on uniaxial tensile specimens (CERT) under load control (i.e., true stress increasing with specimen deformation), whereas the Westinghouse tests were conducted by bend tests (U-bend and C-ring) under displacement control (i.e., true stress decreasing with cracking and creep deformation). Second, in plotting the Westinghouse data of Fig. 21, relaxation of initial stresses during the tests was ignored.

---

\* A. P. L. Turner, Dominion Engineering, Inc., personal communication, 1998.

Crack initiation tests at lower than yield were conducted at B & W<sup>167</sup> with U-bend tests; the results are plotted in Fig. 22. For the mill annealed material, a threshold of  $\approx 55\%$  yield stress at room temperature is indicated. Note that a thermal treatment of 2 h at 600°C increases the crack initiation life by a factor of 2-3. Enough data are not available to indicate if there is any increase in threshold stress when compared with the mill-annealed material.

The effect of strain rate on crack initiation by CERTs was reported by Bulishek and Van Rooyen,<sup>46</sup> who found that, at 325°C, the total strain to failure decreased from 45 to 13% when the strain rate was decreased from  $2.9 \times 10^{-7}/s$  to  $3.9 \times 10^{-8}/s$ . They established that, although the crack depths, dependent on the exposure times, varied significantly, the average CGRs were nearly identical. A similar lack of effect of strain rate on average CGR was also reported by Bandy and van Rooyen.<sup>48</sup> Based on measurement of percent area of SCC at various temperatures and strain rates, Kim and van Rooyen<sup>51</sup> proposed a smooth curve (Fig. 23) that plots limiting strain rate, above which SCC would not occur as a function of temperature in the 300-365°C range.

Gras<sup>10</sup> reported that Alloy 600 exhibited creep deformation in argon at 360°C, with an enhancement of creep rate when exposed to primary water. The presence of grain boundary sliding in mill-annealed and thermally-treated Alloy 600 specimens led Gras to propose that intergranular cracking should be explained in terms of intergranular strain rate (due to grain boundary sliding) and not the macroscopic strain rate.

The relative importance of strain rate and stress for SCC initiation was investigated by Boursier et al.,<sup>168</sup> with two series of tests. In the first series of tests, the specimen was loaded rapidly to a stress above yield in argon, unloaded to zero stress, soaked in primary water for 200 h, and then reloaded rapidly to the first stress level, after which it was subjected to the CERT at  $5 \times 10^{-8}/s$  for 300 h. Specimens with final stresses of 510 and 850 MPa exhibited average crack depths of 30 and 15  $\mu m$ , respectively. In the second series of tests, the specimens were subjected to a constant-load test (850 MPa) for 300 h after a 200 h immersion in primary water. Under these conditions, the creep rate of the alloy was  $\approx 10^{-10}/s$ , and no significant cracking ( $< 2 \mu m$ ) was observed, thus suggesting that strain rate was more important than stress for crack initiation. Using data from five heats of mill-annealed Alloy 600 tubing, Boursier et al.<sup>168</sup> were able to correlate low resistance to SCC with high creep rate and high resistance to SCC with low creep rate. However, a sixth heat, whose creep rate was low, exhibited high SCC. Furthermore, a high-creep-rate (low-resistance-to-SCC) heat, when thermally treated at 700°C for 16 h, retained its high creep rate behavior but developed good resistance to SCC. To explain this lack of correlation of creep rate with SCC, Boursier et al.,<sup>168</sup> made some limited measurements of grain boundary sliding to show that the most susceptible heat had the greatest sliding at the grain boundaries. More data are needed to confirm this observation.

A significant data base on CGR in pure and simulated primary water environments exists for specimens made of Alloy 600 tubing. However, it is difficult to compare data from one laboratory with those from another because small differences in temperature, amount of gaseous hydrogen  $H_2$ , heat treatment, or cold work can cause large discrepancies in CGRs. Szklarska-Smialowska and Rebak<sup>169</sup> have recently collected a

significant body of data (Fig. 24) to show that, in the range 20-40 MPa $\sqrt{m}$ , data scatter is of two orders of magnitude. The overall crack growth data (in  $\mu\text{m}/\text{h}$ ) in a simulated primary water environment was fitted (solid line in Fig. 24) with a correlation factor of 67% to the following equation:

$$\frac{da}{dt} = 1.2348 \times 10^{-3} [K_I]^{1.83} \quad (2)$$

with a threshold  $K_{I\text{SCC}} \approx 10 \text{ MPa}\sqrt{m}$ .

Crack growth data obtained from fracture mechanics-type specimens made from as-hot-rolled Alloy 600 plates are more scarce than data from specimens made from tubes. Foster et al.<sup>170</sup> reported crack growth data in simulated primary water at 300 and 310°C compact-tension (1/2T compact tension) specimens. Their data (denoted by open and filled diamonds) fall within the scatter band of Fig. 24, indicating that crack growth data from tubes and plates in primary water do not differ significantly.

### 3.5.2 Secondary water IGA/IGSCC/ODSCC

Field experience shows that cracks formed in tubes at TSP crevices generally do not grow above or below the TSP. This observation indicates that an aggressive environment can lower the threshold stress for crack initiation substantially below the yield (nominal stress due to pressure and temperature gradient is 10-15 ksi), but that, in the bulk secondary environment, high stresses are needed to sustain crack growth.

Intergranular stress corrosion cracking and IGA are the two most common types of failure of Alloy 600 in caustic environments. In short-term laboratory tests with stressed specimens in caustic environments, both IGSCC and IGA have been observed. But one generally observes more extensive IGSCC and less extensive IGA in the laboratory than in tubing removed from the field. Of the two, IGA is less dependent on stress and has been observed to occur under zero, or even compressive, surface stress conditions.

Crack initiation in 10% NaOH solution was investigated at B & W<sup>167</sup> by using U-bend tests; the results at 289°C are plotted in Fig. 25a. A comparison of Fig. 25a with Fig. 22 shows that initiation time is reduced by a factor of 500 when compared with that in pure water. Note that, as in pure water, a thermal treatment of 2 h at 600°C increases the crack initiation life in 10% NaOH by a factor of 2-3. For both the mill-annealed and thermally treated materials, a threshold of  $\approx 40\%$  yield stress at room temperature is indicated, although more data are needed to verify this.

Pressurized tube tests in 10% NaOH solution at 315°C were conducted at Westinghouse<sup>171</sup> and the results are plotted in Fig. 25b. There appears to be a threshold stress for cracking at  $\approx 20\%$  room-temperature yield strength. Results from 2000-h C-ring tests in 10% NaOH at 315°C were also reported by Airey;<sup>36</sup> they are shown in Fig. 26. Note that although there is a large scatter in the data, a threshold stress is evident. For the mill-annealed material, this stress is  $\approx 50\%$  of yield strength

(which is higher than that observed in pressurized-tube tests, Fig. 25b) and, for the thermally treated material, it is >150% of yield strength.

The French at EDF have observed relatively high threshold stresses for crack initiation in tests on pulled mill-annealed tubes in 10% NaOH solution.<sup>108</sup> Although they have found many low-carbon heats of Alloy 600 with poor IGSCC resistance, no perfect correlation was found between carbon content alone and IGSCC. A better correlation was found between the threshold stress for IGSCC and yield stress of the mill-annealed material at 350°C (Fig. 8). For example, the pulled tubes from Saint-Laurent B1, with low yield stress (220-230 MPa) at 350°C, have shown a high susceptibility to IGSCC ( $\sigma_{th} < 170$  MPa). This negative correlation between yield strength and IGSCC resistance is surprising, because the opposite is observed for PWSCC. However, this negative correlation apparently holds only for certain manufacturers and not for all, thus raising the possibility that the manufacturing process itself might have an important bearing on the susceptibility of Alloy 600 to IGSCC. However, as in the U.S., the French have also observed a slight increase in the threshold stress for IGSCC in thermally treated material when compared with mill-annealed material. Based on extensive tests on pulled tubes, the following threshold values for IGSCC of Alloy 600 tubes in 10% NaOH solution have been proposed by EDF:<sup>108</sup>

Table 1. *Threshold stress, normalized by yield stress, for crack initiation in Alloy 600 tubes in 10% NaOH solution.*<sup>108</sup>

Thermal treatment	320°C	350°C
Mill-annealed	0.8	0.7
Thermally-treated at 700°C	1.0	0.9

C-ring tests in solutions with various concentrations of NaOH at 350°C were conducted at EDF<sup>65</sup> on as received Alloy 600 tubes that were stressed nominally to yield stress (actual stress estimated to be 80% yield stress because of stress relaxation). The data showed a large scatter and the minimum times to initiate a 500- $\mu$ m ( $\approx$ 40% of wall thickness) crack that was deduced from the data are shown in Fig. 27. Note that the resistance to IGSCC of thermally treated material (16 h at 700°C) is superior to that of mill-annealed material, and that a saturation effect is present for both materials with increasing NaOH concentration.

Although the relatively rapid crack initiation in caustic solution, when compared with that in pure water, may suggest that crack propagation should play a more important role in caustic SCC life than in PWSCC life, this is not supported by field observation. Tubes that are shot peened after one fuel cycle continue to develop detectable cracks for several fuel cycles, even though peening before service has been

shown to be very effective in preventing PWSCC.\* This observation implies rapid initiation and slow growth. Therefore, crack growth correlations with a stress intensity factor or other crack driving force parameter would be useful for predicting failure by caustic SCC as well as PWSCC, but such data are scarce. Crack propagation rates have been measured in steam generator tubing by a side-stream model boiler.<sup>172,173</sup> Both chemically-induced and electro-discharge machined (EDM) notch + fatigue-induced part-throughwall precracked specimens have been tested with primary side and secondary side temperature and stresses of 320°C and 15.5 MPa, and 272°C and 5.7 MPa, respectively. The CGRs, estimated from posttest fractography, varied from 0.0017  $\mu\text{m}/\text{h}$  for 50% throughwall thickness precracks to 0.01  $\mu\text{m}/\text{h}$  for deeper precracks. Unfortunately, the stress intensity factors for the cracks were not reported.

Cassagne and Galpi<sup>160</sup> conducted crack growth tests on 5% cold worked Alloy 600 tubular fracture mechanics specimens in AVT-treated water with hydrogen at 360°C. Their results, which compare data from simulated primary and AVT-treated water (Fig. 28a) show that AVT-treated water is more aggressive than primary water for the same hydrogen partial pressure of 0.03 MPa. EDF<sup>65</sup> has obtained crack growth results with fatigue precracked WOL and double cantilevered bending (DCB) specimens (fabricated from Alloy 600 plate) in NaOH solutions of various dilute concentrations at 350°C. They have tested material that was both mill-annealed and thermally treated at 700°C for 16 h. The results in the form of CGR curves are presented in Fig. 28b.

Miglin et al.<sup>174</sup> reported results on the effects of stress on lead-assisted stress corrosion of precracked and smooth (unprecracked) Alloy 600 C-rings. They conducted tests at 23 and 90% of room temperature yield stress at 360°C, with the calculated pH value held constant at 4.5. At 23% of room-temperature yield stress, cracks grew in specimens with precracks and were initiated in smooth specimens. Similar effects of stress on cracking at 23% yield stress was reported by Server,<sup>165</sup> who observed significant cracking at 324°C and less cracking at 288°C. Stress dependency of Alloy 600 C-rings in lead-containing solutions was investigated by Sakai et al.<sup>175</sup> at 340°C. For the mill-annealed alloy, no stress dependency (20, 90, and 150% room-temperature yield stress) was observed in solutions with 3000 ppm lead (where mostly IGA was observed), but stress dependency (as prominent TGSCC) was observed at 300 ppm lead.

A CGR of 0.64  $\mu\text{m}/\text{h}$ , independent of strain rate (between  $5 \times 10^{-8}$  and  $10^{-6}/\text{s}$ ), was measured in CERTs of Alloy 600 tubes that were tested in deionized water with 1% PbO at 320°C.<sup>166</sup> Average CGRs of 0.20-0.43  $\mu\text{m}/\text{h}$ , depending on final crack depth and time, were observed in C-ring tests on mill-annealed Alloy 600 in AVT water with 0.01 M PbO at 320°C.<sup>148</sup> Average CGRs of 0.22-0.26  $\mu\text{m}/\text{h}$  were measured in 0.5%-strain C-ring tests of mill-annealed Alloy 600 tubes in AVT water with 0.1 M PbO at 320°C.<sup>150</sup> This CGR range agrees well with B&W results for C-ring specimens at 100% of room-temperature yield stress in AVT plus 0.01% PbO at the same temperature.<sup>176</sup> The CGRs of C-rings tested at 23% of room-temperature yield stress were an order of magnitude less.

---

\*A. P. L. Turner, Dominion Engineering, Inc., personal communication, 1998.

## 4 Models for IGA/IGSCC of Alloy 600

---

As we have seen, the cracking susceptibility (initiation and growth) of Alloy 600 in high-temperature primary and secondary water depends on internal metallurgical and external environmental factors. The internal metallurgical factors are:

- grain size (gs), cold work (CW) or plastic strain, and their effects on yield stress ( $\sigma_y$ ),
- thermal treatment (TT) and distribution of carbides, and
- grain boundary structure, microchemistry, and segregation (gb).

The external environmental factors are

- applied and residual stress ( $\sigma$ )/stress intensity factor ( $K_I$ ), strain ( $\epsilon$ ), and strain rate ( $\dot{\epsilon}$ ),
- temperature (T),
- solution pH, ECP, and surface oxide films,
- solution chemistry, impurities, and inhibitors (SC), and
- partial pressure of hydrogen ( $p_{H_2}$ ),

Thus, the SCC susceptibility can be written as a generalized function:

$$SCC = f(gs, CW, \sigma_y, TT, gb, \sigma, K_I, \epsilon, \dot{\epsilon}, T, pH, ECP, SC, p_{H_2}). \quad (3)$$

Several theories and mechanistic models have been proposed to explain the cracking susceptibility of Alloy 600 in high-temperature water. Of course, none of them even approximately explains how all of the factors in the above equation interact to cause IGSCC. Therefore, various empirical models have also been proposed.

### 4.1 Influence of Fundamental Variables on IGA/IGSCC

Before discussing the various mechanisms and models for IGA/IGSCC of Alloy 600, it is appropriate to review the effects of some of the more fundamental variables on IGA/IGSCC.

#### 4.1.1 Oxide films

The good performance of Alloy 600 in high-temperature, near-neutral water is primarily due to the protective chromium-rich oxide film that forms on the tube surface. All IGA/IGSCC ultimately boils down to the failure of the protective surface oxide film. In primary water, the film is composed of two layers: a chromium-rich inner  $M_3O_4$

spinel type layer that also contains nickel and iron, and an outer layer of precipitated oxide crystals.<sup>177</sup> The inner protective spinel layer is stable over a wide range of pH and its chromium content increases as the pH decreases.<sup>137</sup> Such a protective film is generally stable in environments in which PWSCC occurs. Therefore, to understand cracking due to IGA/IGSCC, one must understand how the protective effects of the oxide film can be breached either by mechanical (e.g., rupture) or by chemical/electrochemical means.  $\text{Cr}_2\text{O}_3$  is stable in mildly acidic solutions and dissolves in alkaline solutions. Thus, in alkaline solutions, the oxides that form (primarily nickel oxide and magnetite) are less protective.

The stable oxides that are formed on the Alloy 600 surface depend not only on pH but also on potential. Increasing the potential decreases the thickness and increases the Cr/Ni ratio of the chromium-rich oxide. At a potential that is close to the  $\text{H}_2/\text{H}_2\text{O}$  equilibrium in alkaline solution (pH = 10), the oxides are NiO and  $\text{NiFe}_2\text{O}_4$ , and chromium is dissolved. The solubility of NiO is minimal in neutral water (pH  $\approx$  6) and increases in both more acidic and more alkaline solutions. At lower potentials, chromium-containing oxides ( $\text{FeCr}_2\text{O}_4$ ) are also stable.<sup>139</sup> The resistance of Alloy 600 to IGSCC depends on the stability of the chromium-rich oxide. For example, chloride ions are not incorporated in chromium-rich oxides. On the other hand, in nickel-rich oxides formed at high pH, anions are incorporated, producing an increased number of film defects and an increased sensitivity to breakdown.

In general, the oxide film that forms on the surface of steam generator tubes in the field shows a variation in composition with depth. For example, measurements of oxide composition on pulled tubes from Ringhals 3 have shown that parts of the tube that were exposed to alkaline environment, such as the TSP crevice, produced an oxide that was depleted in chromium and enriched in iron and nickel in the outer layer; however, below the outer layer, at the TSP and in the free-span region, the oxide was enriched in chromium.<sup>139</sup>

Cayla et al.<sup>72</sup> and Combrade et al.<sup>73</sup> who have shown that IGA can be promoted in the presence of either sulfides or reducible sulfates in deaerated caustic environments, found no protective layer on the surface. In neutral solutions (boric acid plus LiOH) at the same redox potential that promoted caustic IGA, and with no added hydrogen, IGA was not observed in the presence of sulfides. Surface analysis showed a double layer with an inner chromium-rich oxide and an outer thick sulfide layer. From these observations, they concluded that the onset of IGA is correlated with the absence of a protective oxide film on the surface. Sulfides or reducible sulfates can inhibit the growth of this protective layer in caustic but not in neutral environments (recent Belgian work tends to refute the latter). However, even in the absence of a protective oxide layer, IGA only occurs in a specific range of potential. At a potential that is too high, general corrosion rather than IGA occurs. At a potential that is too low, IGA is not possible, probably because of the decrease of nickel solubility.

In conditions that lead to PWSCC or caustic IGSCC, the alloy surface is always covered by an oxide film, which in neutral environments is essentially  $\text{Cr}_2\text{O}_3$ . In a caustic environment, an inner thin layer of  $\text{Cr}_2\text{O}_3$  is covered by an outer layer of  $\text{Ni}(\text{OH})_2$  or NiO.<sup>178</sup> In deaerated caustic environments, NiO becomes the base of the

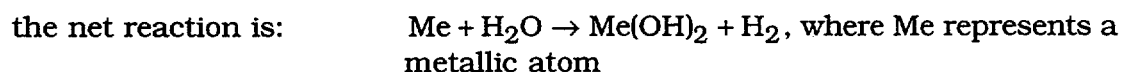
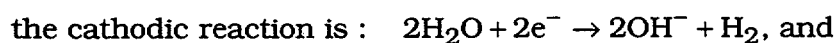
surface films (because of the high solubility of chromium and iron compounds) for potentials above +30/50 mV/RHE. In the absence of hydrogen addition, the free corrosion potential is  $\approx +40$  to  $+70$  mV/RHE, which is in the range of stable NiO. Hydrogen addition lowers the potential to the range of stable nickel, a finding that is consistent with the lack of a detectable surface oxide layer. In fact, Combrade et al.<sup>73</sup> argued that the presence of a surface oxide layer is necessary for IGSCC to occur because no IGSCC was observed in hydrogenated caustic environments.

#### 4.1.2 Hydrogen ion activity (pH) and potential

Information on pH and potentials is important because they control the surface oxide film composition, structure, and stability, all of which have an important bearing on the IGA/IGSCC resistance of the alloy. Potential and pH also influence the oxidation/dissolution rate of the underlying metal. Staehle<sup>178</sup> has identified five submodes of SCC of mill-annealed Alloy 600 and plotted them in a three-dimensional plot, with potential, pH, and threshold strength as coordinates. A simpler potential/pH diagram that shows the main areas where corrosion cracking of Alloy 600 is known to occur in aqueous environments at 300°C is presented in Fig. 29.

Few systematic data are available on the effect of solution pH on IGSCC of Alloy 600 in high-temperature water. The approximate pH values on the primary and secondary sides of PWR steam generator tubing during normal operation are 6-8 and 8.5-9.5, respectively. There is a big difference between the hydrogen concentrations on the two sides:  $\approx 3$  ppm in the primary side vs  $\approx 3$  ppb in the secondary side. In the absence of oxygen, hydrogen fugacity (partial pressure) fixes the redox potential, which for Alloy 600 is practically equivalent to the corrosion potential. Thus, for the same pH at 300°C, corrosion potentials are  $\approx 170$  mV more negative (cathodic) on the primary side than on the secondary side. Depending on the pH, metals dissolve in deaerated water and form either cations (at low pH) or anions (at higher pH). In the case of iron, either  $\text{Fe}^{2+}$  cations or  $\text{HFeO}_2^-$  anions are produced. pH values that separate the respective stabilities of these two ions, when their activities are equal, are 10.0, 8.2, and 6.0 at 25, 100, and 300°C, respectively.<sup>180</sup> Chromium and nickel behave similarly.<sup>53</sup>

Taking into consideration the pH values that occur in the primary and secondary waters, it can be expected that a bare (film-free) Alloy 600 surface would dissolve primarily in the form of anions:



Because the solubility of the anions produced from Alloy 600 is low, hydroxides precipitate when the respective solubility limits are exceeded. In SCC processes, the anodic reaction occurs in the crack tips and the cathodic reaction occurs in the crack flanks or the remaining outer surface of the metal.

The susceptibility of Alloy 600 to IGSCC is minimal in neutral water and increases with both increasing and decreasing pH.<sup>169</sup> However, in the pH range of primary water, the influence of pH on PWSCC is not pronounced. On the other hand, if the pH is increased significantly in secondary-side crevices, risk of higher susceptibility to IGSCC also increases greatly. IGA in caustic solutions is also influenced by pH, generally increasing with increasing pH in the range of pH 10-11.5.<sup>17,81</sup> Furthermore, IGA can proceed in the absence of applied stress or even in the presence of surface compressive stress, although an application of tensile stress during the test may switch it to IGSCC.

The pH inside the cracks formed in Alloy 600 has never been measured. However, measurements in an artificial crevice showed that in pure water, the crevice pH was slightly alkaline and the degree of alkalinity was self-limiting, thereby preventing highly caustic solutions from developing.<sup>181</sup>

As discussed earlier, the idea during the last two decades of associating IGA/IGSCC in the secondary side of a PWR with an aqueous high-pH environment is increasingly being called into question; a neutral to slightly alkaline environment is indicated by examination of pulled tubes. Nevertheless, many similarities with caustic IGA/IGSCC remain. These include a mixed IGA and crack-like morphology, the presence of severely degraded nonprotective oxide, and probable chromium and iron dealloying below unprotective films and on crack flanks.<sup>134,135,138</sup> However, whereas the surface oxide of laboratory specimens in caustic solutions is either absent or mainly NiO, in the case of many of the recently pulled tubes with IGA/IGSCC, a brittle chromium-rich oxide is observed. Although at first sight these might suggest an acidic environment, complementary analyses of hideout return and of tube deposits, which usually incorporate complex silicates, show that the environment in contact with the tube in the occluded region was neither strongly acidic nor strongly alkaline. Chemical species that might be able to cause the degradation of the protective film in neutral to mildly alkaline environments include lead, sulfur, and alumino-silicates, probably assisted by carboxylic acid complexing agents.<sup>75,78</sup>

Inasmuch as the aqueous environment of a PWR steam generator tube remains at its corrosion potential for the given temperature and solution composition, the effects of ECP on SCC susceptibility have not been studied extensively. However, in conventional laboratory immersion tests, long test periods (months) are required to produce SCC and the interpretation of the results is complicated by time-dependent variations in the test environment conditions. Therefore, to study the effects of parameters such as heat treatment or carbon content on IGSCC, some researchers have conducted corrosion tests that allow the specimen potential to be controlled at known values, thereby initiating SCC in a relatively short period of times (days), with associated minimization of variations in the test environment. Anodic polarization curves are useful in this respect because they identify the potential ranges for active, transpassive and passive regions. Because the IGSCC behavior of Alloy 600 is markedly dependent on the potential, one would expect wide variations in its SCC behavior, depending on the hydrogen (or oxygen) concentration in the solution.

Rebak et al.<sup>121</sup> generated anodic polarization curves in 350°C primary water, shown in Fig. 30, to isolate the behavior of Alloy 600, Cr<sub>23</sub>C<sub>6</sub>, and graphite. At open-circuit potential, no preferential dissolution was expected because the corrosion potentials of Alloy 600 and Cr<sub>23</sub>C<sub>6</sub> were nearly identical ( $\approx$  900 mV<sub>SHE</sub>). With a slight anodic potential of 100 mV, the current density of Alloy 600 rose above that of the carbide and graphite, suggesting that the matrix would dissolve preferentially. It was postulated that the carbide would passivate at a lower current density because of its higher chromium content with respect to that of the matrix. Above the transition potential of  $\approx$  250 mV<sub>SHE</sub>, the carbides and graphites would dissolve preferentially.

Lai and Smialowska<sup>54</sup> reported measurements of the open-circuit potential, AC impedance, and anodic polarization curves for Alloy 600 under three heat-treatment conditions; LTMA at 927°C, HTMA at 1024°C, and thermal treatment at 700°C for 28 h, in 25-350°C lithiated water that contained hydrogen. The values of the open-circuit potential for the three heat-treated materials were almost identical at the same temperature. Values of the polarization resistance measured by AC impedance data indicated that the thermally treated material was superior (higher resistance, more protective surface film) to the material that was mill annealed at 1024°C. The LTMA material showed the lowest resistance. Anodic polarization measurements showed lower dissolution rates and greater tendencies to passivation for thermally treated and HTMA materials than for LTMA material.

Bandy et al.<sup>182</sup> have measured the polarization curve of Alloy 600 in 10% NaOH + 1% Na<sub>2</sub>CO<sub>3</sub> at 300°C at a scan rate of 20 mV/min (Fig. 31). Increasing the scan rate to 500 mV/min increased the anodic peak current and the potential for active-to-passive transition to 37.8 mA/cm<sup>2</sup> and 190 mV, respectively. The polarization curve in 10% NaOH + 1% Na<sub>2</sub>SO<sub>4</sub> was essentially the same as in Fig. 31. However, in 10% NaOH solution, although the active peak current density and the potentials for active-to-passive transition were very similar to those in Fig. 31, the passive current density was  $\approx$ 40% less than that in Fig. 31.

The regions of SCC and IGA observed in the tests of Bandy et al.<sup>182</sup> are also shown in Fig. 31. All of the mill-annealed C-ring specimens (constant displacement) that were held between 60 mV (measured against nickel) and 180 mV (measured against nickel), underwent SCC with a maximum crack propagation rate at 137 mV (measured against nickel). Tests in 10% NaOH + 0.1% Na<sub>2</sub>CO<sub>3</sub> gave a very similar potential dependence except that SCC was observed at a more active potential (+40 mV). The onset of rapid SCC generally coincided with the potential that corresponded to the active-to-passive transition, and, at potentials where the passivity was well established (>300 mV vs. nickel), CGR fell sharply. From this they concluded that cracking proceeded by film rupture followed by anodic dissolution along grain boundaries and subsequent repassivation. Intergranular attack (IGA) was observed in this environment in the mill-annealed C-ring specimens from  $\approx$ -84 to  $\approx$ 60 mV (vs. nickel). The maximum depth of IGA varied from 50 to 140  $\mu$ m in 343 h, independent of the potential. The solution-annealed specimens also showed IGA between -50 and 80 mV (vs. nickel) in a ten-day test, although the attack was generally shallower than that in the mill-annealed samples. The most pronounced IGA generally occurred in the crevices under nuts and often on the compressive side.

Essentially similar polarization curves had been reported earlier by Pessall et al.,<sup>183</sup> who used potential control to show that for highly stressed samples tested in 10% NaOH solutions at 315°C, maximum crack depth occurred when the specimen potential was controlled in the active-to-passive transition region. They were able to show that CGR was  $\approx 20$  times greater in mill-annealed material than in thermally treated (705°C for 24 h) material when the tubes were held at their most susceptible potential range. The increased resistance of the thermally treated material was ascribed to the beneficial effect of semicontinuous grain boundary carbides.

Smialowska et al.<sup>53</sup> studied the effect of ECP on the susceptibility of cold worked Alloy 600 to SCC in hydrogenated solutions at 350°C. They found that Alloy 600 suffered SCC at the corrosion potential  $E_{\text{corr}}$ , at cathodic potentials, and in the active dissolution and transpassive regions of anodic potentials. Stress corrosion cracking was not observed in the anodic regions of potentials where the alloy developed a passivating film. The IGA and IGSCC in caustic solutions also depend on the potential.<sup>17,33</sup> The IGA rate in Alloy 600 in 10% NaOH plus 0.1% Na<sub>2</sub>CO<sub>3</sub> solutions at 300°C increases as the potential increases above 0 mV (measured against nickel). However, when a protective film begins to form on the surface at  $\approx 100$  mV more positive (anodic) than nickel, IGA changed to IGSCC.

#### 4.1.3 Composition, structure, and creep of grain boundaries

Bulk chromium content and grain boundary chromium concentration in Alloy 600 are of great interest in the study of IGA/IGSCC. In high-purity, deaerated and hydrogenated water at 360°C, increasing the bulk chromium content from 5 to 17 wt.% dramatically changed the surface film from predominantly Ni(OH)<sub>2</sub> to Cr<sub>2</sub>O<sub>3</sub>.<sup>184</sup> However, the surface film was also a sensitive function of the carbon level. Thus, after 100 h exposure in high-purity hydrogenated water at 360°C, Cr<sub>2</sub>O<sub>3</sub> was the stable surface film in an alloy with 0.002 wt.% carbon, whereas a less protective Ni(OH)<sub>2</sub> film was formed on an alloy that contained 0.03 wt.% carbon.<sup>184</sup> Donati et al.<sup>66</sup> have observed that SCC resistance increased when special heats of Alloy 600 with 19% chromium (instead of the nominal 15%) were tested in deaerated, hydrogenated primary or pure water at 350-360°C or in hydrogenated 200-bar steam at 400°C, but was unaffected in dilute (10g/L NaOH) caustic solution. The increased chromium content did not appreciably change the microstructure or the grain boundary precipitate morphology, except for the occurrence of M<sub>23</sub>C<sub>6</sub>, which is generally absent from Alloy 600.

As already discussed, grain boundary carbide precipitation occurs readily in Alloy 600 because of low carbon solubility. A thermal treatment in the range of 500-900°C following a solution annealing produces incoherent, semicontinuous platelets of M<sub>7</sub>C<sub>3</sub> precipitates in the grain boundary. However, when carbon activity is low, e.g., after extended thermal treatment, M<sub>23</sub>C<sub>6</sub> carbides have also formed. The major consequence of the various carbides is a reduction in the depth of the chromium-depleted zone for M<sub>23</sub>C<sub>6</sub> when compared with M<sub>7</sub>C<sub>3</sub>.<sup>185</sup>

Modeling has proved useful in determining that the chromium depletion profile depends on the stoichiometry and composition of the carbide, the content of carbon and chromium in the alloy, the time at temperature, and the grain size.<sup>185</sup> Chromium depletion in mill-annealed structures can differ significantly from that in SA structures. The mill-annealed structure often shows varying degrees of chromium depletion, depending on the details of the mill annealing. Because, in mill-annealed material, a significant amount of carbon has already been taken out of solution in the form of chromium carbides, subsequent thermal treatments more quickly replenish the depleted region of mill-annealed than solution-annealed material. This is why a thermal treatment of 700°C/10h will usually lead to healing of existing chromium-depleted zones in mill-annealed material but will produce severe chromium depletion in solution-annealed material.

Although chromium depletion is generally detrimental in oxygenated water, such a correlation does not seem to apply in deaerated water where sensitization appears to be beneficial rather than detrimental.<sup>43</sup> Rajan et al.<sup>186</sup> conducted CERTs in 345°C deaerated water of controlled-purity Ni-Cr-Fe-C over a range of chromium depletion levels (5-15 wt.%), which showed no correlation with IGSCC susceptibility in that all levels produced 25-55- $\mu$ m-deep surface cracks. The results were much the same at 360°C.<sup>187</sup> Thus, it appears that grain boundary chromium depletion has no effect on intergranular cracking in deaerated water, Fig. 32.<sup>188</sup> In fact, the percent intergranular cracking starts to increase only after most of the depleted chromium has been replenished by diffusion. Clearly, this cannot be due to the concentration of chromium alone.

The role of chromium depletion in IGSCC of Alloy 600 in 10% NaOH solution at 288°C was investigated by Crum<sup>189,190</sup> in CERTs. The tests showed that thermal treatments at 593°C for 4 h or 704°C for 15 h significantly reduced the percent intergranular failure in samples that contained 0.02-0.05% carbon. Because the former heat treatment would produce severe grain boundary chromium depletion at all carbon levels and the latter heat treatment would probably produce healing, the data seemed to show that chromium depletion did not play a role in this environment. Bandy et al.<sup>182</sup> conducted constant-displacement C-ring tests in 10% NaOH + 0.1% Na<sub>2</sub>CO<sub>3</sub> at 300°C and found an inverse correlation between CGR and severity of chromium depletion (as surmised from heat treatments). However, the results are ambiguous because the differing heat treatments led to differing yield strengths and thus to differing stresses.

The role of carbon in IGSCC of Alloy 600 in 360°C hydrogenated water that contained lithium and boric acid was investigated by Lai and Smialowska,<sup>54</sup> who found that Alloy 600 that was thermally treated at 1100°C for 1 h, followed by 700°C for 26 h, exhibited a lower critical potential for passivation and a lower current density in the passive state than material that was mill annealed at 927°C for 3-5 min. It was suggested that a greater amount of carbon in solid solution at the grain boundaries of the mill-annealed material made passivation more difficult and enhanced the dissolution rate. The anodic polarization measurements showed a lower dissolution rate and increased passivity for the thermally treated material, from which they concluded that carbide precipitation at the grain boundaries had a beneficial effect on the dissolution rate and on the ability of the material to assume a passive state.

Among the grain boundary impurities in Alloy 600, sulfur, phosphorus and silicon have received the most attention. The high resistance of Alloy 600 to IGSCC in deaerated water at 316°C has been reported not to be impaired by carbon, sulfur or phosphorus, even when present in amounts corresponding to the upper limit found in commercial alloys.<sup>116</sup> Apparently sulfur inhibits grain boundary attack and increases general corrosion. Tests have demonstrated that additions of phosphorus, and, to a much lesser extent, silicon, to solution-annealed Alloy 600 cause susceptibility to IA in strongly oxidizing media.<sup>114</sup> Was and Martin<sup>191</sup> have shown that extended thermal treatment at 700°C produced a saturation in the phosphorus level at between 10 and 100 h and that the phosphorus is indeed present as a segregant rather than being incorporated into carbides. Guttman et al.<sup>117</sup> performed AES on intergranular fracture surfaces of Alloy 600 by cathodically charging with hydrogen at elevated temperature in molten salts. They found phosphorus to be the only nonmetallic impurity that appreciably segregated (by equilibrium-type segregation) to the grain boundaries of commercial-purity Alloy 600. However, phosphorus did not appear to be the cause of IGSCC in pure water or caustic environments. Silicon did not segregate appreciably but seemed to be in a precipitate form at the grain boundaries.

As already mentioned, the importance of grain boundary structure on IGSCC has recently received some attention. The coincident-lattice-site (CSL) model of grain boundary structure classifies grain boundaries into three categories, based on the relative misorientation among grains that are adjacent to the grain boundary.<sup>192</sup> Low-angle boundaries (LABs) are misoriented at an angle of up to 15°. Coincident site lattice boundaries are those that are at or sufficiently close to misorientations where two adjacent grain lattices have some coincident points. The CSL boundaries are often characterized by a number  $\Sigma$ , defined as the reciprocal density of the coincident lattice sites. All other boundaries are considered to be general high-angle GHA boundaries or "random" boundaries. Carbides are generally smaller and more closely spaced on boundaries with a low  $\Sigma$  (except they are absent on  $\Sigma = 3$  twin boundaries). It has been shown that grain boundaries that are close to a low  $\Sigma$  ( $\leq 49$ ) orientation, exhibit improved physical, chemical, and creep cavitation resistance properties when compared with high  $\Sigma$  ( $> 49$ ) orientations and GHA boundaries.<sup>192-194</sup>

Palumbo et al.<sup>195</sup> examined the effect of grain boundary structure on intergranular fracture of Alloy 600 exposed to 10% NaOH at 350°C for 6000 h. They found that 35 of 51 grain boundaries that were investigated exhibited  $\Sigma \geq 27$ , and all showed cracking susceptibility. The rest of the boundaries were found to exhibit  $\Sigma < 27$  and nine of them were immune to IGSCC. Aust et al.<sup>196</sup> have tried to improve the intergranular corrosion resistance of nonsensitized commercial Alloy 600 by optimizing its microstructure via alteration of grain boundary structure, i.e., via increasing the fraction of CSL boundaries with  $\Sigma < 27$ . Tests showed that intergranular corrosion rate after sensitization for 1h at 600°C also diminished with increasing fraction of CSL boundaries.

Recent research shows that grain boundary response to creep may be playing an important role in the IGSCC susceptibility of Alloy 600.<sup>197</sup> Several observations in this

study supported a hydrogen-enhanced creep mechanism for intergranular cracking of Ni-Cr-Fe-C alloys in 360°C deaerated high-purity and primary water:

- The fracture surfaces exhibited intergranular facets that were not smooth, but were covered with dimples.
- Incidences of intergranular cracking were preferentially located at the specimen interior, which was excluded from direct contact with the environment.
- The amount of intergranular cracking increased as the applied ECP was decreased.
- The creep rate of Ni-17%Cr-9%Fe-low-C alloy at 360°C and 500 MPa increased by a factor of 9 over that in argon, when exposed to deaerated hydrogenated primary water at  $-1.159 \text{ mV}_{\text{SHE}}$ .

Because dislocation-controlled creep was responsible for intergranular cracking of these alloys in argon, the increase in intergranular cracking in high-temperature water was attributed to an increase in the dislocation-controlled creep without increases in grain boundary cavitation and sliding. However, the observation that changes in the applied potential did not affect the creep rate in 360°C water did not support a hydrogen mechanism.

As discussed earlier, Boursier et al.<sup>168</sup> did not find a direct correlation between total creep rate and IGSCC but did find that the materials with the greatest amount of grain boundary sliding exhibited the least resistance to IGSCC. Using an initial strain rate of  $3 \times 10^{-7}/\text{s}$  in 360°C argon, Thaveprungsripon et al.<sup>198</sup> conducted CERTs on carbon-doped and carbon-free controlled-purity Ni-16Cr-9Fe-xC alloys. They found little grain boundary sliding and little intergranular cracking in the carbon-doped alloys but much higher intergranular cracking and sliding in the carbon-free alloy. The creep rate of the carbon-doped alloy was much lower than that of the carbon-free alloy. They also found that GHA boundaries were more susceptible to grain boundary sliding and cavitation than CSL boundaries and LABs.

## 4.2 Mechanistic Models

Scott and Combrade<sup>199</sup> recently reviewed various intergranular cracking mechanisms for Alloy 600 in PWR water, with particular emphasis on the relationship among corrosion potential, surface oxide film characteristics, and the corresponding corrosion damage. Their assessment led to the following conclusions.

- Caustic cracking occurs in fluids where chromium is too soluble to contribute to passivity and is associated with an active/passive transition in a limited potential range, above Ni/NiO equilibrium, where film repair kinetics are slow.
- Caustic IGA occurs in the absence of a protective film (i.e., at potentials below the Ni/NiO equilibrium) and appears to proceed by the selective dissolution of

iron and chromium, which is assumed to be faster on grain boundaries than in the grains.

- PWSCC is observed over a limited range of potential, centered on the Ni/NiO equilibrium under neutral to slightly alkaline conditions. Composition of the formed spinel oxides changes rapidly over the relevant potential range, but the film repair kinetics do not correlate with cracking sensitivity. They speculated that ion transport in the oxide film or oxygen transport into the metal could be rate controlling.
- The morphology of IGA/IGSCC observed on pulled tubes shows many similarities with that caused by caustic solutions in laboratory specimens. The main observation is a degraded, nonprotective, brittle oxide composed of NiO in the case of caustic, but frequently chromium-rich in the pulled tubes. The latter is caused by impurities that are not necessarily strongly acidic or alkaline. Thus, mechanisms of IGA/IGSCC observed in the pulled tubes should be similar to those observed in caustic solutions.
- They concluded that IGA/IGSCC are not necessarily exclusively liquid phase phenomena and that selective grain boundary oxidation that leads to embrittlement and intergranular cracking is possible. The presence of plugged crevices on the secondary side increases the chances of local dryout and the possibility of generating a medium not unlike the medium doped-steam that is used in the laboratory to test for primary side susceptibility to cracking.

A significant number of mechanistic models, some quantitative some not, based on various postulated mechanisms, has been proposed. These models are briefly reviewed.

#### 4.2.1 Film rupture/dissolution/repassivation model

The slip dissolution/film rupture mechanism of crack propagation was developed at General Electric (GE).<sup>200,201</sup> In this mechanism, crack advance is related to the oxidation reactions that occur at the crack tip as the protective film is ruptured by increasing strain in the underlying matrix. This rupture event occurs with a periodicity  $t_f$ , which is determined by the fracture strain  $\epsilon_f$  of the oxide and the strain rate at the crack tip. The extent of crack advance is related by Faraday's law to the oxidation charge density associated with dissolution, oxide growth (passivation), and spontaneous corrosion on the bared metal surface, as schematically represented in Fig. 33.<sup>199</sup> These reactions vary with time in a complex manner for differing environments and material chemistries. This qualitative description may be quantified by considering various rates of, e.g., bare-surface dissolution  $i_0$ , passivation rate parameters  $t_0$ ,  $n$ , etc., to give a fundamentally derivable relationship of the average CGR  $V_T$ . The model assumes that there is a high degree of separability between the mechanical and chemical contributions to the CGR. The basic concept is that the emergence of slip steps at the crack tip structurally damages the protective oxide film, with consequent oxidation of the underlying matrix and subsequent film repair. The fraction of oxidation related to dissolution can be Faradically related to average CGR by the equation

$$V_T = \frac{M}{z\rho F} \cdot \frac{Q_f}{t_f}, \quad (4)$$

where  $Q_f$  is the oxidation charge density between film rupture events,  $M$  is the atomic weight,  $z$  is the oxidation number,  $\rho$  is the density,  $F$  is the Faraday constant, and  $t_f$  is the time per oxide fracture event.

At a sufficiently high crack tip strain rate, a bare surface is continuously maintained at the crack tip, and the environmentally assisted CGR becomes independent of the crack tip strain rate because it cannot exceed the Faradaic equivalent of the bare-surface dissolution rate. The limiting average CGR is then given by

$$V_T = \frac{M}{z\rho F} \cdot i_0, \quad (5)$$

where  $i_0$  is the bare-surface-dissolution-rate parameter.

At the other extreme, when the average CGR approaches the oxidation rates on the crack sides  $V_s$ , a sharp crack cannot be maintained, the crack propagation rate decreases with exposure time, and crack arrest occurs because of chemical blunting. Between these two extremes, the average CGR can be shown to be given by

$$\begin{aligned} V_T &= \frac{M}{z\rho F} \frac{i_0 t_0^n}{(1-n)\epsilon_f^n} \cdot (\dot{\epsilon}_{ct})^n \\ &= f(n)(\dot{\epsilon}_{ct})^n, \end{aligned} \quad (6)$$

where  $\dot{\epsilon}_{ct}$ , the crack tip strain rate, embodies the mechanical contribution, and  $n$  is a parameter that represents the effects of the environment and material chemistries on environmentally assisted crack growth.

In Eq. 6, the value of the exponent  $n$ , which varies between 0 (highly oxidizing environment with highly sensitized material) and 1 (reducing environment and solution-annealed microstructure), is related to the corrosion potential, coolant conductivity, and EPR, which is a measure of grain boundary chromium depletion. The higher the value of  $n$ , the lower the CGR. By integration of the fundamental relationship, the following equation was derived by Ford and Andresen for Type 304 SS and nickel base alloys in BWR water:

$$V_T = \left(2.808 \times 10^5 n^{3.6}\right) \left(6 \times 10^{-14} K^4\right)^n, \quad (7)$$

where  $V_T$  is the average CGR in  $\mu\text{m}/\text{h}$  and  $K$  is the stress intensity factor in  $\text{MPa}\sqrt{\text{m}}$ .

Ford and Andresen<sup>199</sup> claimed that Eq. 7 can quantitatively predict the observed crack propagation rates for a wide combination of materials, environments, and stress conditions. The apparent activation energy for the CGR IGSCC of SSs in BWR

environments has been found to vary from 25 kcal/mole (105 kJ/mole) at 150°C to 4 kcal/mole (17 kJ/mole) at higher temperatures. These findings have been interpreted in terms of a rate-controlling step that changes from control of solid state diffusion at 150°C to control of liquid diffusion of solvating water molecules to the crack tip at higher temperatures.<sup>201</sup> The apparent activation energy of IGSCC of Alloy 600 in PWR water has been found to be 30-50 kcal/mole (125-210 kJ/mole),<sup>202</sup> which suggests that the rate-limiting step is control of solid-state diffusion rather than liquid diffusion. Also, in the slip dissolution model, coolant conductivity is one of the most important system definers, because it reasonably quantifies non-OH<sup>-</sup> anion activity; in BWR environments, this is directly related to the anionic activity and pH at the crack tip, both of which affect the metal oxidation rate and hence, the crack propagation rate. In PWR environments, the higher conductivity is due to borate and LiOH additions, which do not materially affect the metal oxidation rate.<sup>201</sup> Whether excess conductivity changes due to other anions (e.g., sulfate and chloride) may be correlated with crack propagation rates in PWR system is not known. Thus, the applicability of the slip dissolution model to IGSCC of Alloy 600 in PWR water is open to question.

Nevertheless, Eq. 7 has been used with  $n = 0.65$  and the second coefficient  $6 \times 10^{-14}$  replaced by  $4.1 \times 10^{-14}$ , to give a reasonable correlation between predicted and observed CGRs in Alloy 600 in high-temperature simulated primary water (Fig. 34).<sup>169</sup> However, it is not clear how the environment, alloy chemistry, and temperature combine to give a value of  $n = 0.65$ . The strength of the slip dissolution model is that it provides a practical approach by combining a theoretical model with data fitting. It correctly predicts that, as the environmental effect increases (i.e.,  $n$  decreases), the threshold stress intensity factor  $K_{ISCC}$  decreases. However, it cannot explicitly account for the effects of temperature, pH, grain boundary carbides, cold work, etc. on the CGR. Furthermore, the model does not provide any insight into the parameters that are important for crack nucleation.

#### 4.2.2 Enhanced surface mobility theory

The maximum CGR that is predicted by the slip dissolution model is limited by the bare-surface dissolution rate. In some metal environment systems, CGRs that are much higher than the maximum CGR predicted by the slip dissolution model have been measured. The surface mobility theory of Galvele<sup>203</sup> can, in principle, explain such results. According to this model, an atom at the crack tip is transported by surface diffusion from its highly stressed location to a less stressed crack side, thereby advancing the crack by one atomic step per such movement. In other words, crack propagation is the result of vacancy capture by the stressed lattice at the crack tip. The rate-controlling step is the rate of movement of atoms along the surface of the crack, and the role of the environment is to increase the surface mobility or surface self diffusion of the metal or alloy. The CGR was derived by consideration of how the equilibrium vacancy concentration on a surface is altered by the application of stress and was given as,

$$\text{CGR} = \frac{D_s}{L} \left[ \exp\left(\frac{\sigma a^3}{kT}\right) - 1 \right], \quad (8)$$

where  $D_s$  (in  $m^2/s$ ) is the surface self-diffusion coefficient,  $L$  is the diffusion path (typically  $10^{-8}m$ ),  $a$  is the atomic diameter ( $2.5 \times 10^{-10}m$ ),  $\sigma$  (in  $N/m^2$ ) is the normal stress at the crack tip,  $T$  is temperature in K, and  $k$  is Boltzman's constant ( $1.38 \times 10^{-23}J/K$ ).

Few values have been published for surface diffusion. For the case of environmentally assisted cracking, the diffusion coefficient was given<sup>203</sup> by

$$D_s = 7.4 \times 10^{-2} \exp\left(-\frac{30T_m}{RT}\right) + 1.4 \times 10^{-6} \exp\left(-\frac{13T_m}{RT}\right), \quad (9)$$

where  $R$  is the gas constant ( $1.987 \text{ cal/mole}\cdot\text{K}$ ) and  $T_m$  is the absolute melting temperature of the contaminated surface compound.

Galvele<sup>203</sup> classified the compounds of differing elements as protective, unsafe, and dangerous, according to the magnitude of  $D_s$ . If  $D_s \geq 10^{-16} m^2/s$ , the compound would be dangerous and exhibit a propensity to cause SCC in the metal or alloy. Aqueous SCC of SS in chloride solution was attributed to the formation of a low-melting-point salt (e.g., iron chloride). In this case, the environment merely serves to lower the melting point of the surface by forming a low-melting-point compound. The formation of low-melting-point compounds allows surface diffusional creep processes to occur.

Several theoretical problems are associated with Galvele's analysis.<sup>204</sup> The most serious of these is the fact that the diffusion equation for a problem where stress and curvature effects are important (e.g., in a crack) was set up with concentrations rather than chemical potentials. A second problem stems from the treatment of cracks in ductile materials as atomistically sharp. When atoms move from a region of high negative curvature (crack tip) to zero curvature (crack side), there must be proper accounting of the energetics of the process. Such an accounting was lacking in Galvele's analysis. Using the gradient of chemical potential rather than concentration for computing the vacancy flux, Sieradzki and Friedersdorf<sup>204</sup> obtained CGRs that were 8 (sharp crack) to 14 (blunted crack) orders of magnitude smaller than Galvele's estimates.

Despite the theoretical problems associated with Galvele's analysis, the model has several attractive features. With NiO as the surface contaminant, Eqs. 8 and 9 have been used successfully to predict Stage II CGR data for Alloy 600 in high-temperature water.<sup>169</sup> Galvele's model correctly predicts the formation of NiO that is necessary for IGSCC to occur at  $T > 250^\circ\text{C}$ , which is the equilibrium temperature for the formation of NiO. It also predicts that, when  $T < 250^\circ\text{C}$  (or  $p_{H_2}$  is high), NiO is absent, and  $\text{Cr}_2\text{O}_3$  effectively acts as a protective layer. Galvele's model predicts an apparent activation energy of 28 kcal/mole (118 kJ/mole) for SCC at  $K_I = 20 \text{ MPa}\sqrt{m}$  (slightly lower at higher  $K_I$ ), which is quite reasonable. The beneficial effects of carbides at the grain boundary can be explained by the fact that on the surface, carbides form only  $\text{Cr}_2\text{O}_3$ , which has a very low  $D_s$ . The nucleation time for IGA/IGSCC can be interpreted as the time needed to form the contaminant compound.

### 4.2.3 Hydrogen-assisted-cracking model

Hydrogen formed as a result of electrochemical reactions close to the crack tip may play an important role in crack growth. It has long been known that pickled specimens consistently have shorter IGSCC failure times than unpickled companion specimens.<sup>43</sup> Hydrogen introduced in the specimens by pickling may be responsible for this observation, although this has not been established. Incorporation of hydrogen atoms into the metal may lead to cracking due to hydrogen embrittlement,<sup>52</sup> whereas the presence of molecular hydrogen has been observed to have a great influence on the properties of the oxide films that are formed on the surface of Alloy 600.<sup>205</sup> Many experiments have been conducted to clarify the role of hydrogen and to explain the correlation among partial pressure of hydrogen in the system, hydrogen content of the metal, and cracking behavior. Recently, three hydrogen-related fracture mechanisms have been discussed by Birnbaum et al.:<sup>206</sup> hydrogen-related phase change, hydrogen-enhanced local plasticity, and hydrogen effect on the cohesive energy.

Smialowska et al. have proposed that hydrogen absorption at the grain boundaries would help the anodic dissolution process.<sup>53</sup> Their observation of the development of PWSCC cracks and even the formation of new cracks at room temperature in air on RUB specimens that were previously exposed to primary water would support a hydrogen embrittlement mechanism. They have demonstrated that the hydrogen content in the most highly strained regions where cracking was occurring was much greater (30-80 ppm) than that in the bulk of the specimen (2 ppm). However, in some specimens with high hydrogen content, cracking did not occur. Also, in dry hydrogen gas, no IGSCC was found in Alloy 600, even at a pressure of 35 MPa at 300-400°C. Magnin et al.<sup>70</sup> have also measured the amount of absorbed hydrogen by a melting method in Alloy 600 SCC specimens (RUB and SSRT) after testing for SCC. They found that the amount of hydrogen uptake in the material was independent of the system hydrogen pressure but increased with maximum applied stress. Moreover, the amount of hydrogen uptake was almost nil for specimens without cracks. Totsuka et al.<sup>52</sup> reported similar results. All of these results suggest that if hydrogen takes part in the embrittling process, it is the cathodic hydrogen and not the hydrogen dissolved in the environment that is important. Global hydrogen analyses are unable to provide information about amount of hydrogen that is at or near the crack tip.

Economy et al.<sup>38</sup> found that IGSCC behavior of Alloy 600 in hydrogen-containing steam at 368°C was very similar to its behavior in hydrogen-containing pressurized water at 368°C. Shen and Shewmon<sup>207</sup> observed that a hydrogen overpressure of 0.2 MPa at 380°C prolongs or even stops crack initiation. They also observed that the oxide film color (i.e., its thickness) changed with the hydrogen partial pressure, indicating that the oxide film that formed on the surface influenced the initiation time. They proposed a model in which, within the metal, hydrogen reacts with carbon to form methane, creating voids with high pressure. However, this hydrogen-assisted-cracking mechanism for Alloy 600 has not been confirmed by mass spectroscopy.<sup>208</sup>

Production of hydrogen close to the crack tip during crack propagation has been visually (from photographs) observed in SCC tests on Type 316 SS in 42% magnesium chloride solution.<sup>209</sup> Li and Ferreira<sup>210</sup> suggested a model for hydrogen generation

inside a stress corrosion crack by electrochemical and chemical reactions. Hydrogen is formed close to crack tip because of the low value of the potential difference between the metal and the solution. They also confirmed that hydrogen generation is enhanced by anodic polarization but decreased at negative potentials for SSs in hot chloride solutions.

Assuming that, under certain conditions, the crack tip environment may consist of steam and molecular hydrogen, Persson and Lagerstrom<sup>211</sup> and Lagerstrom et al.<sup>212</sup> also proposed a hydrogen-assisted-cracking model for Alloy 600. According to their model, the most important factor that governs the incorporation of hydrogen is whether or not a gas phase can develop along the crack front. If it can, hydrogen diffuses into the metal, where it may react with carbon to form methane, as suggested by Shen and Shewmon.<sup>207</sup> The pressure inside the gas bubble at the crack tip is the sum of the vapor pressure of water and partial pressure of hydrogen and equals the total pressure of the system. Accordingly, changes in the total pressure and in the temperature of the system produce changes in the partial pressure of hydrogen in the bubble, which in turn should result in changes in CGR. The prerequisites for existence of gaseous hydrogen and water vapor at the crack tip are,

- The potential difference between the metal and the solution close to the crack tip must be low enough for hydrogen production to proceed. This condition should be satisfied in both PWR and BWR water systems.
- A corresponding positive current must pass, because of an anodic reaction (i.e., metal oxidation), to account for charge balance in the system.
- Hydrogen evolution must be extensive enough to exceed the limit of hydrogen solubility in water. The solubility limit is  $\approx 480$  wt-ppm at  $320^{\circ}\text{C}$  and a system pressure of 16 MPa.
- The diffusion of hydrogen from the crack tip must be slow enough to maintain the hydrogen concentration at the crack tip at the solubility limit.

Crack growth tests under cyclic loading were conducted to validate the model.<sup>212</sup> The model was able to provide a qualitative explanation for an increase in CGR (by a factor of 1.5) due to a decrease in hydrogen content from 25 mL to 0 mL  $\text{H}_2/\text{kg}$  of water. A decrease in the bulk content of hydrogen led to an increase in corrosion potential of the bulk sample and thus caused an increase in the anodic reactions (oxidation of metal) in the crack. The increase in the anodic reactions led to increased hydrogen generation at the crack tip. The fractographic results also showed a corresponding decrease in the transgranular component and increase in the intergranular components of crack growth. On the other hand, the model predicted increased CGR if the system temperature was decreased at constant pressure, because water vapor pressure in the bubbles would be decreased and lead to a higher partial pressure of hydrogen. Using a similar argument, the model would predict that a decrease in system pressure at constant temperature would lead to decreased CGR. However, tests showed the reverse trend, i.e., CGR decreased in the first case and increased in the second. It was claimed

that the predictions failed in these two cases because the assumption of simultaneous presence of water vapor and hydrogen at the crack tip was not satisfied in the tests.

There is indirect evidence that links hydrogen with IGSCC and there are some experimental observations that can be qualitatively explained by the hydrogen-assisted-cracking model. However, its main drawback is that currently, the exact mechanisms of hydrogen embrittlement are not known and no quantitative model exists that can predict the cracking behavior of Alloy 600 in PWR water.

#### 4.2.4 Internal-oxidation model

Scott and Calvar<sup>213</sup> have reviewed existing mechanistic models and PWSCC data in PWR steam generators and concluded that any successful mechanistic model must be consistent with at least the following trends in the data:

- great influence of hydrogen partial pressure (or corrosion potential) on IGSCC and the observation of a worst case centered on potentials near the Ni/NiO equilibrium
- apparently continuous mechanism of failure between 300 (subcooled water) and 400°C (superheated steam)
- high and variable activation energy, typically, 43 kcal/mole (180 kJ/mole), with a large scatter band
- influence of carbon content, carbide morphology, and cold work on IGSCC
- high stress exponent of  $\approx 4$  for time to failure

Conventional models, such as film rupture/anodic dissolution or hydrogen embrittlement cannot be reconciled with either the influence of corrosion potential or the high activation energy of PWSCC. Theories based on grain boundary cavities<sup>214</sup> or bubbles<sup>207</sup> address the magnitude of the activation energy, stress exponent, and some aspects of the roles of carbon and carbide morphology but do not provide a satisfactory explanation for the thermodynamics of PWSCC. Because of these deficiencies in existing models, Scott and Calvar<sup>213</sup> concluded that other solid-state grain boundary diffusional processes may be worth examining and it was in this context that they proposed the internal-oxidation model.

Internal oxidation is a particular form of corrosion, typically for nickel-based superalloys in atmospheres with low oxygen partial pressure, in which the less noble alloying elements of the alloy oxidize and leave the solvent metal untouched. The concentration of oxygen must be low enough so alloying elements such as chromium or aluminum cannot form a protective film. Typically, internal-oxidation experiments are carried out at temperatures  $>700^{\circ}\text{C}$ . Scott and Calvar<sup>213</sup> speculated that such a mechanism may also be operating at  $\leq 400^{\circ}\text{C}$ , provided the test time is extended.

Thermodynamic calculations showed that under conditions in which PWSCC is observed, nickel oxide would be stable but chromium, iron, and carbon (which are less noble) and potentially susceptible to internal oxidation could oxidize. For internal oxidation to proceed by grain boundary penetration by oxygen, external oxidation of the alloy must be suppressed. Transition from internal to external oxidation depends on the effectiveness of the external spinel layer to cut off the diffusion of oxygen into the metal and also on factors such as surface finish, grain size, and cold work, all of which affect PWSCC.

Grain boundary embrittlement of nickel-base alloys can occur by formation of gas bubbles ( $\text{CO}/\text{CO}_2$ ) or an internal oxide ( $\text{Cr}_2\text{O}_3$ ), or simply because a layer of oxygen is present at the grain boundaries or other embrittling elements are released. The last possibility was excluded for PWSCC because no impurity elements, such as sulfur and phosphorus, have been detected consistently in the grain boundaries of Alloy 600. Using a gas-bubble-based theory, Scott and Calvar<sup>213</sup> derived the following equation for the time to unstable bubble growth:

$$t_f = \frac{1}{\sigma^2} \left[ \frac{512\gamma^3 a^2}{81kTD_0} \right] \left[ \frac{zx}{\delta N_s} \right]^{1/2}, \quad (10)$$

where

$\sigma$  = applied tensile stress,

$\gamma$  = surface energy =  $1.5 \text{ J/m}^2$ ,

$a$  = interatomic spacing =  $2.2 \times 10^{-10} \text{ m}$  for nickel,

$k$  = Boltzmann constant =  $1.38 \times 10^{-23} \text{ J/K}$ ,

$T$  = absolute temperature in K,

$D_0$  = grain boundary diffusion coefficient for oxygen in nickel

$$= 1.5 \times 10^{-7} \exp(-13800/T) \text{ m}^2/\text{s},$$

$z$  = number of sites explored per jump = 4,

$x$  = diffusion distance,

$\delta$  = grain boundary width =  $10^{-9} \text{ m}$ ,

$N_s$  = surface solubility of oxygen in nickel =  $7 \times 10^{-4}$  mole fraction

Using the concept of a critical fracture process zone, defined by

$$x_p = \frac{1}{6\pi} \left( \frac{K_I}{\bar{\sigma}} \right)^2, \quad (11)$$

where

$K_I$  = Mode I stress intensity factor in  $\text{Pa}\sqrt{\text{m}}$ ,

$\bar{\sigma}$  = "fracture" stress in  $\text{Pa} = 500 \text{ MPa}$ ,

and from Eqs. 10 and 11, we can obtain the following CGR equation:

$$\frac{dx}{dt} = \frac{x_p}{t_f} = \left[ \frac{81kTD_0}{512\gamma^3 a^2} \right] \left[ \frac{\delta N_s}{6\pi z} \right]^{1/2} \bar{\sigma} K_I. \quad (12a)$$

Substituting the values for the various parameters, Eq. 12a reduces to

$$\text{CGR} = 2.1408 \times 10^{-2} K_I, \quad (12b)$$

where CGR is in  $\mu\text{m}/\text{h}$  and  $K_I$  is in  $\text{MPa}\sqrt{\text{m}}$ .

Plots of the prediction of the model<sup>212</sup> and available experimental data, shown in Fig. 35, indicate that the predictions are reasonable. However, it must be realized that the value of  $D_0$ , the key parameter in this model, is highly uncertain because grain boundary diffusion data for oxygen at the temperatures of interest are virtually unavailable. Diffusion data for oxygen in dilute nickel-base alloys at high temperatures (800-1300°C) show that the activation energy is  $\approx 70 \text{ kcal/mole}$  (300  $\text{kJ/mole}$ ). Scott and Calvar<sup>212</sup> chose the diffusion coefficient to match the measured diffusion coefficient at high temperatures but extrapolated it to lower temperatures by using a much shallower slope (i.e., lower activation energy), arguing that the high-temperature diffusion was dominated by lattice diffusion. The lower activation energy was obtained from intergranular crack growth (by internal oxidation) data for nickel-base alloys at 450-760°C. The result is an underprediction of the absolute rate of intergranular penetration by oxygen by a factor of 20. Thus, it is likely that the value of  $D_0$  should be higher than assumed. Furthermore, plastic strain can increase oxygen diffusivity. On the other hand, if grain boundary sliding is inhibited (e.g., at CSL boundaries), grain boundary diffusivity is decreased. Similarly, the presence of precipitates in the grain boundaries of complex alloys can slow down grain boundary diffusivity. All of these complexities increase the probability that no single value of activation energy is appropriate. A second uncertainty in the model is in the "fracture stress" for the process zone (used in Eq. 12); we have used the flow stress value.

Although this model is subject to uncertainties in the values of pertinent parameters, it contains several attractive features. It is gaining credence from the observation of IGSCC along scratches at midspan (SGs at McGuire and Farley) and general IGA in the superheated steam space of OTSGs (primarily Oconee 1, 2 and 3). It is a mechanism that does not require a liquid phase. It explains why grain boundary

structure and carbide morphology (sensitization) influence IGSCC behavior through their influence on oxygen diffusivity.

The reported observation that Alloy 600 continues to crack at room temperature after removal from a primary water environment can be explained in terms of an oxygen-damaged intergranular zone that subsequently cracks by hydrogen embrittlement at low temperature. Hydrogen created during general corrosion would be trapped in the alloy during cooldown, because of its high solubility and low diffusivity. However, without an oxygen-damaged zone, Alloy 600 remains ductile. Gourgues et al.<sup>208</sup> conducted tests to show that grain boundaries of unstressed Alloy 600 are embrittled to a depth of several microns when exposed to primary water. This embrittlement was irreversible by high-temperature degassing and could not be directly due to hydrogen. Although the results seemed to support the hypothesis that oxygen atom penetration of grain boundaries is possible, no evidence was found for the formation of gas bubbles or oxides. Whatever the mechanism, this embrittling process could sequentially act at the tip of a growing stress corrosion crack. Recent analytical TEM and secondary ion mass spectroscopy (SIMS) work is beginning to provide direct metallurgical evidence that supports this mechanism.<sup>215</sup>

#### 4.2.5 Corrosion deformation interaction model

Magnin et al.<sup>70</sup> proposed an SCC model for Alloy 600 in primary water that accounts for the corrosion deformation interaction (CDI) observed during creep tests. This is a crack propagation model based on cleavage cracking due to local environmentally enhanced softening. The major support for this model is the purported increase in creep strain rate in the medium when compared with that in air or argon, indicating that an interaction between corrosion and plastic deformation occurs. According to this model, the following steps are considered.

- A localized anodic dissolution (or oxidation) occurs on the {111} slip planes at the crack tip near grain boundaries after film rupture because of the emergence of a slip line.
- An enhanced localized plasticity occurs because of localized corrosion on {111} slip planes by dissolution (or oxidation) and adsorption of hydrogen. Thus, the role of corrosion is essential but indirect; it enhances local plasticity at the crack tip.
- Dislocations emitted from this enhanced localized zone of plasticity will interact with various obstacles (e.g., precipitates, grain boundaries, etc.) and produce pileups and increased local stress.
- If the obstacles are strong enough and the reduction of  $K_{IC}$  due to hydrogen adsorption is large enough, an embryo crack will form at the obstacle.
- Relaxation of stress at the obstacle can occur on the grain boundary, depending on the orientation of the obstacle, cohesive energy or impurity content (leading to intergranular cracking), or on {111} and {100} macrofacets by decohesion due

to reduction of cohesive energy by hydrogen adsorption (leading to transgranular cracking), or by mixed mode.

According to the CDI model, oxidation first occurs near grain boundaries, a circumstance that allows hydrogen adsorption and absorption to occur. Thus, a hydrogen effect can occur only if a critical defect due to oxidation is present. It correctly explains the lack of correlation between total hydrogen absorption and susceptibility to SCC and the observed increase in severity of SCC between 0 and 4 bar hydrogen pressure and decrease of severity of SCC at high hydrogen overpressure. It takes into account the intrinsic role of both oxidation and hydrogen. Oxidation is first necessary and then hydrogen effect can follow. The crack propagates neither by dissolution nor by hydrogen accumulation, but by cleavage. Well-known SCC effects such as carbide precipitates and cold work are taken into account by the proposed model. Unfortunately, no quantitative model based on CDI that can predict the cracking behavior of Alloy 600 in PWR water is available.

#### **4.2.6 Selective dissolution-vacancy-creep model for IGSCC**

According to this model,<sup>216</sup> the rate-determining step is the generation of cation vacancies by selective dissolution of metal cations through the existing passive film at the crack tip. For Alloy 600 in primary water, the oxide is most often spinel and the diffusivity of an iron cation is greater than that of nickel and much greater than that of chromium in spinel-type oxides. Thus, the generation of cation vacancies is dominated by dissolution of iron cations.

By dissolution we mean that the iron cations are transported through the existing passive film into the solution, without film rupture. The cation vacancies that move in the opposite direction and reach the metal/oxide interface exhibit a high driving force for transport toward the zone of high triaxial stress ahead of the crack tip. Because vacancy generation is highest at the crack tip and because the driving force for vacancy migration keeps vacancies in the plane of the crack, dislocations that are in the plane and directly ahead of the crack tip are the preferential sinks for the vacancies. This process continues until a relatively dislocation-free planar zone that extends from the crack tip is formed. On both sides of this zone the dislocation density remains very high and thus a shear band can form at the crack tip. Further deformation concentrates in the shear band and enhances local creep processes.

The vacancies that are generated can now move to the zone of high triaxial stress without being consumed by dislocations and the local concentration of vacancies in the zone of high triaxial stress increases and approaches the equilibrium concentration of vacancies that correspond to the high triaxial stress. As the vacancy concentration exceeds a critical value, the load-bearing capability of the ligament between the crack tip and the maximum stress area is exceeded and the crack advances a jump.

As justification, it was reported that the measured activation energies for diffusion of iron cation through magnetite, ferrite spinels, and the growing oxides on 316 stainless steel are all  $\approx 36$  kcal/mole, which is comparable to the apparent activation energies (30 to 50 kcal/mole) reported for IGSCC of Alloy 600. Furthermore, the model

is able to qualitatively explain the effects of temperature, pH, hydrogen overpressure, zinc injection, yield stress, and grain boundary carbide distribution on IGSCC.

However, to date, a quantitative model based on SDVC that can predict the cracking behavior of Alloy 600 in PWR water has not been developed.

### 4.3 Empirical Models

Because of the extreme complexity of IGA/IGSCC processes, quantitative models based on fundamental mechanisms that can predict all or even the major experimentally observed trends are not feasible at the present time or in the foreseeable future. Therefore, several empirical models have been proposed for correlating observed data. However, as with all empirical approaches, these models are valid only within the range of experimental parameters from which they were derived and should be extrapolated with caution.

#### 4.3.1 Scott model for PWSCC

Scott<sup>217</sup> developed an empirical model for PWSCC growth rates at 330°C, based on SCC growth kinetics and tube data of McIlree et al.<sup>218</sup> Scott first developed CGR as a function of the stress intensity factor and then reduced it by a factor of 5 because the laboratory test specimens had higher cold work than the field tubes. The factor of 5 was based on the observation by Cassagne and Gelpi<sup>74</sup> that CGR increased by a factor of 5-10 for cold-worked material (Fig. 16). Scott's equation at 330°C was

$$\frac{da}{dt} = 1.008 \times 10^{-2} (K_I - 9)^{1.16} \quad (13a)$$

where  $da/dt$  is in  $\mu\text{m}/\text{h}$  and  $K_I$  is in  $\text{MPa}\sqrt{\text{m}}$ .

The threshold stress intensity factor was considered to be  $9 \text{ MPa}\sqrt{\text{m}}$ . The above equation has been generalized to other temperatures by using an activation energy of 33 kcal/mole to give<sup>170</sup>

$$\frac{da}{dt} = 9.216 \times 10^9 \exp\left(-\frac{33,000}{RT}\right) (K_I - 9)^{1.16} \quad (13b)$$

where  $R = 1.987 \text{ cal/mole/K}$ .

Crack growth rates predicted by Eq. 13a and obtained experimentally are shown in Fig. 36, which also includes the predictions by Scott's internal oxidation model (Eq. 12b). The two predictions are within a factor of 2 of each other in the high- $K_I$  regime and differ from each other in the low- $K_I$  regime only because the threshold effect is built into Eq. 13a but not into Eq. 12b.

#### 4.3.2 Strain rate damage model of Garud for PWSCC

Garud and Gerber<sup>99</sup> proposed a strain rate damage model for estimating the expected time to stress corrosion crack initiation, i.e., nucleation and growth to a detectable size. The model assumes that initiation of SCC occurs when the damage reaches a critical value  $D_c$ . In this model, the damage  $D$  is defined as follows:

$$D = \int_0^t f(\dot{\epsilon}) dt \quad (14a)$$

where  $\dot{\epsilon}$  = strain rate,  $t$  = time, and  $f = \alpha \dot{\epsilon}^p$  is a damage function.

The strain rate in this model is considered to be the principal mechanical variable. The critical damage  $D_c$  depends on the material, microstructure, temperature, and environment. Note that for CERTs,  $D_c$  is given by the equation:

$$D_c = \alpha \dot{\epsilon}^p t_f \quad (14b)$$

where  $t_f$  is the time to failure.

The values of  $p$  and  $\alpha$  (assuming  $D_c = 1$ ) can be determined from a series of CERT or SSRT tests. To predict failure under a constant stress loading condition, it is necessary to compute strain rate as a function of time. Garud used the Bodner-Partom formulation for constitutive equations, which assumes that the strain rate  $\dot{\epsilon}$  equals the sum of elastic and nonelastic strain rates, which are given by

$$\dot{\epsilon}_e = \frac{\dot{\sigma}}{E} \quad (15a)$$

and

$$\dot{\epsilon}_n = \frac{2D_0}{\sqrt{3}} \exp \left[ -0.5 \left( \frac{Z}{\sigma} \right)^{2n} \right], \quad (15b)$$

where  $E$  = Young's modulus,  $D_0$  and  $n = a/T$  are material parameters,  $\sigma$  = true stress,  $\epsilon_e$  = elastic strain,  $\epsilon_n$  = nonelastic strain, and  $Z$  = hardness function such that (ignoring thermal recovery)

$$\frac{dZ}{dt} = m(Z_1 - Z)\sigma\dot{\epsilon}_n, \quad (15c)$$

where  $Z_1$  and  $m$  are constants.

Strictly speaking, the stress  $\sigma$  in Eq. 15c should be the net section stress, which is related to the nominal stress  $\sigma_{nom}$  by the equation

$$\sigma = \frac{\sigma_{\text{nom}}}{1 - \frac{2D}{h}}, \quad (15d)$$

where D is interpreted as the crack depth (symmetrical on both sides), with h as the section thickness.

However, for computing crack initiation time,  $\sigma = \sigma_{\text{nom}}$  and Eq. 15c can be integrated to

$$Z = Z_1 - (Z_1 - Z_0)\exp(-mW_p), \quad (15e)$$

where  $W_p$  = cumulative work due to nonelastic deformation,  $m = m_0T + c_0$ , and  $Z_0 = (m_1T + c_1)Z_1$ .

In general, Eqs. 14 and 15 represent a system of differential equations that must be solved numerically. For the special case of constant stress, and where  $m\sigma\epsilon$  is small when compared with unity, the strain rate can be approximated by

$$\dot{\epsilon} = \frac{\dot{\epsilon}_s}{(k\dot{\epsilon}_s t + 1)}, \quad (16a)$$

where

$$k = mn(Z_1 - Z_s)(Z_s / \sigma)^{2n-1}, \quad (16b)$$

$\dot{\epsilon}_s$  and  $Z_s$  are the initial values of  $\dot{\epsilon}$  and Z, respectively, at which the stress hold begins; and the time to failure under constant stress is given by

$$t_f = (1 - p) \left( \frac{a_f}{A} \right)^{\frac{1}{1-p}} k^{\frac{p}{1-p}}. \quad (16c)$$

The parameters p and  $a_f/A$  were used as fitting parameters to fit each data set; the other common model parameters suggested by Garud and McIlree<sup>159</sup> are listed in Table 2. They were able to fit the BNL crack initiation data (Fig. 20) at 365°C with  $p = 0.662$  and  $a_f/A = 5.59702$ , together with the model parameters for the as-received material in Table 2.

Later developments have included the modeling of crack growth through the thickness of a flat specimen and through the wall of a 360° circumferential crack.<sup>219,220</sup> The damage rate equation was cast in terms of net section stress and strain rate as follows:

$$\dot{D} = \alpha_0 \exp\left[-\frac{Q}{RT}\right] \dot{\epsilon}_{\text{net}}^\phi \quad \text{when } \dot{\epsilon}_{\text{net}} \leq \dot{\epsilon}_{\text{ucr}}. \quad (17)$$

Table 2. Garud's model parameters for as-received and mill-annealed Alloy 600

Parameter	As-Received	Mill-Annealed
$D_0$ (1/s)	10	10
$Z_1$ (ksi)	145.63	116.87
$a$ (K)	2868	5950
$m_0$ (1/ksi-K)	$1.307 \times 10^{-4}$	$0.703 \times 10^{-4}$
$c_0$ (1/ksi)	0.05826	0.13393
$m_1$ (1/K)	$-3.37 \times 10^{-5}$	$-16.35 \times 10^{-5}$
$c_1$	0.41323	0.42481

As before, Garud was able to fit van Rooyen's IGSCC depth data<sup>48</sup> at 365°C in primary water by using the following values of the parameters:

$$\phi = 0.5$$

$$\alpha_0 = 7.338 \times 10^{14}$$

$$Q = 138.07 \text{ kJ/mole}$$

$$\dot{\epsilon}_{\text{ucr}} = 5 \times 10^{-6} / \text{s},$$

where  $\dot{D}$  is in  $\mu\text{m/h}$  and the value of  $\dot{\epsilon}_{\text{ucr}}$  was suggested by the experimental data.

#### 4.3.3 Numerical model of Rebak and Smialowska

Rebak and Smialowska<sup>169</sup> used available crack growth data for Alloy 600 and fitted it with temperature, cold work (% cold work in bending), stress intensity factor ( $K_I$  in  $\text{MPa}\sqrt{\text{m}}$ ) and pH by multivariate analysis without making any assumption about mechanisms. For example at 330°C, they proposed the following correlations for CGR (in  $\mu\text{m/h}$ ):

$$\left. \frac{da}{dt} \right|_{\text{I}} = 4.7 \times 10^{-3} K_I^{1.09} \text{CW}^{0.75} \text{ for } K_I < 30 \text{ MPa}\sqrt{\text{m}} \quad (18a)$$

and

$$\left. \frac{da}{dt} \right|_{\text{II}} = 8.4 \times 10^{-3} K_I^{0.38} \text{CW}^{0.38} \text{pH}^{1.67} \text{ for } K_I > 30 \text{ MPa}\sqrt{\text{m}} \quad (18b)$$

The functional relationships of CGR with cold work in Eqs. 18a and b are valid only for cold work introduced by bending, and may change for other types of cold work. The effect of pH is approximately linear in the region of  $7 < \text{pH} < 9$  at high temperature.

#### 4.3.4 Gorman model for PWSCC

As a practical approach for utility engineers, Gorman et al.<sup>221</sup> advocated the use of an empirical equation for predicting PWSCC life (i.e., when a given fraction of population, e.g., 1%, is likely to experience PWSCC) and a two-parameter Weibull distribution for predicting how the fraction that is experiencing PWSCC varies with time. The empirical model for time to 1% PWSCC is given by

$$t_{1\%} = At_{\text{ref}} \left( \frac{\sigma}{\sigma_{\text{ref}}} \right)^n \exp \left[ \frac{Q}{R} \left( \frac{1}{T} - \frac{1}{T_{\text{ref}}} \right) \right], \quad (19)$$

where

$t_{1\%}$  = mean time at which 1% of population will fail by PWSCC

A = nondimensional material constant

$t_{\text{ref}}$  = time to 1% failure of a reference case

$\sigma$  = total stress at the material surface (MPa)

$\sigma_{\text{ref}}$  = reference stress

n = stress exponent set at 4

Q = apparent activation energy set at 50 kcal/mole

R = gas constant, 1.986 cal/mole/K

T = absolute temperature (K)

$T_{\text{ref}}$  = reference temperature.

To predict how the fraction that is experiencing PWSCC is likely to vary with time, they proposed the use of a two-parameter Weibull distribution

$$F = 1 - \exp \left[ -0.0101 \left( \frac{t}{t_{1\%}} \right)^b \right], \quad (20)$$

where

F = fraction of population experiencing PWSCC

t = time in effective full-power years (EFPY)

b = Weibull slope, a fitted parameter determined by analysis of failure data.

$$A=1$$

$$t_{\text{ref}} = 6.83 \text{ effective full power year (EFPY)}$$

$$\sigma_{\text{ref}} = 345 \text{ MPa}$$

$$T_{\text{ref}} = 589 \text{ K}$$

To determine the reference parameters they conducted statistical analyses of PWSCC data on LTMA tubes that were manufactured by a single vendor and for which the largest data base was available.

The reference time described above is the time for crack initiation plus crack growth to a size detectable by bobbin coil, i.e., to a length of  $\approx 6$  mm in the kiss roll transitions (1% cold work). This reference value must be adjusted by adjusting parameter A for cases where the amount of cold work or the crack length at detection differ from the reference case. Plant experience and laboratory tests suggest that the constant A, which is equal to 1 for LTMA material, should be set equal to 4 for HTMA material. However, if operational experience at a plant shows that the time to PWSCC is earlier or later than industry norms, the material constant A should be adjusted accordingly.

#### 4.3.5 Hernalsteen model for PWSCC

Hernalsteen\* argued that because of our current incomplete knowledge about the exact mechanisms of IGSCC, development of a predictive model for degradation of operating steam generators cannot be based on a physical model but should be based on an analytical approximation that involves a minimal number of empirical parameters derived from a thorough analysis of an inspection data base. He has proposed the following procedure:

- represent the available distribution of crack lengths during cycle n by a simple analytical function  $y_n(a)$ ,
- the distribution of crack length increments between two prior consecutive inspections by another analytical function  $z(\delta a)$ , which is assumed to be constant as long as the operational parameters are unchanged.
- a combination algorithm for the propagation law over several operational cycles.

It was claimed that a stochastic combination, where the propagation rate of a crack during any cycle is independent of the rates observed during prior cycles, seemed to fit the experimental data. Thus, the propagation law over two consecutive cycles is given by

---

\* P. Hernalsteen, *A Predictive Model for Steam Generator Degradation through PWSCC in Roll Transitions*, SMIRT-10, Vol. D, p. 183, Los Angeles, 1989.

$$z_2(\delta a) = \int_0^{\delta a} z(t)z(\delta a - t)dt, \quad (21)$$

and the distribution curve for crack length after two cycles can be obtained by either

$$y_{n+2}(a) = \int_0^a y_n(t)z_2(a - t)dt \quad (22a)$$

or the repetitive application of the equation:

$$y_{n+1}(a) = \int_0^a y_n(t)z(a - t)dt. \quad (22b)$$

The general shape of the observed histograms (Figs. 37 a and b) for crack sizes and crack length increments suggested a curve-fitting by a gamma distribution function as follows:

$$f_\alpha(t) = \beta^\alpha t^{\alpha-1} e^{-\beta t} / \Gamma(\alpha), \quad (23)$$

where  $\alpha$  is a shape factor,  $\beta$  is a scaling factor, and  $\Gamma$  is the gamma function. From the properties of the assumed distribution curve and Eqs. 21 and 22a and b, the following simple relationships were derived:

$$z(\delta a) = f_1(\delta a) = \beta e^{-\beta \delta a} \quad (24a)$$

$$z_m(\delta a) = f_m(\delta a) \quad (24b)$$

$$y_n(a) = f_n(a) \quad (24c)$$

$$y_{n+m}(a) = f_{n+m}(a). \quad (24d)$$

The measured crack length increment data (from 186 cracked tubes) could be fitted initially by assuming  $\beta = 0.8/\text{mm}$ , which corresponds to an average crack length increment of 1.25 mm/cycle. However, after 100% rotating pancake coil (RPC) inspection data from 1585 cracked tubes became available, the best fit of crack length measurement data led to

$$\alpha = 9.09, \text{ and } \beta = 1.26,$$

with an excellent correlation coefficient of  $R^2 = 99\%$ .

However, the inspection data clearly indicated that the longest cracks are likely to propagate less during the next cycle than shorter cracks. To account for this, the following improved model was postulated.

For a population subset of crack length  $x$ , a fraction  $e^{-kx}$  will not propagate during the next cycle, while the remaining fraction  $1 - e^{-kx}$  will follow a similar probability law as assumed earlier. This assumption led to a more complicated expression for crack length evolution with cycle,

$$y_n(a) = \beta e^{-\beta a} (1 - e^{-ka})^{n-1} \prod_{i=1}^{n-1} \left(1 + \frac{\beta}{ik}\right). \quad (25)$$

A value of  $k = 0.11/\text{mm}$  correctly reproduced the dependence of crack length increment on initial crack length.

#### 4.3.6 EPRI model for caustic SCC

Eason and Nelson<sup>222</sup> have analyzed C-ring caustic stress corrosion cracking data that was generated at Westinghouse from five heats of Alloy 600 tubes in both mill-annealed and thermally treated condition to produce a model for the crack initiation time and CGR. The model is valid over a range of the data, which included 1, 10, and 50% caustic solutions at temperatures that ranged from 288 to 343°C. The model consists of two parts, a probabilistic model of time to crack initiation (chosen because of the large scatter in initiation data) and a deterministic model of CGR, given that initiation has occurred (IGSCC initiation was defined as a 20- $\mu\text{m}$ -deep crack,  $a_0$ ). Both parts of the model depend on heat treatment, caustic concentration, temperature, and strain (after converting from the reported displacement data). Because more mill-annealed material than thermally treated material cracked, the model was developed for the mill annealed material, with the assumption that the same model with different fitting constants would apply to the thermally treated material.

For each category of caustic concentration, temperature, and strain, the time to crack initiation ( $t_0$ ) was fitted by a two-parameter Weibull distribution:

$$F(t_0) = 1 - \exp(-t_0/\eta)^\beta, \quad (26)$$

where  $\beta$  = slope and  $\eta$  = characteristic time.

The dependence of these fitting parameters on caustic concentration, temperature, and strain was determined by regression analyses. It was found that the slope parameter  $\beta$  was not a strong function of any of these variables. An average value was used for each heat treatment and caustic concentration. On the other hand, the value of  $\eta$  strongly depended on all of the variables. The model fitted to  $\eta$  (in h) was as follows:

$$\eta = a_1 + a_2 T + a_3 \ln(\epsilon/0.002), \quad (27)$$

where T is in °F, and  $a_1$ ,  $a_2$ , and  $a_3$  are constants (in h) for each caustic concentration.

For example, in 10% NaOH solution,

$a_1 = 24422$ ,  $a_2 = -33.303$ ,  $a_3 = -242.39$ , and  $\beta = 1.569$  for the mill-annealed material

$a_1 = 105054$ ,  $a_2 = -157.82$ ,  $a_3 = -248.96$ , and  $\beta = 1.778$  for the thermally treated material.

The crack growth data were represented as follows:

$$a / t = b_1 + b_2 T + b_3 \epsilon \quad \text{for } \epsilon \geq 0.002 \quad (28a)$$

$$a / t = (a / t)|_{\epsilon=0.002} \left( \frac{\epsilon}{0.002} \right) \quad \text{for } \epsilon < 0.002, \quad (28b)$$

where a is the crack length at time t after initiation. For example, in 10% NaOH solution (a/t is in  $\mu\text{m}/\text{h}$ ),

$b_1 = -5.724$ ,  $b_2 = 1.04 \times 10^{-2}$ ,  $b_3 = 1.988$ , for the mill-annealed material

$b_1 = -0.2586$ ,  $b_2 = 4.679 \times 10^{-4}$ ,  $b_3 = 0.6368$  at  $T < 630^\circ\text{F}$  for the thermally-treated material

$b_1 = -7.498$ ,  $b_2 = 1.196 \times 10^{-2}$ ,  $b_3 = 0.6368$  at  $T \geq 630^\circ\text{F}$  for the thermally-treated material.

## 5 Discussion and Conclusions

---

The literature on IGA/IGSCC of Alloy 600 in PWR water is vast, with contributions from every country that has operating PWRs. Although more than 200 publications have been reviewed for this report, the search has not been exhaustive. The literature exclusively reports crack initiation and growth. A literature search on the phenomena of crack arrest and crack reinitiation in Alloy 600 in PWR water did not identify any publication that systematically studied the criteria or conditions under which they occur. Examples of "crack arrest" in tubes in steam generators can be found in Europe, where not all defective tubes are plugged or sleeved on detection. In spite of extensive research that extends over four decades, the definitive mechanisms responsible for PWSCC on the primary side and IGA/IGSCC on the secondary side still remain elusive. However, a large body of experimental work has helped to establish several empirical facts about IGA/IGSCC of Alloy 600. Certain conclusions are common to both primary and secondary side SCC:

- Alloy 600 is susceptible to IGA/IGSCC in aqueous and steam environments at high temperature (>280°C). The level of susceptibility, threshold stresses, and CGRs depend on material conditions (i.e., heat-treatment and microstructure), but IGA/IGSCC will occur in some environments for virtually all conditions of the alloy.
- An HTMA or thermally treated Alloy 600 with continuous or semicontinuous grain boundary carbide is generally more resistant to IGA/IGSCC (both initiation and propagation) than LTMA material.
- The threshold stress and CGRs for IGSCC in Alloy 600 depend on the environment. Stress near yield is required to cause cracking in environments such as pure or primary water. Lower threshold stresses are observed in concentrated environments (e.g., NaOH and acid sulfates). Details of what constitutes an aggressive environment for Alloy 600 are not well understood, but recent field experience indicates that high or low pH is not required, i.e., cracking will occur at moderate stresses in near-neutral environments.
- A key to understanding IGA/IGSCC is the effect of the environment on the composition, structure, and stability of the surface oxide film. Formation of a stable, thin, adherent, and dense chromium-rich spinel oxide is the reason for the high resistance of Alloy 600 to IGSCC in mildly acidic to neutral water. The breakdown of such a protective oxide in high-pH water is partly responsible for the aggressive effect of such water on Alloy 600. However, work to date on protective oxides has been suggestive but not definitive.
- Increase in temperature leads to shorter IGA/IGSCC life, both for crack initiation and crack propagation. The relatively high apparent activation energy of  $\approx 30\text{-}40$  kcal/mole with a large scatter band indicates that the rate-limiting step cannot be liquid diffusion and probably represents a combination of several processes. The high apparent activation energy (50-54 kcal/mole) derived from

field experience does not correlate with any known physical mechanism; a single mechanism with an activation energy that high would not be observed at 300°C (600 K) because it would be too slow.

- Resistance to IGSCC is very high at neutral pH and decreases with increasing or decreasing pH.
- Lead is detrimental to TGSCC/IGSCC at acidic to caustic pH values.
- Grain boundary sliding rate (rather than total creep strain rate) appears to be important for IGSCC. Coincident-site-lattice (or low  $\Sigma$ ) boundaries are more resistant to grain boundary sliding and IGSCC than random high-angle boundaries.

### 5.1 Deaerated Hydrogenated Pure Water

- A high stress close to yield is needed for PWSCC. Crack initiation life is inversely proportional to approximately the fourth power of stress. When compared with mill-annealing, cold work reduces life by a factor of 3-4 and thermal treatment increases life by a factor of 2-3. The threshold stress for PWSCC is relatively high,  $\approx 50-70\%$  of yield stress, for mill-annealed Alloy 600.
- The smaller the grain size and the higher the yield stress, the more susceptible the alloy is to PWSCC.
- Life decreases with increasing hydrogen partial pressure for tests in high-temperature water or steam. However, the effect saturates at a partial pressure of  $\approx 0.05$  MPa, beyond which, life improves.
- Crack growth rate data from various sources as a function of stress intensity factor show that, at a given stress intensity factor, the scatter in the CGR data is approximately a factor of 100. The threshold stress intensity factor is  $\approx 10$  MPa $\sqrt{m}$ .
- Experimental data fail to show any consistent influence of trace impurities, such as sulfur, phosphorus, and silicon, on PWSCC.

### 5.2 Deaerated Caustic Solution

- The deleterious effect of a caustic environment increases with increasing caustic concentration from 1 to 10%, beyond which a saturation effect is observed. The threshold stress for IGSCC initiation in a caustic environment (10% NaOH) is relatively low,  $\approx 40-50\%$  of yield stress, for mill-annealed material. However, the French have reported a much higher threshold stress (80% of yield stress). Threshold stress for thermally-treated material is significantly higher than that for mill-annealed material.

- Unlike PWSCC, higher yield stress may not necessarily be detrimental for IGA/IGSCC in caustic environments because some data tend to indicate that threshold stress for IGA/IGSCC increases with increasing yield stress. Indirect field evidence for this is the occurrence of either PWSCC or ODSCC as the main degradation mechanism in many plants. However, a mixture of both ID and OD cracking mechanisms is also sometimes observed.
- Crack growth rate in caustic water is approximately a factor of 2 greater than that in primary water at the same stress intensity factor. For crack depths  $\leq 25 \mu\text{m}$  in caustic ( $>1\%$  NaOH), the kinetics are one order of magnitude slower for IGA than for IGSCC.
- Intergranular attack occurs (with or without applied stress) in high pH solutions near the normal corrosion potential (0 mV measured against nickel) of Alloy 600 and generally increases with increasing potential up to 80 mV. In this regime, Alloy 600 does not appear to have a protective film. In the absence of stress, IGA depth follows a parabolic growth law. The kinetics of IGA are accelerated by stress and gradually change from parabolic to linear with increasing stress. Currently, it is hard to distinguish IGA from IGSCC of short corrosion cracks.

### 5.3 Deaerated Acidic Solution

- At low pH and high sulfate-to-chloride ratios, wastage outpaces crack growth and IGSCC is not observed in Alloy 600. As sulfate is replaced by chloride while pH is maintained constant, wastage is decreased and IGSCC occurs.
- Alloy 600 in the LTMA or HTMA condition shows the least resistance to IGSCC, with sensitized Alloy 600 and thermally treated Alloy 600 following in order.

### 5.4 PWSCC Mechanisms

PWSCC is observed over a limited range of potential that is centered on the Ni/NiO equilibrium in neutral to slightly alkaline solutions. The composition of the protective spinel oxide scale that is formed changes rapidly in this region. The film rupture/dissolution/repassivation mechanism suggests itself as a natural candidate, because of the known importance of the oxide scale to IGSCC resistance. However, the film repair kinetics do not appear to correlate with PWSCC sensitivity. The apparent activation energy for PWSCC is too high for liquid diffusion to be the rate-controlling process in a film rupture/dissolution/repassivation mechanism. It has been speculated that ion transport in the oxide, or oxygen transport into the metal could be rate controlling. Although available PWSCC crack growth data on Alloy 600 have been correlated with the film rupture/anodic dissolution model by treating the exponent in the CGR equation as a fitting parameter, it is not clear how the environment, material chemistry, and temperature combine to give such a value for the exponent.

Pickled specimens have long been known to exhibit shorter IGSCC lives than companion nonpickled specimens. Specimens exposed to SCC testing in primary water

have been reported to continue to crack intergranularly (or initiate new cracks) after being transferred from the environment to room temperature air. In some IGSCC testing, incidences of intergranular cracking were located preferentially at the specimen interior, where the cracking is excluded from direct contact with the environment. Creep rate of Alloy 600 in deaerated, hydrogenated, high-temperature water has been found to be significantly enhanced as compared with that in argon. All of these observations are indirect evidence that link hydrogen with SCC. However, the lack of dependence of creep rate in hydrogenated water on applied potential does not support a hydrogen mechanism. No IGSCC is found in Alloy 600 when tests are conducted in dry hydrogen at high pressure. It is generally agreed that if hydrogen has any effect at all, it is the cathodic hydrogen and not the hydrogen dissolved in the environment that is important for IGSCC. However, currently, a quantitative hydrogen-assisted-cracking-based model for predicting PWSCC life is not available.

Each of the various other mechanisms that have been discussed in this report has some attractive features that explain, at least qualitatively, some but not all aspects of PWSCC. The enhanced-surface-mobility model correctly predicts the formation of NiO that is necessary for IGSCC to occur above 250°C, which is the equilibrium temperature for its formation. Nucleation time, according to this model, can be interpreted as the time to form a low-melting-point compound. The internal-oxidation model explains the influence of surface finish, grain size, cold work, grain boundary structure, and carbide morphology on IGSCC through their influence on oxygen diffusivity; it does not require a liquid phase and is gaining credence from the observation of IGSCC along scratches and general IGA in the superheated steam space of OTSGs. Recent ATEM and SIMS work is beginning to provide direct metallurgical evidence that supports this mechanism.

The CDI model correctly explains the observed lack of correlation between total hydrogen absorption and SCC susceptibility; it also explains the observed increase in severity of SCC with increasing hydrogen pressure from 0 to 4 bars that is followed by decreased severity at higher hydrogen pressure.

The SDVC model correctly predicts an activation energy (that corresponds to diffusion of iron cations through growing oxides) that is in the range of activation energies reported for IGSCC. However, no quantitative models are available for crack growth based on the CDI or SDVC mechanisms.

Although the exact mechanisms of PWSCC initiation and growth are not well understood, on a more practical level, the empirical models for PWSCC have been used extensively because they can represent the available crack growth data in a user-friendly fashion. The crack initiation data for PWSCC appear to fall into a relatively broad scatter band in the temperature range of interest. Some of the approaches take into consideration the statistical nature of PWSCC failure and make use of available nondestructive evaluation inspection data from existing plants. Because of the relatively well-controlled chemistry of the primary water and the lack of concentrating crevices in the primary side, such empirical approaches appear to be adequate as long as the maximum stress (applied plus residual) can be estimated correctly. Currently

lacking is data on slow growth (near threshold) of short cracks. Most of the available crack growth data are for fast growing, relatively long cracks.

## 5.5 IGA/ODSCC Mechanisms

In contrast to the chemical and electrochemical environment on the primary side, the corresponding environment in the secondary side is vastly more complex, because the control of secondary-water chemistry is less stringent and also because much of the secondary-side cracking occurs in crevices and under sludge piles at the TTS and TSP junctions. The exact environment in these inaccessible regions is still largely unknown because it is next to impossible to obtain direct measurements in these regions. Data from model boilers may not be representative of plant conditions, because studies are performed in bulk water in which the concentration of impurities is increased to accelerate the tests. It was traditionally assumed that local boiling and poor circulation would tend to concentrate caustic impurities in superheated crevices and under sludge piles. This position was backed up by calculations performed with codes like MULTEQ, with inputs from hideout return data. Therefore, many experimental data have been generated on the IGA/IGSCC behavior of Alloy 600 in highly caustic solutions and a good understanding of the mechanisms of IGA/IGSCC of Alloy 600 in caustic solutions has been developed.

It has sometimes been suggested that local environments might be more appropriately represented by molten salts (or steam to simulate steam blanketing) rather than caustic solutions. This suggestion has been made even though a molten-salt (or steam) environment is not necessarily more aggressive than concentrated caustics, because the enhanced possibility that separated anodic and cathodic reactions can proceed in aqueous solutions would give them a catalytic advantage over processes that are direct chemical oxidations, especially at lower temperatures.

It is known that IGSCC is stress assisted and occurs in the active/passive transition in a limited potential range above the Ni/NiO equilibrium, where chromium is too soluble to contribute to passivity, and film repair kinetics are slow. Caustic IGA can occur without applied tensile stress (or even under applied compressive stress) in the absence of protective oxide film at potentials below the Ni/NiO equilibrium and proceed by the selective dissolution of iron and chromium, which is faster along the grain boundaries than in the grains.

The morphology of IGA/IGSCC in pulled tubes shows many similarities with that caused by caustic solutions in the laboratory, e.g., the presence of a degraded, nonprotective, brittle oxide film composed of NiO in the case of caustics but frequently chromium-rich for the pulled tubes. All of the SCC results from Alloy 600 in strong caustic solutions are consistent with a classical anodic-dissolution mechanism concentrated at the more active grain boundaries. A troubling aspect is the high apparent activation energy of 20-60 kcal/mole associated with IGA/IGSCC. The high activation energy for IGSCC is possibly associated with transport of iron through the oxide film.

In the case of IGA, selective dissolution of the grain boundaries could be controlled by intergranular diffusion of iron and chromium, a process that is more rapid than diffusion through the grains themselves. One consequence of a very alkaline crevice is a significant difference in potential between the crevice and the free-span tube. However, it is unlikely that the crevice surfaces are anodically polarized because of the high resistances of the bulk water and the tortuous diffusion path in heavily fouled crevices (see discussions later). It is even more unlikely in steam-blanketed crevices with a small volume of concentrated liquid.

Recent analyses of the deposits on pulled tubes suggest that the environment in the crevices is neither highly caustic nor highly acidic, but is near neutral to slightly alkaline. We have already alluded to other uncertainties in the concentrating mechanisms in the crevices. The presence of plugged crevices increases the potential for local dryouts and the crevice environment may approach that of laboratory tests with doped steam. It is difficult to explain some of the secondary-side cracking observed in plants as having occurred in a liquid environment because not enough impurities enter the steam generators to fill the crevice volumes in which the cracking occurs. A possible explanation for the cracking over the full height of the crevice, despite the crevice not being filled by liquid, is that much of it occurred in a contaminated steam environment.

On the surface, steam blanketing of most of the crevice would suggest that the inside and outside of the crevice are not electrically connected. Although it has been estimated that a minor continuous path of liquid through a tortuous path is all that is required to polarize the crevice, the limits for such a minor path are not certain. If polarization of crevices is to be effective, voltage drop through the solution path must be small when compared with the ECP difference that is due to differences in pH between the crevice environment and the bulk water plus an additional ECP drop due to the presence of oxidants in the bulk water. A similar concern exists about the differences in pH and potential between the crack tip and the bulk water.

Recently, it has been observed that SCC of some steam generator tubes depends more on the number of cycles and shutdowns than on the time of exposure itself.<sup>223</sup> Although the results are preliminary, it has been hypothesized that secondary side corrosion may be driven by a galvanic effect due to the presence of an oxidizing agent such as copper oxide. Corrosion rate decreases during operation as the oxidized metal is reduced to the metallic form; it could decrease very rapidly during service because of the highly reducing environment. During an outage, under uncontrolled aerated conditions, the metallic copper might be oxidized again, resulting in corrosion during the next cycle. Nedden et al.<sup>224</sup> have claimed that this hypothesis is consistent with observed ODS/SCC behavior at the TSP of the Doel 4 plant; they verified it in the laboratory with simulated cold shutdowns in which they used a series of capsule tests in an acid sulfate environment that contained metallic copper.

As is clear from the above discussions, the greatest uncertainty in predicting IGA/IGSCC life of steam generator tubing is in predicting the local environment within crevices or under sludge piles, where crack initiation occurs. Furthermore, crack initiation data that are generated in autoclave systems are not directly applicable to the

prediction of the crack initiation life of steam generator tube bundles, because the bulk of the time necessary to nucleate cracks in a steam generator is spent in developing the necessary local chemistry for cracking within the crevices. This process is, of course, dependent on the operational details of each steam generator. Model boiler data are not very helpful for this purpose because the concentration of bulk impurities is usually increased to accelerate the tests. From laboratory data on caustic or acidic SCC, one could argue that once the appropriate chemistry is established within the crevices or under sludge piles, crack initiation should occur relatively quickly. However, it must be emphasized that OD-initiated SCC has also been observed in noncrevice regions such as surface scratches at mid-spans. These observations, together with IGA observed in the superheated steam space of an OTSG, would require the invocation of corrosion mechanisms other than crevice corrosion (e.g., internal oxidation).

By applying linear elastic fracture mechanics (LEFM) techniques, crack propagation data (usually from a single, long, dominant crack) that are generated in autoclaves can be useful for predicting the crack growth life during the final rapid propagation stage of a single crack or of widely separated cracks. But early cracking in the secondary side often involves slow growth of closely spaced multiple cracks or cellular cracks, for which the usual LEFM techniques may not be applicable.

## **6 Recommended Future Tests**

---

### **6.1 PWSCC**

An extensive data base on crack initiation and crack propagation of Alloy 600 in hydrogenated deaerated water at high temperatures is already compiled. Much of the crack growth data is, in reality, average CGR over the life of the test and is subject to large uncertainty because of uncertainty in crack initiation time. Crack growth data on relatively short cracks (both axial and circumferential), generated by systems for monitoring crack length during the tests, are needed.

### **6.2 IGA/ODSCC**

An extensive autoclave-generated data base on crack initiation and crack propagation of Alloy 600 in high conductivity acidic and caustic environments is available. If crevice environments in steam generators are near neutral and not steam blanketed, they still must exhibit high ionic conductivity because they must be concentrated to be in equilibrium with the temperature. The data base should be augmented by additional controlled-ionic-conductivity crack initiation and crack propagation tests in near-neutral water and in "doped" steam environments. The CGR studies should emphasize testing of specimens with short cracks and should be conducted with a crack length monitoring system.

However, the biggest obstacle to developing an IGA/ODSCC life prediction methodology for a steam generator tube bundle is the uncertainty in the environment. Recent European attempts to better define the chemical state of crevices by analyzing deposits from TSP and TS crevices of retired steam generators should be continued. In particular, deposits in crevices from TSPs and TSs with cracks should be compared with those without cracks. Model boiler tests (with multiple tubes) with superheated crevices can be helpful in shedding some light on the crack initiation processes in prototypic crevices. The problem with model boilers is, of course, that for practical reasons, the test must be accelerated either by increasing the impurity content or the temperature of the bulk secondary water. Although the results from model boiler tests are not directly applicable to actual steam generators, they can be used to develop and validate models for predicting the development of crevice chemistry and stress corrosion cracks with time. Also, they can be used to test the validity of the hypothesis that the number of startup and shutdown cycles is more important for IGSCC than the time of exposure.

### **6.3 Crack Arrest and Reinitiation**

Currently, data that would help develop criteria for crack arrest and crack reinitiation in Alloy 600 steam generator tubing are not available. As mentioned earlier, tubes with throughwall cracks at kiss roll transitions have been known to be in service for many years with no apparent crack growth. Basically the cracks stop growing or grow very slowly once the tips get out of the high-stress region. Most likely, these cracks would start growing without any reinitiation step if a source of high stress (e.g., denting) was introduced. However, experimental evidence is lacking. Because these

data are necessary for developing our capability to predict IGSCC lives of steam generator tubing, they should be generated in the future to assist the development of criteria for crack arrest and crack reinitiation.

## References

---

1. F. L. LaQue, *Personal communication*, as reported by W. L. Williams and J. F. Eckel in, *Corrosion and Wear Handbook for Water Cooled Reactors*, Chapter 10, D. J. Paul, ed., USAEC TID 7006 (March 1957), pp. 117,165.
2. W. J. Singley, I. H. Welinsky, S. F. Whirl, and H. A. Klein, *Stress Corrosion of Stainless Steel and Boiler Water Treatment at Shippingport Atomic Power Station*, pp. 748–768 in *Proc. Amer. Power Conf.*, Vol. XXI (1959).
3. I. H. Welinsky, W. F. Brindley, W. E. Berry, and S. F. Whirl, *Final Evaluation of Shippingport Power Station's Stainless Steel Generator after Five Years*, pp. 1–13 in *Proc. Symp. on High Purity Water Corrosion of Metals*, 23rd NACE Conf., National Association of Corrosion Engineers, Houston, TX (1968).
4. C. F. Cheng, *Intergranular Stress-Assisted Corrosion Cracking of Austenitic Alloys in Water-Cooled Nuclear Reactors*, *J. Nucl. Mater.*, Vol. 56 (1975), pp. 11–33.
5. R. H. McKane, H. C. Minton, and J. W. Wade, *Stainless Steel Failure in Savannah River Plant Reactor Areas*, DP-539, DuPont Co., Wilmington, DE (Oct. 1960).
6. W. E. Berry, O. M. Stewart, and F. W. Fink, *Examination of a Nonregenerative Heat Exchanger from the USS Nautilus (SNN-571)*, BMI-1416, Battelle Memorial Institute (Feb. 1960).
7. W. K. Kratzer, *304 Stainless Steel Steam Generator Tube Experience at N-Reactor*, DUN-SA-178, DuPont Co., Wilmington, DE (Sept. 1971).
8. S. H. Bush and R. L. Dillon, *Stress Corrosion in Nuclear Systems*, CONF-730605-2, Battelle Northwest Laboratory (March 1973).
9. H. A. Wagner, *Light Water Reactor Experience in the United States of America*, pp. 503–520 in *Performance of Nuclear Power Reactor Components*, CONF-691115, International Atomic Energy Agency, Vienna (1970).
10. J. M. Gras, *Stress Corrosion Cracking of Steam Generator Tubing Materials*, in *Proc. Parkins Symp. on Fundamental Aspects of Stress Corrosion Cracking*, S. M. Bruemmer et al., eds., The Minerals, Metals, & Materials Society, Warrendale, PA (1992), pp. 411–432.
11. *Steam Generator Progress Report, Revision 13*, Worldwide web address <http://www.epri.com/npg/cr/sgims13/index.html>, Electric Power Research Institute, Palo Alto, CA (May 1998).
12. Steam Generator Owners Group, *Steam Generator Reference Book*, Electric Power Research Institute, Palo Alto, CA (1985).

13. H. Coriou, L. Grall, C. Mahieu, and M. Pelas, *Sensitivity to Stress Corrosion and Intergranular Attack of High-Nickel Austenitic Alloys*, Corrosion, Vol. 22 (1966), pp. 280-290. Coriou's first paper (in French) *Corrosion Fissurante Sous Contrainte De L'Inconel Dans L'Eau a Haute Temperature*, appeared in 3rd Colloque de Metallurgie - Corrosion, Centre D'Etudes Nuclearies de Saclay (1959).
14. H. R. Copson and W. E. Berry, *Corrosion of Inconel Nickel-Chromium Alloy in Primary Coolants of Pressurized Water Reactors*, Corrosion, Vol. 18 (1962), pp. 21t-26t.
15. *PWR primary water chemistry guidelines: Revision 2*, EPRI NP-7077, Final report, Electric Power Research Institute, Palo Alto, CA (Nov. 1990).
16. *Steam Generator Reference Book*, EPRI TR-103824 (Dec. 1994).
17. J. P. N. Paine, R. S. Pathania, and C. E. Shoemaker, *Effect of Caustic Environment on Intergranular Attack and Stress Corrosion Cracking of Alloy 600*, Proc. 3rd Int. Symp. on Environmental Degradation of Materials in Nuclear Power Systems—Water Reactors, Traverse City, MI, The Metallurgical Society/AIME, Warrendale, PA (1988), pp. 501-509.
18. *PWR secondary water chemistry guidelines - Revision 3*, prepared by Secondary Water Chemistry Guidelines Revision Committee, EPRI-TR-102134, Electric Power Research Institute, Palo Alto, CA (May 1993).
19. S. J. Green and J. P. N. Paine, *Materials Performance in Nuclear Pressurized Water Reactor Steam Generators*, Nucl. Technol., Vol. 55 (1981), pp. 10-29.
20. C. S. Welty, Jr. and J. C. Blomgren, *Steam Generator Issues*, Proc. of the Fourth Int. Symp. on Environmental Degradation of Matls. in Nuclear Power Systems - Water Reactors, Ed. D. Cubicciotti, ed., NACE, Houston, TX (1990), pp. 1-27, 1-36.
21. H. R. Copson and S. W. Dean, *Effects of Contaminants on Resistance to Stress Corrosion Cracking of Ni-Cr Alloy 600 in Pressurized Water*, Corrosion, Vol. 21 (1965), pp. 1-8.
22. H. R. Copson and G. Economy, *Effects of Some Environmental Conditions on Stress Corrosion Behavior of Ni-Cr-Fe Alloys in Pressurized Water*, Corrosion, Vol. 24 (1968), pp. 55-65.
23. A. J. Sedriks, S. Floreen, and A. R. Mc Ilree, *The Effect of Nickel Content on the Stress Corrosion Resistance of Fe-Cr-Ni Alloys in an Elevated-Temperature Caustic Environment*, Corrosion, Vol. 32 (1976), pp. 157-158.
24. A. R. Mc Ilree and H. Y. Michels, *Stress Corrosion Behavior of Fe-Cr-Ni and Other Alloys in High-Temperature Caustic Solutions*, Corrosion, Vol. 33 (1977), pp. 60-67.

25. G. J. Theus, *Caustic Stress Corrosion Cracking of Inconel-600, Incoloy-800, and Type 304 Stainless Steel*, Nucl. Technol., Vol. 28 (1976), pp. 388-397.
26. G. J. Theus, *Relationship Between Acid Intergranular Corrosion and Caustic Stress Corrosion Cracking of Alloy 600*, Corrosion, Vol. 33 (1977), pp. 20-26.
27. H. A. Domian, R. H. Emanuelson, L. W. Sarver, G. J. Theus, and L. Katz, *Effect of Microstructure on Stress Corrosion Cracking of Alloy 600 in High-Purity Water*, Corrosion, Vol. 33 (1977), pp. 26-37.
28. G. J. Theus, *Materials Degradation in Water Reactors*, Proc. of 1988 JAIF Int. Conf. on Water Chemistry in Nuclear Power Plants - Operational Experience and New Technologies for Management, Vol. 1, Japan Atomic Ind. Forum, Tokyo, Japan (1988), pp. 69-80.
29. F. P. Vaccaro, G. J. Theus, B. P. Miglin, and S. Roy, *The Effect of Steam Generator Tube Temperature on the Stress Corrosion Cracking of Alloy 600*, Proc. of the Water Chemistry and Materials Performance Conf., Pub. Canadian Nuclear Society, Toronto, Ont., Canada (1986), pp. 45-54.
30. G. J. Theus, *Primary Side Stress Corrosion Cracking and Remedial Measures*, Trans. Am. Nucl. Soc., Vol. 53 (1986), pp. 207-208.
31. R. H. Emanuelson, D. F. Levstek, K. E. Moore, and G. J. Theus, *Materials Model Boiler Tests for the Babcock & Wilcox Once-Through Steam Generators*, Nucl. Tech., Vol. 55 (1981), pp. 422-435.
32. G. J. Theus and R. H. Emanuelson, *Stress Corrosion Cracking of Alloy 600 and Alloy 690 in All Volatile Treated Water at Elevated Temperatures. Final Report (PWR)*, EPRI-NP-3061, Electric Power Research Institute, Palo Alto, CA (1983).
33. B. P. Miglin, L. W. Sarver, J. V. Monter, and G. J. Theus, *Predicting Caustic IGA in Nuclear Steam Generator Tubing*, Proc. 3rd Int. Symp. on Environmental Degradation of Materials in Nuclear Power Systems—Water Reactors, Traverse City, MI, The Metallurgical Society/AIME, Warrendale, PA (1988), pp. 535-544.
34. S. L. Harper, B. P. Miglin, J. V. Monter, and G. J. Theus, *The Role of Sulfur in the Corrosion of NSG*, Proc. 3rd Int. Symp. on Environmental Degradation of Materials in Nuclear Power Systems—Water Reactors, Traverse City, Michigan, The Metallurgical Society/AIME, Warrendale, PA (1988), pp. 457-463.
35. F. W. Pement, I. L. W. Wilson, and R. G. Aspden, *Stress Corrosion Cracking Studies of High Nickel Austenitic Alloys in Several High-Temperature Solutions*, Materials Performance, Vol. 19 (1980), pp. 43-49.
36. G. P. Airey, *Optimization of Metallurgical Variables to Improve Corrosion Resistance of Inconel 600*, EPRI NP-3051, Electric Power Research Institute, Palo Alto, CA (1983).

37. G. P. Airey, *The Stress Corrosion Cracking Performance of Inconel Alloy 600 in Pure and Primary Water Environments*, EPRI Workshop on Primary-Side SCC of PWR Steam Generator Tubing, Clearwater Beach, FL, EPRI NP-5498, Electric Power Research Institute, Palo Alto, CA (1987).
38. G. Economy, R. J. Jacko, and F. W. Pement, *IGSCC Behavior of Alloy 600 Steam Generator Tubing in Water or Steam Tests above 360°C*, *Corrosion*, Vol. 43 (1987), pp. 727-734.
39. J. N. Esposito, G. Economy, W. A. Byers, J. B. Esposito, F. W. Pement, R. J. Jacko, and C. A. Bergmann, *The Addition of Zinc to Primary Reactor Coolant for Enhanced PWSCC Resistance*, Proc. 5th Int. Symp. on Environmental Degradation of Materials in Nuclear Power Systems—Water Reactors, Monterey, CA, American Nuclear Society, La Grange Park, IL (1991), pp. 495-500.
40. R. J. Jacko, G. Economy, and F. W. Pement, *The Influence of Dissolved Hydrogen on Primary Water Stress Corrosion Cracking of Alloy 600 at PWR Steam Generator Operating Temperatures*, Proc. 5th Int. Symp. on Environmental Degradation of Materials in Nuclear Power Systems—Water Reactors, Monterey, CA, American Nuclear Society, La Grange Park, IL (1991), pp. 613-620.
41. G. L. Webb, *Environmental Degradation of Alloy 600 and Welded Filler Metal EN82 in an Elevated-Temperature Aqueous Environment*, Proc. 6th Int. Symp. on Environmental Degradation of Mats. in Nucl. Power Systems—Water Reactors, San Diego (1993), The Metallurgical Society/AIME, Warrendale, PA, pp. 687-695.
42. G. L. Webb and M. G. Burke, *Stress Corrosion Cracking Behavior of Alloy 600 in High-Temperature Water*, Proc. 7th Int. Symp. on Environmental Degradation of Mats. in Nucl. Power Systems—Water Reactors, Breckenridge, CO, NACE, Houston, TX (1995), pp. 41-56.
43. D. van Rooyen, *Review of the Stress Corrosion Cracking of Inconel 600*, *Corrosion*, Vol. 31 (1975), pp. 327-337.
44. T. S. Bulischeck, Y. S. Park, and D. van Rooyen, *Stress Corrosion Cracking of Inconel 600 Tubing in Deaerated High-Temperature Water*, NUREG/CR-0858, Brookhaven National Laboratory, Upton, NY (1979).
45. T. S. Bulischeck and D. van Rooyen, *Experimental Investigation of the SCC of Inconel 600 and a Predictive Model for Evaluating Service Performance*, NUREG/CR-1675, Brookhaven National Laboratory, Upton, NY (1980).
46. T. S. Bulischeck and D. van Rooyen, *Stress Corrosion Cracking of Alloy 600 Using the Constant Strain Rate Test*, *Corrosion*, Vol. 37 (1981), pp. 597-607.

47. T. S. Bulischeck and D. van Rooyen, *Effect of Environmental Variables on the Stress Corrosion Cracking of Inconel 600 Steam Generator Tubing*, Nucl. Technol., Vol. 55 (1981), pp. 383-393.
48. R. Bandy and D. van Rooyen, *Stress Corrosion Cracking of Inconel Alloy 600 in High-Temperature Water - An Update*, Corrosion, Vol. 40 (1984), pp. 425-430.
49. R. Bandy and D. van Rooyen, *Mechanisms of Intergranular Failures in Alloy 600 in High-Temperature Environments*, BNL-NUREG-34270 (1984).
50. R. Bandy, R. Roberge and D. van Rooyen, *Intergranular Failures of Alloy 600 in High-temperature Caustic Environments*, Paper 179, Corrosion 84, New Orleans (1984).
51. U. C. Kim and D. van Rooyen, *Strain Rate and Temperature Effects on the Stress Corrosion Cracking of Inconel 600 Steam Generator Tubing in the Primary Water Conditions*, Proc. 2nd Int. Symp. on Environmental Degradation of Materials in Nuclear Power Systems—Water Reactors, Monterey, CA, American Nuclear Society, La Grange Park, IL (1985), pp. 448-455.
52. N. Totsuka, E. Lunarska, G. Cragolino, and Z. Szklarska-Smialowska, *Effect of Hydrogen on the Intergranular stress Corrosion Cracking of Alloy 600 in High-Temperature Aqueous Environments*, Corrosion, Vol. 43 (1987), pp. 505-514.
53. Z. Szklarska-Smialowska, *Factors Influencing IGSCC of Alloy 600 in Primary and Secondary Waters of PWR Steam Generators*, Proc. 4th Int. Symp. on Environmental Degradation of Materials in Nuclear Power Systems—Water Reactors, Jekyll Island, GA, NACE, Houston, TX (1989), pp. 6-1 to 6-24.
54. W. K. Lai and Z. Szklarska-Smialowska, *Effect of Heat treatment on the Behavior of Alloy 600 in Lithiated Water Containing Dissolved Hydrogen at 25 to 350°C*, Corrosion, Vol. 47 (1991), pp. 40-47.
55. R. B. Rebak and Z. Szklarska-Smialowska, *About the Mechanism of Stress Corrosion Cracking of Alloy 600 in High-Temperature Water*, Proc. 7th Int. Symp. on Environ. Degradation of Mats. in Nucl. Power Systems—Water Reactors, Breckenridge, CO, NACE, Houston, TX (1995), pp. 855-865.
56. K. Norring, J. Engström, and P. Norberg, *Intergranular Stress Corrosion Cracking in Steam Generator Tubing. Testing of Alloy 690 and Alloy 600 Tubes*, Proc. 3rd Int. Symp. on Environ. Degradation of Mats. in Nucl. Power Systems—Water Reactors, Traverse City, MI, The Metallurgical Society/AIME, Warrendale, PA (1988), pp. 587-593.
57. K. Norring, J. Engström, and H. Törnblom, *Intergranular Stress Corrosion Cracking of Steam Generator Tubing. 25000 Hours Testing of Alloy 600 and Alloy 690*, Proc. 4th Int. Symp. on Environmental Degradation of Mats. in Nucl. Power

Systems—Water Reactors, Jekyll Island, GA, NACE, Houston, TX (1989), pp. 12-1 to 12-10.

58. K. Norring, B. Rosborg, J. Engström, and J. Svenson, *Influence of LiOH and H<sub>2</sub> on Primary Side IGSCC of Alloy 600 Steam Generator Tubes*, Int. Symp. on Contribution of Materials Investigation to the Resolution of Problems Encountered in PWR Plants. Fontevraud II, Vol. 1 (1990), pp. 243-249.
59. K. Stiller, J. O. Nilsson, and K. Norring, *Structure, Chemistry, and Stress Corrosion Cracking of Grain Boundaries in Alloys 600 and 690*, Metallurgical and Materials Transactions A (Physical Metallurgy and Materials Science), Vol. 27A, No. 2 (1996) pp. 327-341.
60. H. Coriou, L. Grall, Y. LeGall, and S. Vettier, *Stress Corrosion Cracking of Inconel in High-Temperature Water*, 3rd Metallurgy Conf. on Corrosion, Saclay, 1959, North Holland, Amsterdam (1960), pp. 161-169.
61. J. Daret and G. P. Legry, *Intergranular Attack (IGA) of PWR Steam Generator Tubing: Evaluation of Remedial Properties of Boric Acid*, Proc. 3rd Int. Symp. on Environmental Degradation of Materials in Nuclear Power Systems—Water Reactors, Traverse City, MI, The Metallurgical Society/AIME, Warrendale, PA (1988), pp. 517-523.
62. G. Santarini, *Comprehensive Interpretation of CERTs: A Method for the Characterization and the Prediction of IGSCC*, Corrosion, Vol. 45 (1989), pp. 369-381.
63. J. Daret, *Intergranular Corrosion of Alloy 600 Tubing in PWR's Steam Generators at the Tube Support Plate Elevation: A Model Boiler Study*, Proc. 4th Int. Symp. on Environmental Degradation of Materials in Nuclear Power Systems—Water Reactors, Jekyll Island, GA, NACE, Houston, TX (1989), pp. 7-45 to 7-69.
64. P. Berge, J. R. Donati, B. Prieux, and D. Villard, *Caustic Stress Corrosion of Fe-Cr-Ni Austenitic Alloys*, Corrosion, Vol. 33 (1977), pp. 425-435.
65. P. Berge and J. R. Donati, *Materials Requirements for Pressurized Water Reactor Steam Generator Tubing*, Nucl. Technol., Vol. 55 (1981), pp. 88-104.
66. J. R. Donati, M. Guttman, Y. Rouillon, P. Saint-Paul, and J. C. Van Duysen, *Stress Corrosion Cracking Behavior of Nickel-Base Alloys with 19% Chromium in High-Temperature Water*, Proc. 3rd Int. Symp. on Environmental Degradation of Materials in Nuclear Power Systems—Water Reactors, Traverse City, MI, The Metallurgical Society/AIME, Warrendale, PA (1988), pp. 697-701.
67. P. Berge, F. De Keroulas, O. Menet, A. Rocher, P. Pitner, A. Gelpi, and G. Pinard-Legry, *The Effects of Chemical Factors on Stress Corrosion of Alloy 600 Exposed to the Cooling Medium in Pressurized Water Reactors*, Proc. 5th Int. Symp. On Environ.

- Degradation of Mats. in Nucl. Power Systems—Water Reactors, Monterey, CA, American Nuclear Society, La Grange Park, IL (1991), pp. 533-538.
68. P. Saint Paul and G. Slama, *Steam Generator Materials Degradation*, Proc. 5th Int. Symp. on Environmental Degradation of Mats. in Nucl. Power Systems—Water Reactors, Monterey, CA, American Nuclear Society, La Grange Park, IL (1991), pp. 39-49.
  69. F. Cattant, D. Garriga-Majo, F. De Keroulas, P. Todeschini, and J. C. Van Duysen, *Effectiveness of 700°C Thermal Treatment on Primary Water Stress Corrosion Sensitivity of Alloy 600 Steam Generator Tubes: Laboratory tests and In-Field Experience*, Proc. 5th Int. Symp. on Environmental Degradation of Materials in Nuclear Power Systems—Water Reactors, Monterey, CA, American Nuclear Society, La Grange Park, IL (1991), pp. 901-911.
  70. T. Magnin, J. M. Boursier, D. Noel, R. Rios, and F. Vaillant, *Corrosion Deformation Interaction During Stress Corrosion Cracking of Alloy 600 in Primary Water*, Proc. 6th Int. Symp. on Environmental Degradation of Mats. in Nucl. Power Systems—Water Reactors, San Diego, The Metallurgical Society/AIME, Warrendale, PA (1993), pp. 669-677.
  71. F. Vaillant, D. Buisine, and B. Prioux, *Comparative Behavior of Alloys 600, 690, and 800*, Proc. 7th Int. Symp. on Environmental Degradation of Mats. in Nucl. Power Systems—Water Reactors, Breckenridge, CO, NACE, Houston, TX (1995), pp. 219-225.
  72. O. Cayla, P. Combrade, and G. Slama, *About some possible causes of IGA of Alloy 600 tubes in hot caustic solutions*, Proc. 2nd Int. Symp. on Environmental Degradation of Mats. in Nucl. Power Systems—Water Reactors, Monterey, CA, American Nuclear Society, La Grange Park, IL (1985), pp. 464-471.
  73. P. Combrade, O. Cayla, M. Foucault, D. Vançon, A. Gelpi, and G. Slama, *About the Role of Surface Films on Alloy 600 Corrosion in High-Temperature Deaerated Environments*, Proc. 3rd Int. Symp. on Environmental Degradation of Materials in Nuclear Power Systems—Water Reactors, Traverse City, MI, The Metallurgical Society/AIME, Warrendale, PA (1988), pp. 525-533.
  74. T. B. Cassagne and A. Gelpi, *Crack Growth Rate Measurements on Alloy 600 Steam Generator Tubes in Steam and Primary Water*, Proc. 5th Int. Symp. on Environmental Degradation of Mats. in Nucl. Power Systems—Water Reactors, Monterey, CA, American Nuclear Society, La Grange Park, IL (1991), pp. 518-524.
  75. B. Sala, P. Combrade, R. Erre, and A. Gelpi, *Local Chemistry and Formation of Deposits on the Secondary Side of Steam generators - A Laboratory Study*, Proc. 6th Int. Symp. on Environmental Degradation of Mats. in Nucl. Power Systems—Water Reactors, San Diego, The Metallurgical Society/AIME, Warrendale, PA (1993), pp. 215-226.

76. P. Scott, B. Liblin, J. Vincent, A. Lorthioir, B. Granger, and B. Bussy, *Factors Affecting PWR Steam Generator Tube Denting Above the Tube Sheet*, Proc. 6th Int. Symp. on Environmental Degradation of Mats. in Nucl. Power Systems—Water Reactors, San Diego, The Metallurgical Society/AIME, Warrendale, PA (1993), pp. 227-232.
77. B. Michaut, F. Steltzlen, B. Sala, Ch. Laire, and J. Stubbe, *Nickel Electroplating as a Remedy to Steam Generator Tubing PWSCC*, Proc. 6th Int. Symp. on Environmental Degradation of Mats. in Nucl. Power Systems—Water Reactors, San Diego, The Metallurgical Society/AIME, Warrendale, PA (1993), pp. 713-719.
78. B. Sala, M. Organista, K. Henry, R. Erre, A. Gelpi, F. Cattant, and M. Dupin, *Laboratory Study of Corrosion of Steam Generator Tubes: Preliminary Results*, Proc. 7th Int. Symp. on Environmental Degradation of Mats. in Nucl. Power Systems—Water Reactors, Breckenridge, CO, NACE, Houston, TX (1995), pp. 259-275.
79. P. Hernalsteen and F. Van Zeveren, *Leak and Burst Testing Practice on Pulled-out Steam Generator Tubes*, Int. Symp. on Contribution of Materials Investigation to the Resolution of problems encountered in PWRs. Fontevraud III, Vol. 2 (1994), pp. 425-433.
80. A. Kishida, H. Takamatsu, H. Katamura, S. Isobe, K. Onimura, K. Arioka, T. Hattori, T. Arai, and M. Sato, *The Causes and Remedial Measures of Steam Generator Tube Intergranular Attack in Japanese PWR*, Proc. 3rd Int. Symp. on Environmental Degradation of Materials in Nuclear Power Systems—Water Reactors, Traverse City, MI, The Metallurgical Society/AIME, Warrendale, PA (1988), pp. 465-471.
81. H. Takamatsu, K. Matsueda, K. Onimura, K. Arioka, S. Tokunaga, and K. Katsura, *IGA/IGSCC Propagation Behaviors of Alloy 600*, Proc. 4th Int. Symp. on Environmental Degradation of Materials in Nucl. Power Systems—Water Reactors, Jekyll Island, GA, NACE, Houston, TX (1989), pp. 7-29 to 7-44.
82. K. Yamanaka, *The Role of Grain Boundary Chromium Carbides on the IGA Resistance of Nickel Base Alloy 600*, Proc. 6th Int. Symp. on Environmental Degradation of Materials in Nucl. Power Systems—Water Reactors, San Diego, The Metallurgical Society/AIME, Warrendale, PA (1993), pp. 105-111.
83. H. Nagano and H. Kajimura, *Clarification of Stress Corrosion Cracking Mechanism on Nickel Base Alloys in Steam Generators*, Proc. 7th Int. Symp. on Environmental Degradation of Materials in Nucl. Power Systems—Water Reactors, Breckenridge, CO, NACE, Houston, TX (1995), pp. 291-301.
84. R. H. Thompson and R. L. Tapping, *Inferring Steam Generator Fouling Mechanisms from Visual Inspections and Deposit Analyses*, CORROSION/88, Paper 255, NACE, Houston, TX (1988).

85. J. P. N. Paine, S.A. Hobart, and S. G. Sawochka, *Predicting Steam Generator Crevice Chemistry*, Proc. 5th Int. Symp. on Environmental Degradation of Materials in Nucl. Power Systems—Water Reactors, Monterey, CA, American Nuclear Society, La Grange Park, IL (1991), pp. 739-744.
86. G. O. Hayner, C. R. Frye, and G. J. Theus, *Examination of Tubes Removed from St. Lucie Unit 1 and Investigation of Causes of the Corrosion*, Proc. 3rd Int. Symp. on Environmental Degradation of Materials in Nuclear Power Systems—Water Reactors, Traverse City, MI, The Metallurgical Society/AIME, Warrendale, PA (1988), pp. 449-456.
87. G. P. Airey, *The Effect of Carbon Content and Thermal Treatment on the SCC Behavior of Inconel Alloy 600 Steam Generator Tubing*, Corrosion, Vol. 35 (1979), pp. 129-136.
88. S. M. Bruemmer and C. H. Henager, Jr., *Microstructure, Microchemistry, and Microdeformation of Alloy 600 Tubing*, Proc. 2nd Int. Symp. on Environmental Degradation of Materials in Nucl. Power Systems—Water Reactors, Monterey, CA, American Nuclear Society, La Grange Park, IL (1985), p. 293.
89. S. M. Bruemmer, L. A. Charlot, and C. H. Henager, Jr., *Microstructure and Microdeformation Effects on IGSCC of Alloy 600 Steam Generator Tubing*, Corrosion, Vol. 44 (1988), pp. 782-788.
90. R. Bandy and D. Van Rooyen, *Effect of Thermal Stabilization on the Low Temperature Stress Corrosion Cracking of Inconel 600*, Corrosion, Vol. 40 (1984), pp. 281-289.
91. K. Norring, J. Engstrom, and B. Rosborg, *Ringhals 2. Primary and Secondary Side Steam Generator Tube Cracking*, Int. Symp. on Contribution of Materials Investigation to the Resolution of problems encountered in PWRs. Fontevraud I (1985), pp. 209-216.
92. C. M. Owens, *Role of Processing on the Development of Alloy 600 Tubing Microstructure*, in EPRI 1985 Workshop on Primary-Side SCC of PWR Steam Generator Tubing, San Diego, EPRI NP-5158, Electric Power Research Institute, Palo Alto, CA (1985).
93. J. A. Gorman, *Status and Suggested Course of Action for Nondenting Related Primary Side IGSCC of Westinghouse-Type Steam Generators*, EPRI-NP-4594-LD, Electric Power Research Institute, Palo Alto, CA (May 1986).
94. C. M. Owens, *The Primary Side Stress Corrosion Cracking Performance of Mill-Annealed Inconel 600 Tubing in C-E Designed Steam Generators*, NEA/CSNI-UNIPEDD specialists meeting on steam generators, Stockholm, (Oct. 1984).
95. T. P. Magee and P. J. Plante, *Examination of a Steam Generator Tube Removed from Maine Yankee*, Proc. 5th Int. Symp. on Environmental Degradation of Materials in

Nuclear Power Systems—Water Reactors, Monterey, CA, American Nuclear Society, La Grange Park, IL (1991), pp. 628-635.

96. H. Tas, P. Hernalsteen, R. Houben, and L. Driesen, *Relationship between Microstructural Features and Tube Cracking as Observed on Tube Samples of a Doel 2 Steam Generator*, in EPRI 1985 Workshop on Primary-Side SCC of PWR Steam Generator Tubing, San Diego, EPRI NP-5158, Electric Power Research Institute, Palo Alto, CA (1985).
97. A. A. Stein and A. R. McIlree, *Relationship of Annealing Temperature and Microstructure to Primary Side Cracking of Alloy 600 Steam Generator Tubing and the Prediction of Stress Corrosion Cracking in Primary Water*, Proc. 2nd Int. Symp. on Environmental Degradation of Materials in Nuclear Power Systems—Water Reactors, Monterey, CA (1985), pp. 47-51.
98. E. Serra, *Stress Corrosion Cracking of Alloy 600*, EPRI Report NP-2114-SR, Electric Power Research Institute, Palo Alto, CA (1981).
99. Y. S. Garud and T. L. Gerber, *Intergranular Stress Corrosion Cracking of Ni-Cr-Fe Alloy 600 Tubes in PWR Primary Water—Review and Assessment for Model Development*, EPRI Report NP-3057, Electric Power Research Institute, Palo Alto, CA (1983).
100. T. B. Cassagne, P. Combrade, M. A. Foucault, and A. Gelpi, *The Influence of Mechanical and Environmental Parameters on the Crack Growth Behavior of Alloy 600 in Primary Water*, Proc. 12th Scandinavian Corrosion Congress and EUROCORR '92, Vol. 2, Espoo, Finland, pp. 55-67 (1992).
101. R. B. Rebak, Z. Xia, and Z. Szklarska-Smialowska, *Effect of Temperature and Cold Work on the Crack Growth Rate of Alloy 600 in Primary Water*, Corrosion, Vol. 51, pp. 689-697 (1995).
102. D. C. Crawford and G. S. Was, *The Effect of Grain Boundary Misorientation on Intergranular Cracking of Ni-16Cr-9Fe in 360°C Argon and High Purity Water*, Proc. 5th Int. Symp. on Environmental Degradation of Materials in Nuclear Power Systems—Water Reactors, Monterey, CA, American Nuclear Society, La Grange Park, IL (1991), pp. 488-494.
103. J. C. Fournel, *A Statistical Insight in the Suspected Relations between PWSCC in RTZ and IGASCC on TSPs*, presented at the IGA/SCC EPRI workshop, Minneapolis, MN (October 1993).
104. P. Lemaire, *Current Status of ODSCC at EDF Plants*, *ibid.*
105. M. Kowaka, H. Nagano, T. Kudo, Y. Okada, M. Yagi, O. Takaba, T. Yonezawa, and K. Arioka, *Effect of Heat Treatment on the Susceptibility to Stress Corrosion Cracking of Alloy 600*, Nucl. Technol., Vol. 55, pp. 394-404 (1981).

106. G. J. Theus, *Relationship between Acid Intergranular Corrosion and Caustic Stress Corrosion Cracking of Alloy 600*, Corrosion, Vol. 33, pp. 20-26 (1977).
107. R. J. Jacko, *IGSCC and IGA behavior of I-600*, Proc. 1984 Workshop on secondary side stress corrosion cracking and intergranular corrosion of PWR steam generator tubing, EPRI NP-4478, Electric Power Research Institute, Palo Alto, CA (1986).
108. F. Vaillant, D. Buisine, B. Prioux, J. C. Fournel, and A. Gelpi, *Effects of Microstructure and Mechanical Properties of Alloys 600 and 690 on Secondary Side SCC*, Proc. of Conf. on Control of Corrosion on the Secondary Side of Steam Generators, Airlie Conference Center, Airlie, VA, sponsored jointly by the EPRI and Argonne National Laboratory, NACE, Houston, TX, pp. 321-335 (1995).
109. J. F. Newman, *Stress Corrosion of Alloys 600 and 690 in Acid Sulfate Solutions at Elevated Temperatures*, EPRI Final Report NP-3043, Electric Power Research Institute, Palo Alto, CA (Oct. 1983).
110. W. H. Cullen, M. J. Partridge, J. A. Gorman, and J. P. N. Paine, *IGA/IGSCC of Alloy 600 in Acid Sulfate Solutions*, Proc. 4th Int. Symp. on Environmental Degradation of Materials in Nuclear Power Systems—Water Reactors, Jekyll Island, GA, NACE, Houston, TX (1989), pp. 7-60 to 7-69.
111. G. J. Theus, EPRI 1980 Workshop on Primary-Side SCC of PWR Steam Generator Tubing, Denver, EPRI WS-80-0136, Electric Power Research Institute, Palo Alto, CA (1980).
112. J. V. Monter, *Influence of Carbon Content and Mill-Annealing Temperature on SCC in High-Temperature Caustic*, EPRI 1985 Workshop on Primary-Side SCC of PWR Steam Generator Tubing, San Diego, EPRI NP-5158, Electric Power Research Institute, Palo Alto, CA (1985).
113. T. Yonezawa and K. Onimura, *Effect of Chemical Composition and Microstructure on the Stress Corrosion Cracking Resistance of Nickel-Base Alloys in High-Temperature Water*, EPRI meeting: Intergranular corrosion and primary water IGSCC mechanisms, Washington, DC (1987).
114. D. A. Vermilyea, C. S. Tedmon, Jr., and D. E. Broecker, *Effect of Phosphorous and Silicon on the Intergranular Corrosion of a Nickel-Base Alloy*, Corrosion, Vol. 31 (1975), pp. 222-223.
115. Y. Fujiwara, R. Nemoto, K. Osozawa, K. Ebato, K. Yamauchi, and T. Okazaki, *Influence of C, N and Nb Contents on Intergranular Corrosion, Stress Corrosion Cracking and Mechanical Strength of Alloy 600*, Corrosion Cracking: Proc. of Corrosion Cracking Program: Related papers, ed. V. S. Goel, ASM, Metals Park, OH (1986), p. 167.

116. A. R. McIlree, H. T. Michels, and P. E. Morris, *Effects of Variation of Carbon, Sulfur and Phosphorous on the Corrosion Behavior of Alloy 600*, Corrosion, Vol. 31 (1975), pp. 441-448.
117. M. Guttman, Ph. Dumoulin, N. Tan-Tai, and P. Fontaine, *An Auger Electron Spectroscopic Study of Phosphorous Segregation in the Grain Boundaries of Nickel Base Alloy 600*, Corrosion, Vol. 37 (1981), pp. 416-425.
118. J. E. Truman and R. Perry, *The Resistance to Stress Corrosion Cracking of Some Cr-Ni-Fe Austenitic Steels and Alloys*, Brit. Corr. J., Vol. 1 (1966), pp. 60-66.
119. I. L. W. Wilson and R. G. Aspden, *Caustic SCC of Fe-Ni-Cr Alloys*, paper G-22 presented at Stress corrosion cracking and hydrogen embrittlement of iron base alloys, Firminy, France (June 1973).
120. N. Nagano, *Alkaline Intergranular Corrosion and Stress Corrosion Cracking of Alloy 600*, Proc. of Conf. on Control of Corrosion on the Secondary Side of Steam Generators, Airlie Conference Center, Airlie, VA, sponsored jointly by the EPRI and Argonne National Laboratory, NACE, Houston, TX, pp. 259-271 (1995).
121. R. B. Rebak, Z. Xia, and Z. Szklarska-Smialowska, *Effects of Carbides on Susceptibility of Alloy 600 to Stress Corrosion Cracking in High-Temperature Water*, Corrosion, Vol. 49, pp. 867-876 (1993).
122. G. Economy, R. J. Jacko, J. A. Begley, and F. W. Pement, *Influence of Hydrogen Partial Pressure on the IGSCC Behavior of Alloy 600 Tubing in 360°C Water or 400°C Steam*, Corrosion/87, Paper No. 92, NACE, Houston, TX (1987).
123. A. Rocher, T. Cassagne, V. Durbec, D. G. Briceno, M. L. C. Marin, and A. Gelpi, *The Influence of Chemical Factors on the Initiation of Primary Side IG-SCC in Alloy 600 Steam Generator Tubing*, Int. Symp. on Contribution of Materials Investigation to the Resolution of problems encountered in PWRs. Fontevraud III, Vol. 1 (1994), pp. 337-346.
124. S. S. Pathania and A. R. McIlree, *A Review of the Effect of Hydrogen on Stress Corrosion Cracking of Alloy 600 in 300°C Water*, Proc. 3rd Int. Symp. on Environmental Degradation of Materials in Nuclear Power Systems—Water Reactors, Traverse City, MI, The Metallurgical Society/AIME, Warrendale, PA (1988), pp. 551-554.
125. J. N. Esposito, G. Economy, W. A. Byers, J. B. Esposito, F. W. Pement, R. J. Jacko, and C. A. Bergmann, *The Addition of Zinc to Primary Reactor Coolant for Enhanced PWSCC Resistance*, Proc. 5th Int. Symp. on Environmental Degradation of Materials in Nuclear Power Systems—Water Reactors, Monterey, CA, American Nuclear Society, La Grange Park, IL (1991), pp. 495-501.

126. P. L. Andresen and T. Diaz, *Effect of Zinc Additions on the Crack Growth Rate of Fe and Ni Base Alloys in 288°C Water*, Paper 93184, Corrosion 93, NACE, New Orleans (March 7-12, 1993).
127. W. A. Byers and R. J. Jacko, *The Influence of Zinc Additions and PWR Primary Water Chemistry on Surface Films that Form on Nickel Base Alloys and Stainless Steels*, *Ibid.*, pp. 837-844.
128. P. L. Andresen and T. M. Angeliu, *Effects of Zinc Additions on the Stress Corrosion Crack Growth Rate of Sensitized Stainless Steel, Alloy 600 & Alloy 182 Weld Metal in 288°C Water*, Paper No. 409, Corrosion 95, Orlando, (March 26-31, 1995), NACE, Houston TX.
129. D. S. Morton, D. Gladding, M. K. Schurman, and C. D. Thompson, *Effect of Soluble Zinc Additions on the SCC Performance of Nickel Alloys in Deaerated Hydrogenated Water*, Proc. 8th Int. Symp. on Environmental Degradation of Materials in Nuclear Power Systems—Water Reactors, Amelia Island, FL, American Nuclear Society, La Grange Park, IL (1997), pp. 387-394.
130. R. Bandy, R. Roberge, and R. C. Newman, *Low Temperature Stress Corrosion Cracking of Sensitized Inconel 600 in Tetrathionate and Thiosulfate Solutions*, Corrosion, Vol. 39 (1983), pp. 391-398.
131. R. Bandy, R. Roberge, and R. C. Newman, *Low-Temperature Stress Corrosion Cracking of Inconel 600 under Two Different Conditions of Sensitization*, Corr. Sci., Vol. 23 (1983), pp. 995-1006.
132. R. C. Hermer and C. R. Wolfe, *Field Identification and Laboratory Simulation of IGA and SCC in Alloy 600 Mill-Annealed Tubing*, Int. Symp. on Contribution of Materials Investigation to the Resolution of problems encountered in PWR Plants. Fontevraud I (1985), pp. 280-288.
133. A. Baum and P. Greaney, *Steam generator sludge pile model boiler testing*, EPRI Final Report on Project S119-1-NP-1941, Electric Power Research Institute, Palo Alto, CA (July 1981).
134. C. Laire, G. Platbrood, and J. Stubbe, *Characterization of the Secondary Side Deposits of Pulled Steam Generator Tubes*, Proc. 7th Int. Symp. on Environmental Degradation of Materials in Nuclear Power Systems—Water Reactors, Breckenridge, CO, NACE, Houston, TX (1995), pp. 387-397.
135. L. Albertin, F. Cattant, A. Baum, and P. Kuchirka, *Characterization of Deposits in Dampierre-1 Steam Generator Support Plate Crevices*, *Ibid.*, pp. 399-409.
136. T. P. Magee, J. P. Molkenhain, J. F. Hall, M. A. Melton, D. E. Sachs, K. M. Sweeney, and J. Begley, *Corrosion of Palo Verde 2 Upper Bundle Steam Generator Tubing*, *Ibid.*, pp. 411-421.

137. J. B. Lumsden, P. J. Stocker, and A. R. McIlree, *In Sight of Local Chemistry from Examination of Tubes*, in *Control of Corrosion on the Secondary Side of Steam Generators*, R. Staehle, J. Gorman, and A. R. McIlree, eds., NACE Int., (1996) p. 473.
138. A. M. Lancha, D. Gomez-Briceno, M. Garcia, and E. Lopez Toribio, *AES and SEM/EDS Analysis of Deposits in Pulled Steam Generator Tubes*, Proc. 6th Int. Symp. on Environmental Degradation of Materials in Nuclear Power Systems—Water Reactors, San Diego, The Metallurgical Society/AIME, Warrendale, PA (1993), pp. 89-95.
139. L. Björnkvist, K. Norring, and L. Nyborg, *Comparative Study of Water Chemistry and Surface Oxide Composition on Alloy 600 Steam Generator Tubing*, *Ibid.*, pp. 207-213.
140. W. M. Connor, D. Smith-Magowan, G. Economy, R. H. Kunig, and R. G. Aspden, *Evaluation of Environmental Effects on Intergranular Attack of Alloy 600*, EPRI Final Report NP-4802, Palo Alto, CA (1986).
141. W. H. Cullen, M. J. Partridge, J. A. Gorman, and J. P. N. Paine, *IGA/IGSCC of Alloy 600 in Acidic Sulfate and Chloride Solutions*, Proc. 5th Int. Symp. on Environmental Degradation of Materials in Nuclear Power Systems—Water Reactors, Monterey, CA, American Nuclear Society, La Grange Park, IL (1991), pp. 780-788.
142. W. H. Cullen, M. J. Partridge, and J. P. N. Paine, *Corrosion of Alloys 600 and 690 in Acidified Sulfate and Chloride Solutions*, Proc. 6th Int. Symp. on Environmental Degradation of Materials in Nuclear Power Systems—Water Reactors, San Diego, The Metallurgical Society/AIME, Warrendale, PA (1993), pp. 197-206.
143. P. Berge, D. Noel, J. Gras, and B. Prioux, *Chloride Stress Corrosion Cracking of Alloy 600 in Boric Acid Solutions*, Proc. 8th Int. Symp. on Environmental Degradation of Materials in Nuclear Power Systems—Water Reactors, Amelia Island, FL, American Nuclear Society, La Grange Park, IL (1997), pp. 189-199.
144. P. J. King, F. Gonzalez, and J. Brown, *Stress Corrosion Cracking Experience in Steam Generators at Bruce NGs*, Proc. 6th Int. Symp. on Environmental Degradation of Materials in Nuclear Power Systems—Water Reactors, San Diego, The Metallurgical Society/AIME, Warrendale, PA (1993), pp. 233-243.
145. A. Rocher, F. Cattant, D. Buisine, B. Prioux, and M. Helie, *Effect of Lead on the OD Degradation of Steam Generator Tubes*, Int. Symp. on Contribution of Materials Investigation to the Resolution of problems encountered in PWRs. Fontevraud III, Vol. 2 (1994), pp. 537-547.
146. S. S. Hwang, K. M. Kim, and U. C. Kim, *Stress Corrosion Aspects of Nuclear Steam Generator Tubing Materials in the Water Containing Lead at High Temperature*, Proc. 8th Int. Symp. on Environmental Degradation of Materials in Nuclear Power

- Systems—Water Reactors, Amelia Island, FL, American Nuclear Society, La Grange Park, IL (1997), pp. 200-203.
147. H. Takamatsu, T. Matsunaga, B. P. Miglin, J. M. Sarver, P. A. Sherburne, K. Aoki, and T. Sakai, *Study on Lead-Induced Stress Corrosion Cracking of Steam Generator Tubing under AVT Water Chemistry Conditions*, Proc. 8th Int. Symp. on Environmental Degradation of Materials in Nuclear Power Systems—Water Reactors, Amelia Island, FL, American Nuclear Society, La Grange Park, IL (1997), pp. 216-223.
  148. M. L. Castano-Marin, D. Gomez-Briceno, and F. Hernandez-Arroyo, *Influence of Lead Contamination on the Stress Corrosion Resistance of Nickel Alloys*, Proc. 6th Int. Symp. on Environmental Degradation of Materials in Nuclear Power Systems—Water Reactors, San Diego, The Metallurgical Society/AIME, Warrendale, PA (1993), pp. 189-196.
  149. W. A. Byers, J. Barkich, M. W. Rootham, and F. Hundley, *Control of Lead-Assisted Stress Corrosion Cracking of Alloy 600 Tubing in Steam Generator Free Span Locations*, Proc. 8th Int. Symp. on Environmental Degradation of Materials in Nuclear Power Systems—Water Reactors, Amelia Island, FL, American Nuclear Society, La Grange Park, IL (1997), pp. 224-231.
  150. B. P. Miglin and J. M. Sarver, *Investigation of Lead as a Cause of Stress Corrosion Cracking at Support Plate Intersections*, EPRI-NP-7367-S, Palo Alto, CA (June 1991).
  151. B. Sala, S. Chevalier, M. Organista, and A. Gelpi, *The Role of Silica Compounds in the Corrosion Process of the Secondary Side of Steam Generators: An Electrochemical Study*, Proc. 8th Int. Symp. on Environmental Degradation of Materials in Nuclear Power Systems—Water Reactors, Amelia Island, FL, American Nuclear Society, La Grange Park, IL (1997), pp. 80-90.
  152. A. J. Baum, P. J. Prabhu, M. Rootham, and N. L. Zupetic, *Development of Improved PWR Secondary Water Chemistry Guidelines*, Proc. 8th Int. Symp. on Environmental Degradation of Materials in Nuclear Power Systems—Water Reactors, Amelia Island, FL, American Nuclear Society, La Grange Park, IL (1997), pp. 74-79.
  153. S. W. Lurie and P. B. Radsky, *Boric Acid Neutralization of Denting at Maine Yankee Station*, Proc. 2nd Int. Symp. on Environmental Degradation of Materials in Nuclear Power Systems—Water Reactors, Monterey, CA, American Nuclear Society, La Grange Park, IL (1985), pp. 566-570.
  154. R. S. Pathania, J. P. N. Paine, and C. E. Shoemaker, *Inhibition of Intergranular Attack and Stress Corrosion Cracking with Boric Acid*, Proc. 3rd Int. Symp. on Environmental Degradation of Materials in Nuclear Power Systems—Water Reactors, Traverse City, MI, The Metallurgical Society/AIME, Warrendale, PA (1988), pp. 511-516.

155. J. Daret and G. P. Legry, *Intergranular Attack (IGA) of PWR's Steam Generator Tubing: Evaluation of Remedial Properties of Boric Acid*, *Ibid.*, pp. 517-523.
156. B. P. Miglin and J. P. Paine, *Slow Strain Rate Testing to Evaluate Inhibitors for Stress Corrosion Cracking of Alloy 600*, Proc. 6th Int. Symp. on Environmental Degradation of Materials in Nuclear Power Systems—Water Reactors, San Diego, The Metallurgical Society/AIME, Warrendale, PA (1993), pp. 303-307.
157. J. A. Gorman, R. A. Ogren and J. P. N. Paine, *Correlation of Temperature with Steam Generator Tube Corrosion Experience*, Proc. 5th Int. Symp. on Environmental Degradation of Materials in Nuclear Power Systems—Water Reactors, Monterey, CA, American Nuclear Society, La Grange Park, IL (1991), pp. 609-612.
158. A. R. McIlree, T. Olberg and J. Nestell, *Primary Side Stress Corrosion Cracking*, Steam generator reference book, EPRI-SGOG, Chapter 7, Electric Power Research Institute, Palo Alto, CA (1985), p. 14.
159. Y. S. Garud and A. R. McIlree, *Intergranular Stress Corrosion Cracking Damage Model: An Approach and Its Development for Alloy 600 in High Purity Water*, *Corrosion*, Vol. 42 (1986), pp. 99-105.
160. T. Cassagne and A. Gelpi, *Crack Growth Rate Measurement on Alloy 600 Steam Generator Tubing in Primary and Hydrogenated AVT Water*, Proc. 6th Int. Symp. on Environmental Degradation of Materials in Nuclear Power Systems—Water Reactors, San Diego, The Metallurgical Society/AIME, Warrendale, PA (1993), pp. 679-686.
161. R. Bandy, *Mechanisms of IGA and IGSCC of Alloy 600 in High-Temperature Caustic and Pure Water*, Proc. 1984 Workshop on Secondary Side Stress Corrosion Cracking and Intergranular Corrosion of PWR Steam Generator Tubing, EPRI NP-4478, Electric Power Research Institute, Palo Alto, CA (1986).
162. P. Malagola, *IGA of Inconel 600: Role of Physical Parameters*, 1984 Workshop on secondary side stress corrosion cracking and intergranular corrosion of PWR steam generator tubing, EPRI NP-4478, Electric Power Research Institute, Palo Alto, CA (1986).
163. *Mechanisms of Intergranular Attack and Stress Corrosion Cracking of Alloy 600 by High-Temperature Caustic Solutions Containing Impurities*, EPRI, Final Report NP-5129, Palo Alto, CA (1987)
164. *Production of Eddy Current Standards for Caustic Intergranular Corrosion*, EPRI, Final Report, NP-5109, Palo Alto, CA (1987).
165. J. M. Sarver, *Effect of Processing Parameters on the PbSCC of Alloy 600*, paper presented at the EPRI IGA/SCC Workshop (Dec. 1992).

166. M. Helie, I. Lambert, and G. Santarini, *Some Considerations about the Mechanisms of Lead Assisted Stress Corrosion Cracking of Steam Generator Tubing*, Proc. 7th Int. Symp. on Environmental Degradation of Materials in Nuclear Power Systems—Water Reactors, Breckenridge, CO, NACE, Houston, TX (1995), pp. 247-258.
167. G. J. Theus, *Summary of the Babcock & Wilcox Company's Stress Corrosion Cracking Tests on Alloy 600*, EPRI WS-80-136, EPRI Workshop on cracking of Alloy 600 U-bend tubes in steam generators, Denver (Aug. 1980).
168. J.M. Boursier, D. Desjardins, and F. Vaillant, *The Influence of the Strain Rate on the Stress Corrosion Cracking of Alloy 600 in High-Temperature Primary Water*, Corr. Sci., Vol. 37 (1995), pp. 493-508.
169. Z. Szklarska-Smialowska and R. B. Rebak, *Stress Corrosion Cracking of Alloy 600 in High-Temperature Aqueous Solutions: Influencing Factors, Mechanisms and Models*, Proc. of Conf. on Control of Corrosion on the Secondary Side of Steam Generators, Airlie Conference Center, Airlie, VA, sponsored jointly by the EPRI and Argonne National Laboratory, NACE, Houston, TX (1995), pp. 223-257.
170. J. P. Foster, W. H. Bamford, and R. S. Pathania, *Initial Results of Alloy 600 Crack Growth Rate Testing in PWR Environment*, Proc. 7th Int. Symp. on Environmental Degradation of Materials in Nuclear Power Systems—Water Reactors, Breckenridge, CO, NACE, Houston, TX (1995), pp. 25-40.
171. I. L. W. Wilson, F. W. Pement, R. G. Aspden, and R. T. Begley, *Caustic Stress Corrosion Behavior of Fe-Ni-Cr Nuclear Steam Generator Tubing Alloys*, Nucl. Technol., Vol. 31 (1976), pp. 70-84.
172. H. Takamatsu, K. Matsueda, T. Matsunaga, T. Kitera, K. Arioka, T. Tsuruta, and S. Okamoto, *IGA/SCC Crack Propagation Measurements on Alloy 600 Steam Generator Tubing Using a Side Stream Model Boiler*, Proc. 6th Int. Symp. on Environmental Degradation of Materials in Nuclear Power Systems—Water Reactors, San Diego, The Metallurgical Society/AIME, Warrendale, PA (1993), pp. 81-88.
173. T. Tsuruta, S. Okamoto, T. Kitera, H. Takamatsu, and T. Matsunaga, *IGA/SCC Crack Propagation Rate Measurements on Alloy 600 SG Tubing and Evaluation of Crevice Environments Using a Side Stream Model Boiler*, Proc. 7th Int. Symp. on Environmental Degradation of Materials in Nuclear Power Systems—Water Reactors, Breckenridge, CO, NACE, Houston, TX (1995), pp. 187-197.
174. B. P. Miglin, J. M. Sarver, D. W. Koch, K. Aoki, and H. Takamatsu, *Accelerated IGA/SCC Testing of Alloy 600 in Contaminated PWR Environments*, Proc. 5th Int. Symp. on Environmental Degradation of Materials in Nuclear Power Systems—Water Reactors, Monterey, CA, American Nuclear Society, La Grange Park, IL (1991), pp. 757-763.

175. T. Sakai, T. Senjuh, K. Aoki, T. Shigemitsu, and Y. Kishi, *Lead-induced stress corrosion cracking of Alloy 600 and 690 in high temperature water*, Proc. 5th Intl. Symp. On Environ. Degradation of Mats. in Nucl. Power Systems—Water Reactors, Monterey, CA, American Nuclear Society, La Grange Park, IL (1991), pp. 764-772.
176. B. P. Miglin, J. M. Sarver, M. J. Psaila-Dombrowski, and P. E. Doherty, *Lead Assisted Stress Corrosion Cracking of Nuclear Steam Generator Tubing Materials*, Proc. of Conf. on Control of Corrosion on the Secondary Side of Steam Generators, Airlie Conference Center, Airlie, VA, sponsored jointly by the EPRI and Argonne National Laboratory, NACE, Houston, TX (1995), pp. 305-320.
177. O. Kerrec, S. Gardey, D. Noel, E. Riquelme, P. Miguet, and J. P. Massoud, *Study of the Mechanisms of Stress Corrosion Cracking of Alloy 600 and 690 in Primary Water Reactor Conditions*, Eurocorr 96, Nice (24-26 Sept. 1996).
178. N. S. McIntyre, D. G. Zetaruk, and D. Owen, *X-ray Photoelectron Studies of the Aqueous Oxidation of Inconel 600 Alloy*, J. Electrochem. Soc., Vol. 126 (1979), p. 750.
179. R. W. Staehle, *Occurrence of Modes and Submodes of SCC*, Proc. of Conf. on Control of Corrosion on the Secondary Side of Steam Generators, Airlie Conference Center, Airlie, VA, sponsored jointly by the EPRI and Argonne National Laboratory, NACE, Houston, TX (1995), pp. 135-208.
180. *Computer-Calculated Potential-pH Diagram to 300°C, Vol. 2*, Prepared by the Babcock & Wilcox Company, EPRI NP-3137, Project 1167-2, Electric Power Research Institute, Palo Alto, CA (1983).
181. D. F. Taylor, *Crevice Corrosion of Alloy 600 in High-Temperature Aqueous Environment*, Corrosion, Vol. 35 (1970), pp. 550-559.
182. R. Bandy, R. Roberge, and D. Van Rooyen, *Intergranular Failures of Alloy 600 in High-Temperature Caustic Environment*, Corrosion, Vol. 41 (1985), pp. 142-150.
183. N. Pessall, G. P. Airey, and B. P. Lingenfelter, *The Influence of Thermal Treatment on the SCC Behavior of Inconel Alloy 600 at Controlled Potentials in 10% Caustic Soda Solutions at 315°C*, Corrosion, Vol. 35 (1979), pp. 100-107.
184. T. M. Angeliu and G. S. Was, *The Effect of Chromium, Carbon, and Yttrium on the Oxidation of Nickel-Base Alloys in High Temperature Water*, J. Electrochem. Soc., Vol. 140 (1993), pp. 1877-1883.
185. G. S. Was and R. M. Kruger, *A Thermodynamic and Kinetic Basis for Understanding Chromium Depletion in Ni-Cr-Fe Alloys*, Acta Metall., Vol. 33 (1985), pp. 841-854.

186. V. B. Rajan, J. K. Sung, and G. S. Was, *Stress Corrosion Cracking of Controlled-Purity Inconel 600 Type Alloys in High-Purity Water and Caustic Solutions*, Proc. 3rd Int. Symp. on Environmental Degradation of Materials in Nuclear Power Systems—Water Reactors, Traverse City, MI, The Metallurgical Society/AIME, Warrendale, PA (1988), pp. 545-550.
187. J. K. Sung and G. S. Was, *The Role of Grain Boundary Chemistry in Pure Water Intergranular Stress Corrosion Cracking of Ni-16Cr-9Fe Alloys*, Proc. 4th Int. Symp. on Environmental Degradation of Materials in Nuclear Power Systems—Water Reactors, Jekyll Island, GA, NACE, Houston, TX (1989), p. 6-25.
188. G. S. Was, *Micromechanical and Microstructural Effects of Stress Corrosion Cracking of Nickel-Base Alloys*, in Proc. Parkins Symp. on Fundamental Aspects of Stress Corrosion Cracking, S. M. Bruemmer et al., eds., The Minerals, Metals, & Materials Society, Warrendale, PA (1992), p. 371.
189. J. R. Crum, *Effects of Composition and Heat Treatment on Stress Corrosion Cracking of Alloy 600 Steam Generator Tubes in Sodium Hydroxide*, Corrosion, Vol. 38 (1982), pp. 40-45.
190. J. R. Crum, *Stress Corrosion Cracking Testing of Inconel Alloys 600 and 690 under High-Temperature Caustic Conditions*, Corrosion, Vol. 42 (1986), pp. 368-372.
191. G. S. Was and J. R. Martin, *The Influence of Grain Boundary Precipitation on the Measurement of Chromium Redistribution and Phosphorous Segregation in Ni-16Cr-9Fe*, Metall. Trans. A., Vol. 16A (1985), p. 349.
192. P. H. Pumphrey, *Special High Angle Grain Boundaries*, in Grain Boundary Structure and Properties, D. A. Chadwick and G. A. Smith, eds., Academic Press, London (1976), p. 139.
193. T. Watanabe, *An Approach to Grain Boundary Design for Strong and Ductile Polycrystals*, Res. Mechanica, Vol. 11 (1984), p. 47.
194. J. Don and S. Majumdar, *Creep Cavitation and Grain Boundary Structure in Type 304 Stainless Steel*, Acta. Metall., Vol. 34 (1986), pp. 961-967.
195. G. Palumbo, P. J. King, K. T. Aust, U. Erb, and P. C. Lichtenberg, *Grain Boundary Design and Control for Intergranular Stress Corrosion Resistance*, Scr. Metall. Mater., Vol. 25 (1991), pp. 1775-1780.
196. K. T. Aust, U. Erb, and G. Palumbo, *Interface Control for Resistance to Intergranular Cracking*, Mater. Sci. Eng., Vol. 176A (1994), pp. 329-334.
197. T. M. Angeliu, D. J. Paraventi, and G. S. Was, *Creep and Intergranular Cracking Behavior of Nickel-Chromium-Iron-Carbon Alloys in 360°C Water*, Corrosion, Vol. 51 (1995), pp. 837-848.

198. V. Thaveeprungsriporn, T. M. Angeliu, D. J. Paraventi, and J. L. Herzberg, *Grain Boundary Deformation of Ni-Cr-Fe-C at 360°C*, Proc. 6th Int. Symp. on Environmental Degradation of Materials in Nuclear Power Systems—Water Reactors, San Diego, The Metallurgical Society/AIME, Warrendale, PA (1993), pp. 721-727.
199. P. M. Scott and P. Combrade, *On the Mechanisms of Secondary Side PWR Steam Generator Tube Cracking*, Proc. 8th Int. Symp. on Environmental Degradation of Materials in Nuclear Power Systems—Water Reactors, Amelia Island, FL, American Nuclear Society, La Grange Park, IL (1997), pp. 65-73.
200. F. P. Ford and P. L. Andresen, *Development and Use of a Predictive Model of Crack Propagation in 304/316L, A533B/A508, and Inconel 600/182 Alloys in 288°C Water*, Proc. 3rd Int. Symp. on Environmental Degradation of Materials in Nuclear Power Systems—Water Reactors, Traverse City, MI, The Metallurgical Society/AIME, Warrendale, PA (1988), pp. 789-800.
201. P. Ford, P. Andresen, H. Solomon, G. Gordon, S. Ranganath, D. Weinstein, and R. Pathania, *Application of Water Chemistry Control, On-Line Monitoring and Crack Growth Rate Models for Improved BWR Material Performance*, Proc. 4th Int. Symp. on Environmental Degradation of Materials in Nuclear Power Systems—Water Reactors, Jekyll Island, GA, NACE, Houston, TX (1989), pp. 4-26 to 4-51.
202. R. Bandy and D. Van Rooyen, *Quantitative Examination of Stress Corrosion Cracking of Alloy 600 in High-Temperature Water*, Nucl. Eng. Design, Vol. 86 (1985), pp. 49-56.
203. J. R. Galvele, *A Stress Corrosion Cracking Mechanism Based on Surface Mobility*, Corr. Sci., Vol. 27 (1987), pp. 1-33.
204. K. Sieradzki and F. J. Friedersdorf, *Notes on the Surface Mobility Mechanism of Stress Corrosion Cracking*, Corr. Sci., Vol. 36, (1994), pp. 669-675.
205. U. Ehrnsten, J. Lagerstrom, T. Saario, J. Piippo, P. Aaltonen, S. Tahtinen, T. Laitinen, and H. Hanninen, *Environmentally Assisted Cracking of Alloy 600 in PWR Primary Water*, Eurocorr 96, Nice (24-26 Sept. 1996).
206. H. K. Birnbaum, I. M. Robertson, P. Sofronis, and D. Teter, *Mechanisms of Hydrogen-Related Fracture - A Review*, J. Inst. Mater. Conf. Proc. on Corrosion Deformation Interactions, European Federation of Conference Publication, Nice, France (1996).
207. C. H. Shen and P. G. Shewmon, *A Mechanism for Hydrogen-Induced Intergranular Stress Corrosion Cracking in Alloy 600*, Metal. Trans. A, Vol. 21A (1990), pp. 1261-1271.
208. A. Gourgues, P. M. Scott, and E. Andrieu, *A Study of the Mechanism of Primary Water Stress Corrosion Cracking of Alloy 600*, Proc. 7th Int. Symp. on

Environmental Degradation of Materials in Nuclear Power Systems—Water Reactors, Breckenridge, CO, NACE, Houston, TX (1995), pp. 829-839.

209. J. M. Silcock and P. R. Swann, *Microstructural Aspects of Environment Sensitive Failure of Austenitic Stainless Steel*, in *Mechanisms of Environment Sensitive Cracking of Materials*, P. R. Swann, F. P. Ford, and A. R. Westwood, eds., The Metals Society, London (1977), pp. 66-82.
210. R. Li and M. G. S. Ferreira, *The Thermodynamic Conditions for Hydrogen Generation Inside a Stress Corrosion Crack*, *Corr. Sci.*, Vol. 38 (1996), pp. 317-327.
211. B. Persson and J. Lagerstrom, *The Effect of Varying Loads and Degree of Subcooling on PWSCC in Alloy 600*, Proc. 1994 EPRI Workshop on PWSCC of Alloy 600 in PWRs, Part 2, EPRI TR-105406, Palo Alto, CA (Aug. 1995).
212. J. Lagerstrom, U. Ehrnsten, T. Saario, and H. Hanninen, *Model for Environmentally Assisted Cracking of Alloy 600 in PWR Primary Water*, Proc. 8th Int. Symp. on Environmental Degradation of Materials in Nuclear Power Systems—Water Reactors, Amelia Island, FL, American Nuclear Society, La Grange Park, IL (1997), pp. 349-356.
213. P. M. Scott and M. Le Calvar, *Some Possible Mechanisms of Intergranular Stress Corrosion Cracking of Alloy 600 in PWR Primary Water*, Proc. 6th Int. Symp. on Environmental Degradation of Materials in Nuclear Power Systems—Water Reactors, San Diego, The Metallurgical Society/AIME, Warrendale, PA (1993), pp. 81-88.
214. J. K. Sung and G. S. Was, *Intergranular Cracking of Ni-16Cr-9Fe Alloys in High-Temperature Water*, *Corrosion*, Vol. 47 (1991), pp. 824-834.
215. T. S. Gendron, P. M. Scott, S. M. Bruemmer, and L. E. Thomas, *Internal Oxidation as a Mechanism for Steam Generator Tube Degradation*, presented at the 3rd Intl. Steam Generator and Heat Exchanger Conf. (June 21-24, 1998), Toronto.
216. T. Saario, P. Aaltonen, P. K. Roikonen, J. Piippo, K. Makela, S. Tahtinen, and H. Hanninen, *Selective Dissolution - Vacancy - Creep Model for IGSCC of Alloy 600*, Proc. 7th Int. Symp. on Environmental Degradation of Materials in Nuclear Power Systems—Water Reactors, Breckenridge, CO, NACE, Houston, TX (1995), pp. 841-854.
217. P. M. Scott, *An Analysis of Primary Water Stress Corrosion Cracking in PWR Steam Generators*, Proc. of the Specialists Meeting on Operating Experience with Steam Generators, Brussels, Belgium (Sept. 1991), pp. 5-6.
218. A. R. McIlree, R. B. Rebak, and S. Smialowska, *Relationship of Stress Intensity to Crack Growth Rate of Alloy 600 in Primary Water*, Int. Symp. on Contribution of Materials Investigation to the Resolution of problems encountered in PWR Plants. Fontevraud II, Vol. 1 (1990), pp. 258-267.

219. Y. S. Garud, *An Incremental Damage Formulation for Stress Corrosion Cracking and Its Application to Crack Growth Interpretation Based on CERT Data*, Corrosion, Vol. 46 (1990), pp. 968-974.
220. Y. S. Garud, *An Incremental Damage Formulation and Its Application to Assess IGSCC Growth of Circumferential Cracks in a Tube*, Corrosion, Vol. 47 (1991), pp. 523-527.
221. J. A. Gorman, K. D. Stavropoulos, and A. R. McIlree, *Guidelines for Prediction of PWSCC in Steam Generator Tubes*, Int. Symp. on Contribution of Materials Investigation to the Resolution of problems encountered in PWRs. Fontevraud III, Vol. 1 (1994), pp. 311-318.
222. E. D. Eason and E. E. Nelson, *A Model of Caustic Stress Corrosion Crack Initiation and Growth in Alloy 600*, EPRI TR-104073, Palo Alto, CA (June 1994).
223. J. Stubbe and P. Hernalsteen, *Is Corrosion Dependent on the Duration of In-service Cycle?*, Int. Symp. on Contribution of Materials Investigation to the Resolution of problems encountered in PWRs. Fontevraud III, Vol. 1 (1994), pp. 365-373.
224. L. Z. Nedden, J. Stubbe, and E. Pierson, *Effect of Simulated Outage Conditions in Acid Environment Containing Copper on Corrosion of Steam Generator Tubes*, Proc. 8th Int. Symp. on Environmental Degradation of Materials in Nuclear Power Systems—Water Reactors, Amelia Island, FL, American Nuclear Society, La Grange Park, IL (1997), pp. 91-99.

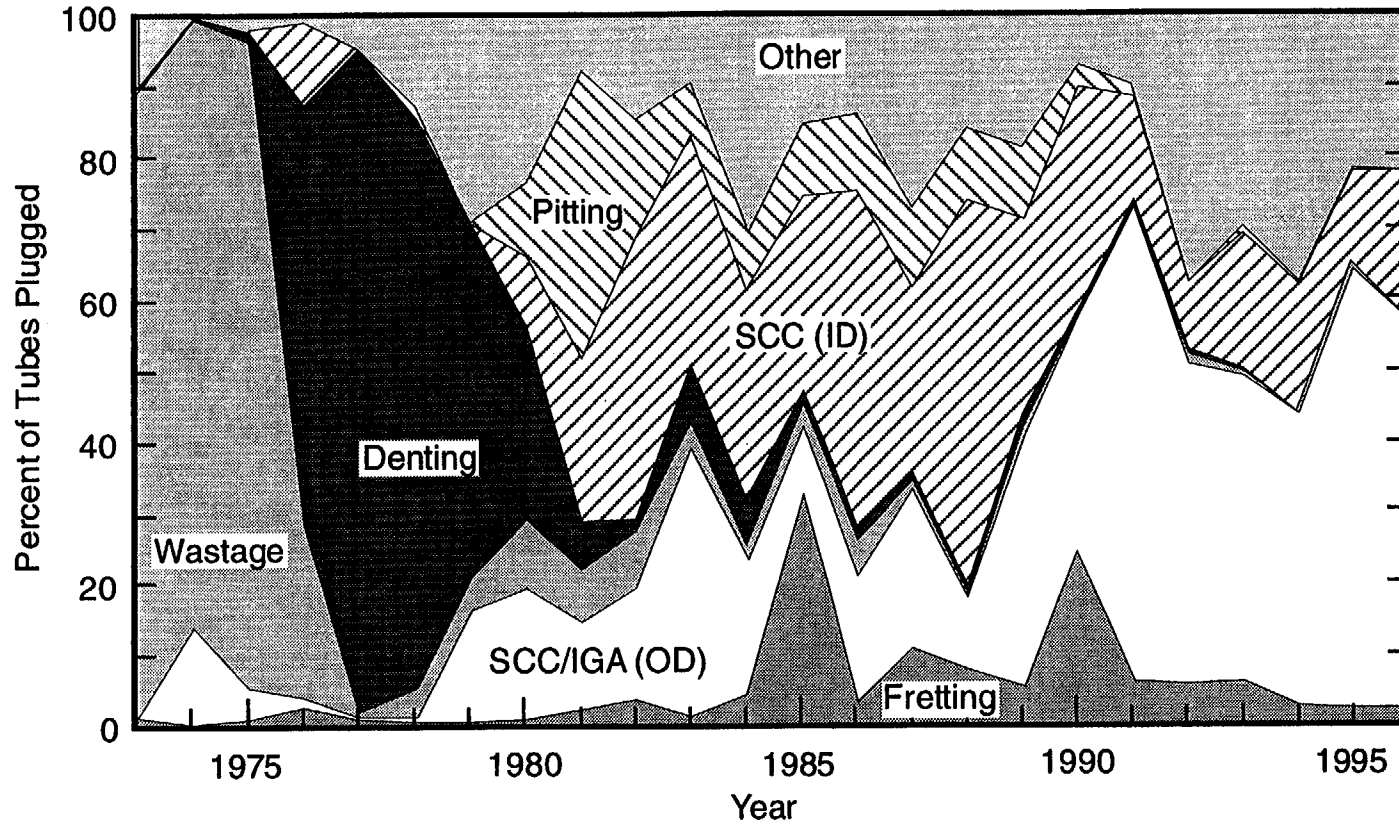
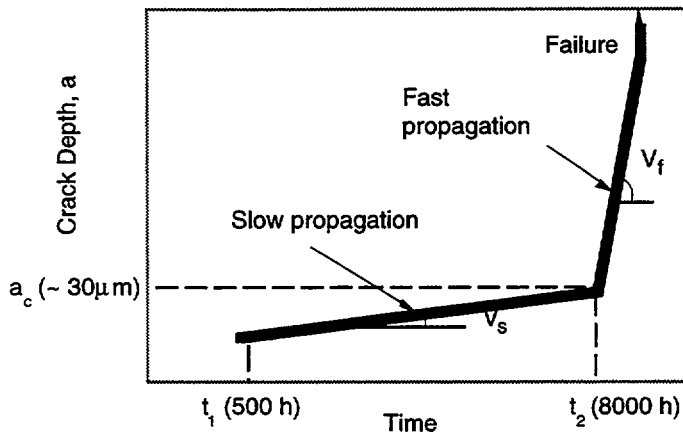
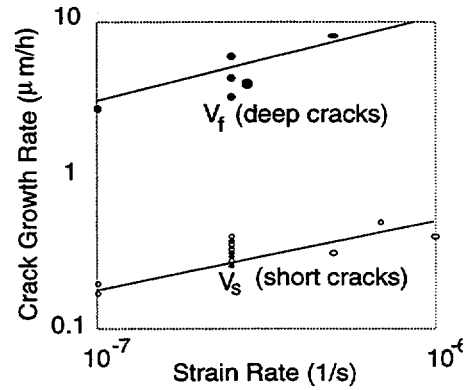


Figure 1. Causes of steam generator tube plugging in U.S. by year (adapted from Ref. 11).



(a)



(b)

Figure 2. Crack growth rate of mill-annealed Alloy 600 tubes: (a) schematic representation of crack depth vs. time (values in bracket are for a constant load test at 450 MPa [65 ksi] in pure hydrogenated water)<sup>10</sup> and (b) CERT in primary water at 360°C.<sup>62</sup>

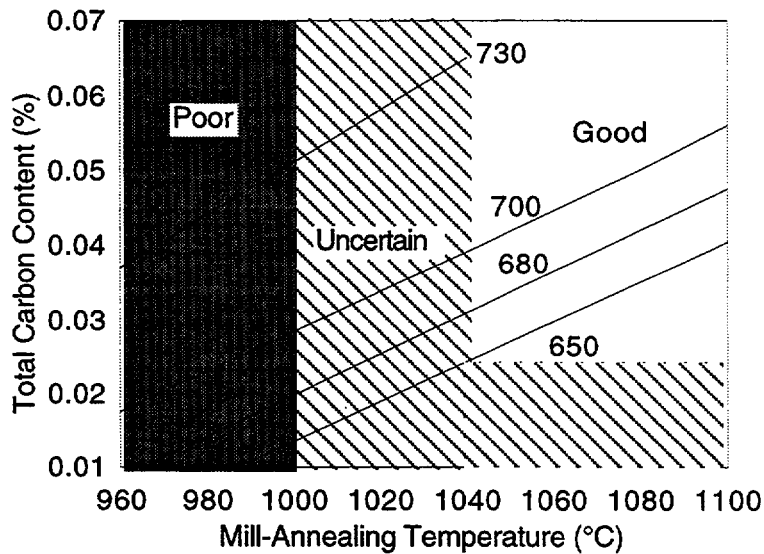


Figure 3. Regions of poor, uncertain, and good resistance to IGSCC of mill-annealed Alloy 600 (without thermal treatment) in pure hydrogenated water at 350°C. Also shown are lines of constant ultimate tensile strength (in MPa) at 350°C.<sup>10</sup>

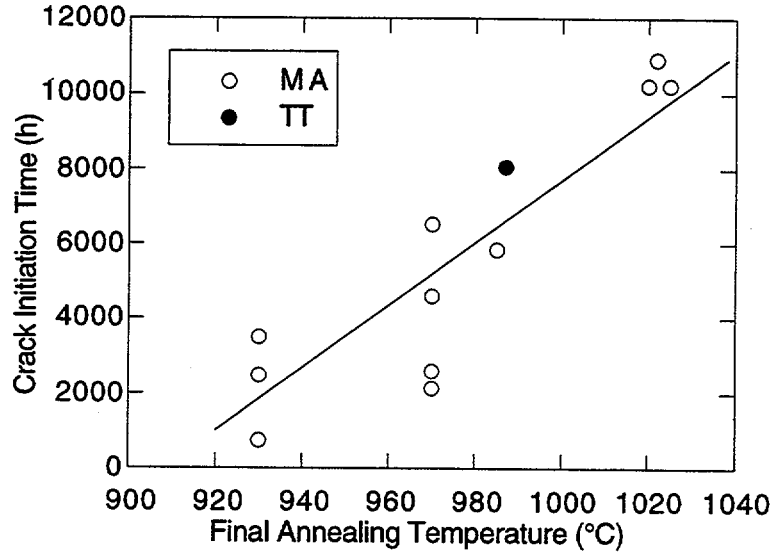


Figure 4. Influence of final annealing temperature on the crack initiation time as determined from RUB tests in high-purity water with hydrogen for 19.1-mm (0.75-in.)-diam Alloy 600 tube at 365°C.<sup>56</sup> MA = mill-annealed; TT = thermally treated.

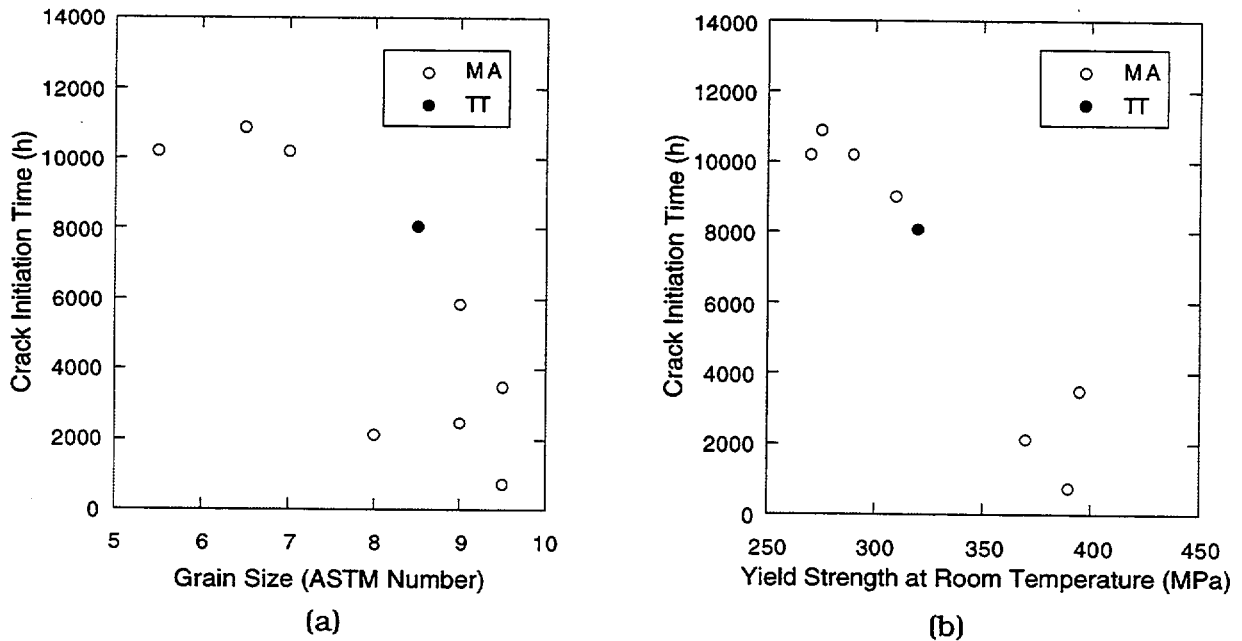


Figure 5. Variation of stress corrosion crack initiation time in Alloy 600 with (a) grain size and (b) room temperature yield strength.<sup>56</sup> MA = mill-annealed; TT = thermally treated.

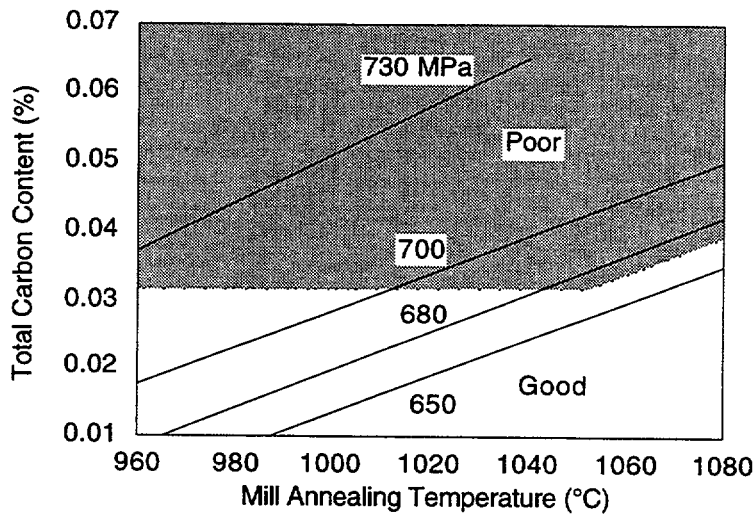


Figure 6. Regions of poor and good resistance to IGSCC of Alloy 600, thermally treated at 700°C, in pure hydrogenated water at 350°C.<sup>10</sup> Also shown are lines of constant ultimate tensile strength (in MPa) at 350°C.

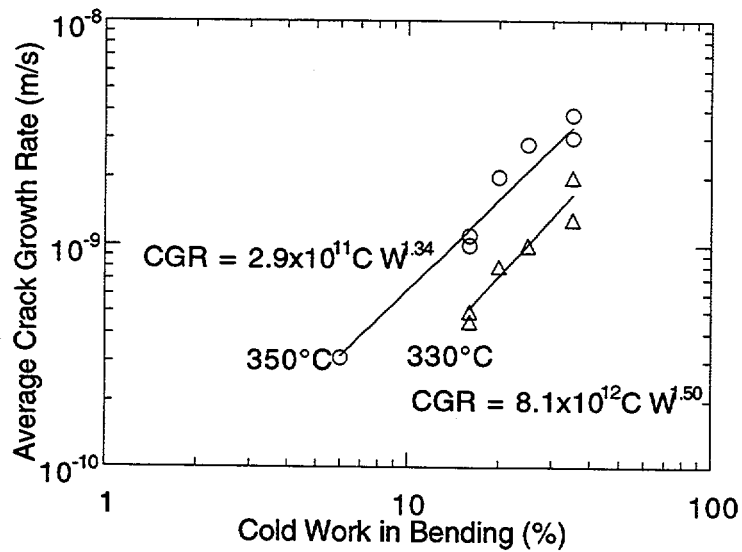


Figure 7. Average CGRs in CERTs vs. cold work in bending for low-temperature mill-annealed Alloy 600 tubes.<sup>101</sup>

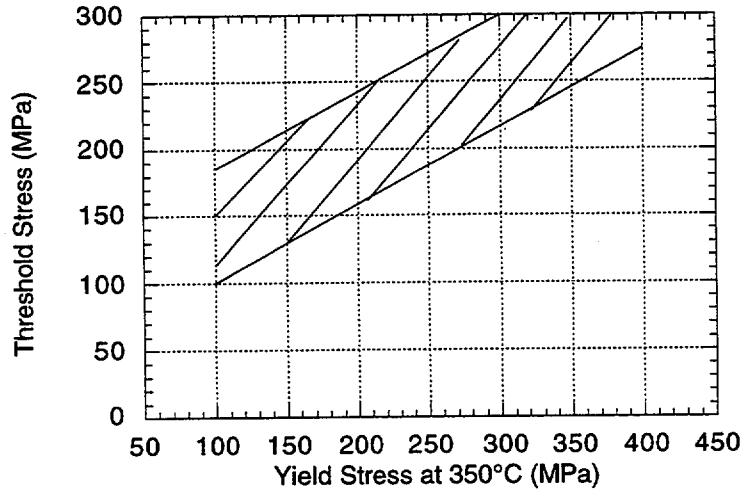


Figure 8. Relationship between stress threshold for IGSCC of mill-annealed Alloy 600 in NaOH (100g/L) at 350°C and yield stress at 350°C.<sup>71</sup>

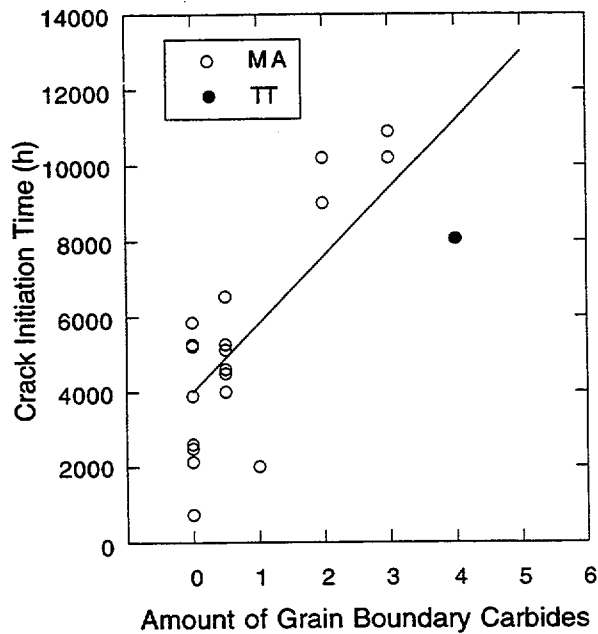


Figure 9. Variation of time for initiation of SCC in Alloy 600 with amount of grain boundary carbides (0 = no carbides in grain boundaries, 5 = grain boundaries are completely covered with carbides).<sup>56</sup> MA = mill-annealed; TT = thermally treated.

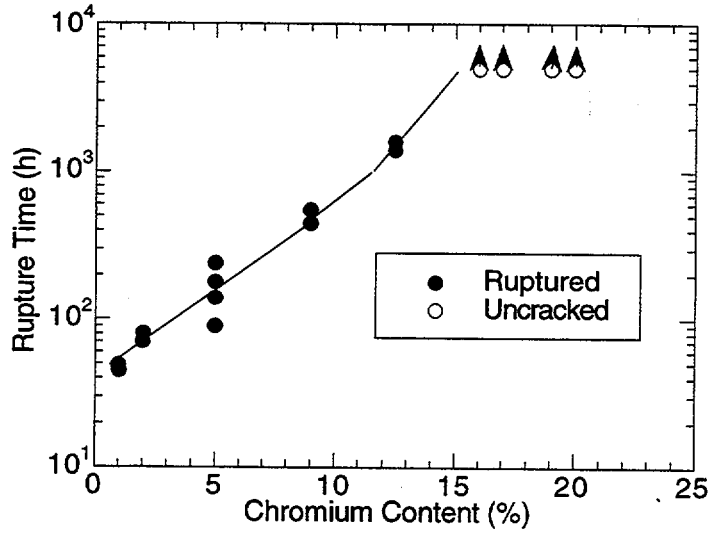


Figure 10. Effect of chromium content on rupture time of solution-annealed Ni-base-Cr-Fe-alloys in lithiated water at 360°C.<sup>113</sup>

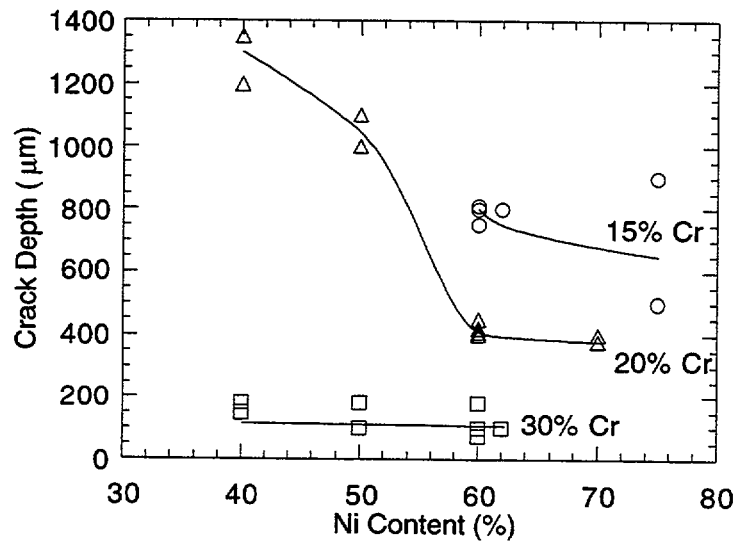
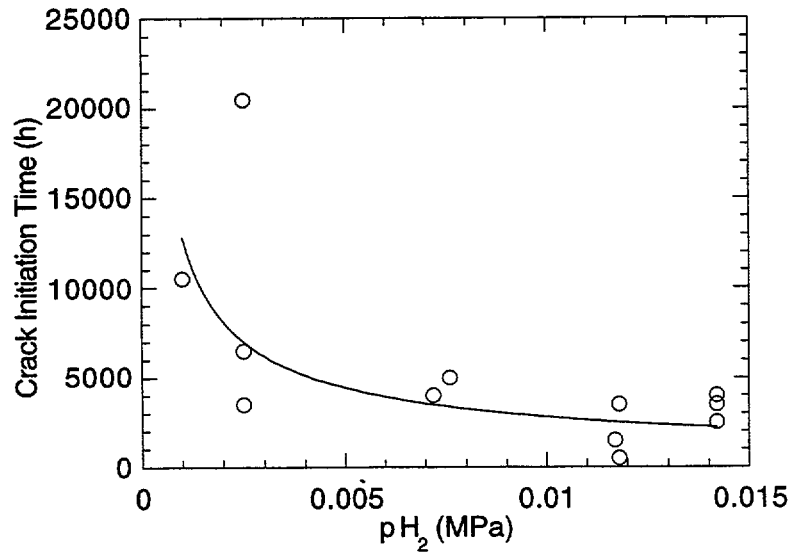
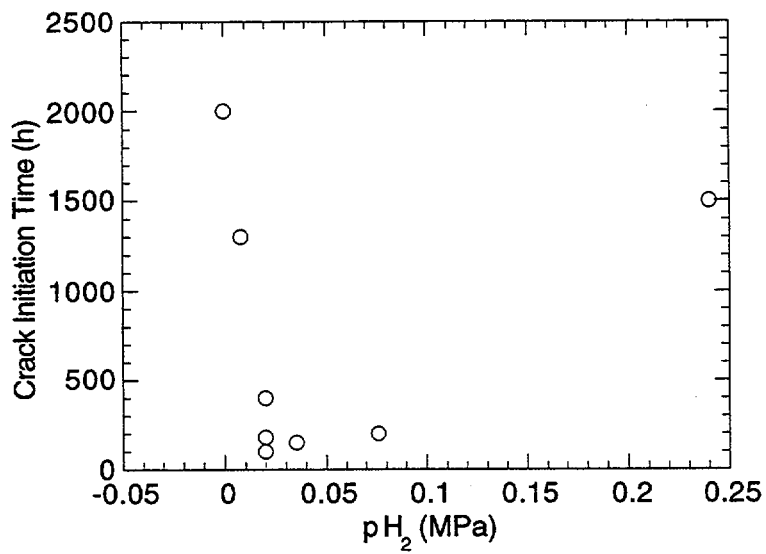


Figure 11. Effect of chromium and nickel contents on caustic SCC resistance of 0.02%C-x%Ni-y%Cr-bal. Fe alloys (mill-annealed at 1100°C and water quenched) in deaerated 10% NaOH solution at 325°C for 500 h (single U-bend).<sup>120</sup>

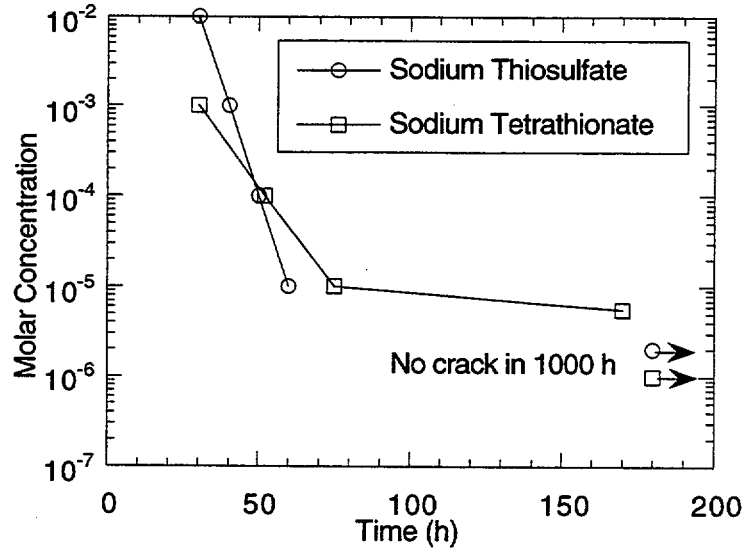


(a)

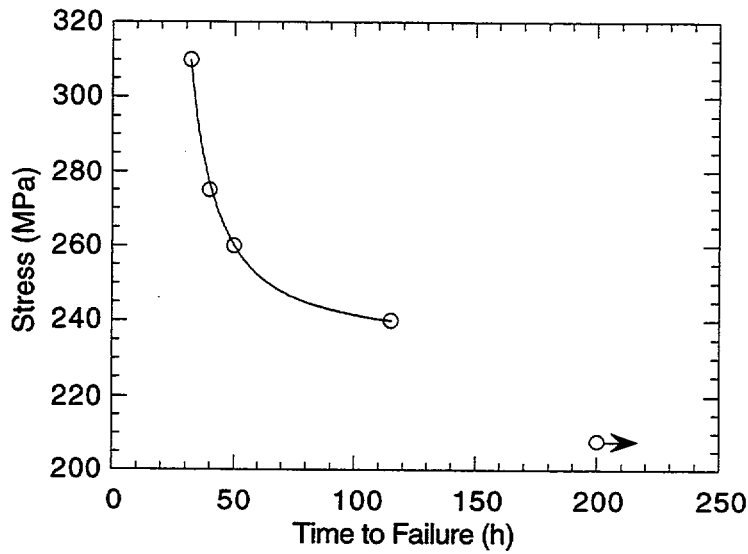


(b)

Figure 12. Effect of hydrogen partial pressure on crack initiation time in (a) high-temperature water,<sup>58</sup> and (b) 400°C steam.<sup>122</sup>



(a)



(b)

Figure 13. (a) Effect of concentration of sodium thiosulfate and sodium tetrathionate on time to failure of SAS U-bends<sup>58</sup> and (b) plot of nominal stress (constant load) vs. time to failure for SAS tensile specimens in 1.3% boric acid with 0.7 ppm sulfur as thiosulfate and 0.7 ppm lithium as lithium hydroxide.<sup>131</sup> All tests were conducted in air-saturated environment at room temperature.

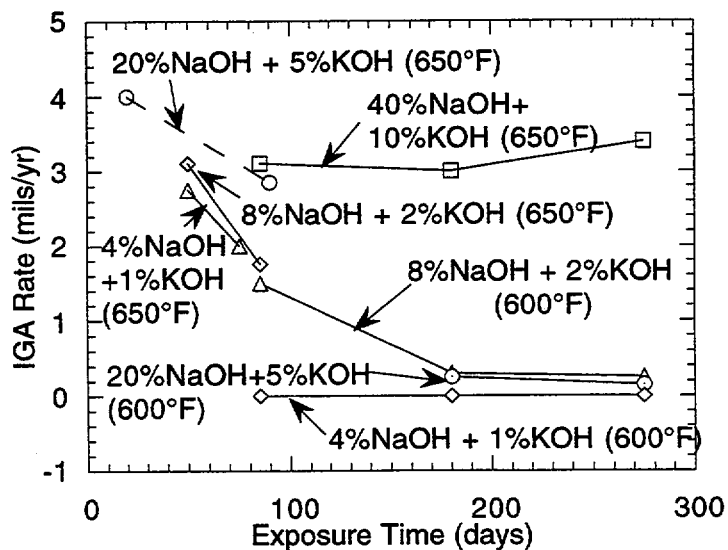


Figure 14. Average IGA rates of Alloy 600, as influenced by caustic concentration and temperature.<sup>140</sup>

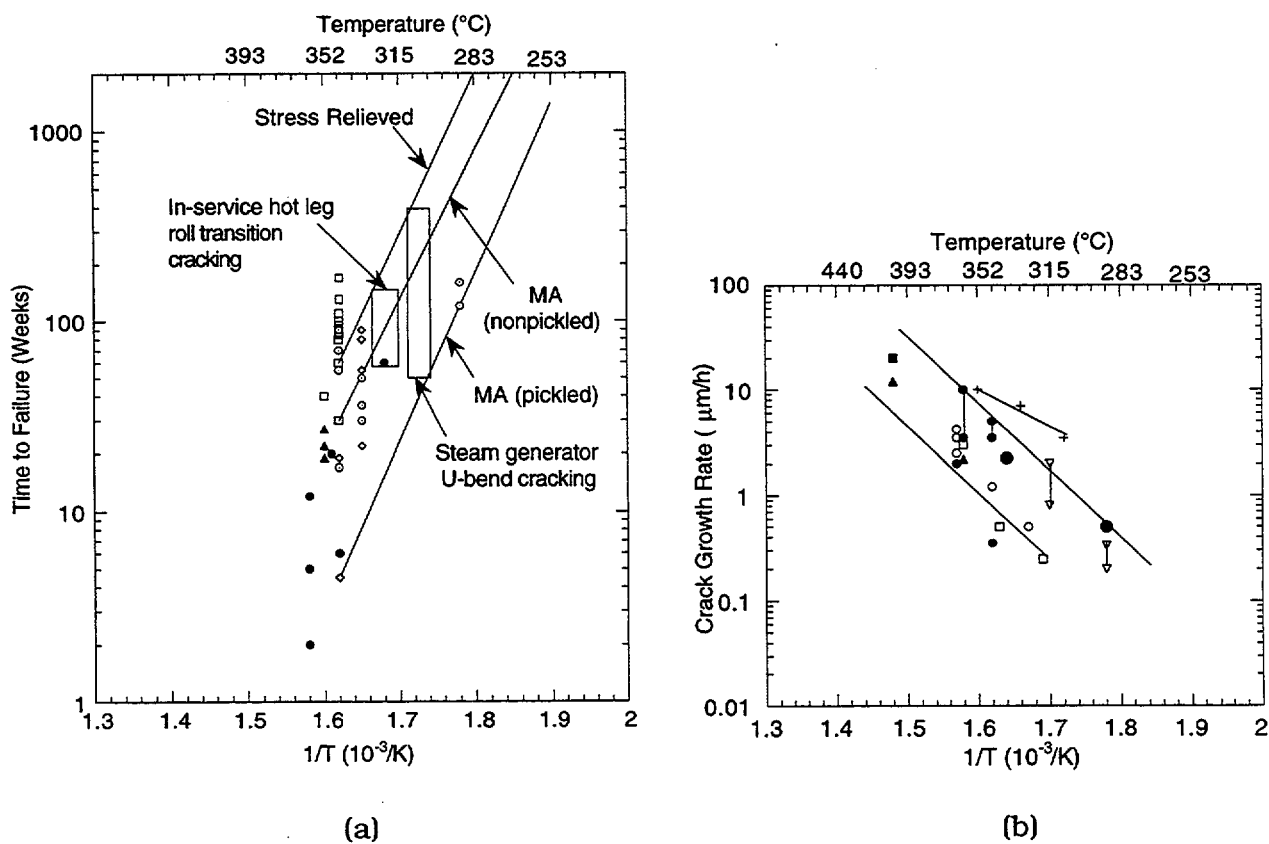


Figure 15. Effect of temperature on SCC (a) crack initiation<sup>158</sup> and (b) crack propagation<sup>10</sup> of mill-annealed Alloy 600 tube. MA = mill annealed.

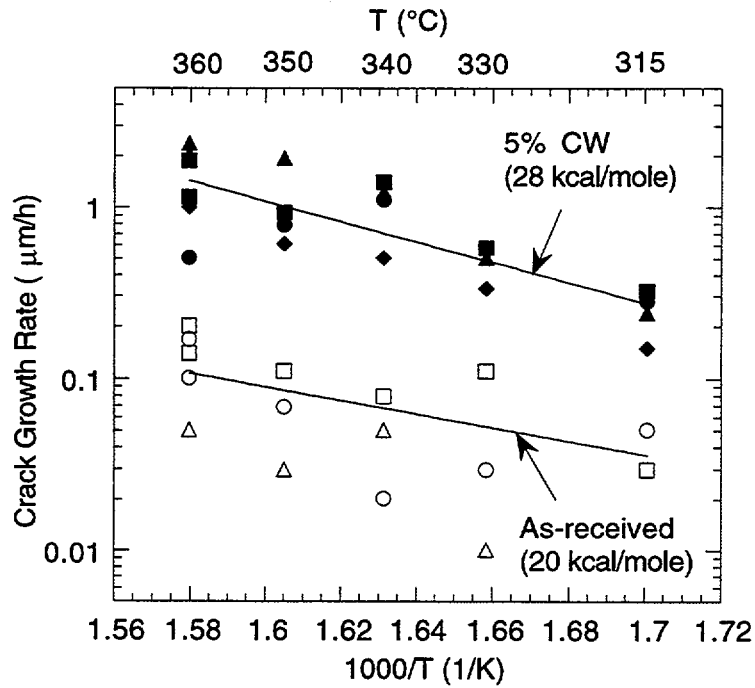


Figure 16. Effect of temperature on CGRs in as received and 5% cold-worked mill-annealed Alloy 600 tubes in primary water with a hydrogen partial pressure of 0.03 MPa (4 psi) and  $20 < K_I < 30 \text{ MPa}\sqrt{m}$ .<sup>160</sup> CW = cold-worked.

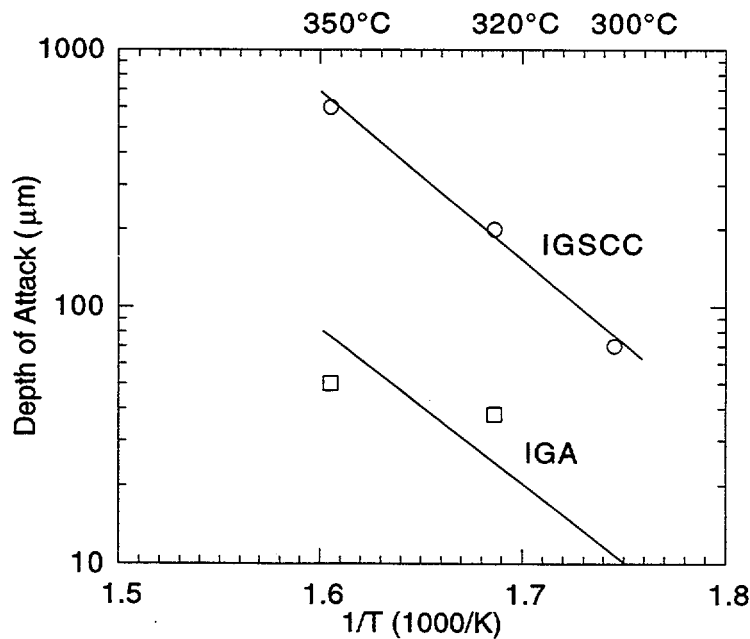


Figure 17. Temperature effect on the corrosion of mill-annealed Alloy 600 C-rings in 240-h tests in 9% NaOH + 1% KOH + 1% Na<sub>2</sub>SO<sub>4</sub>.<sup>17</sup>

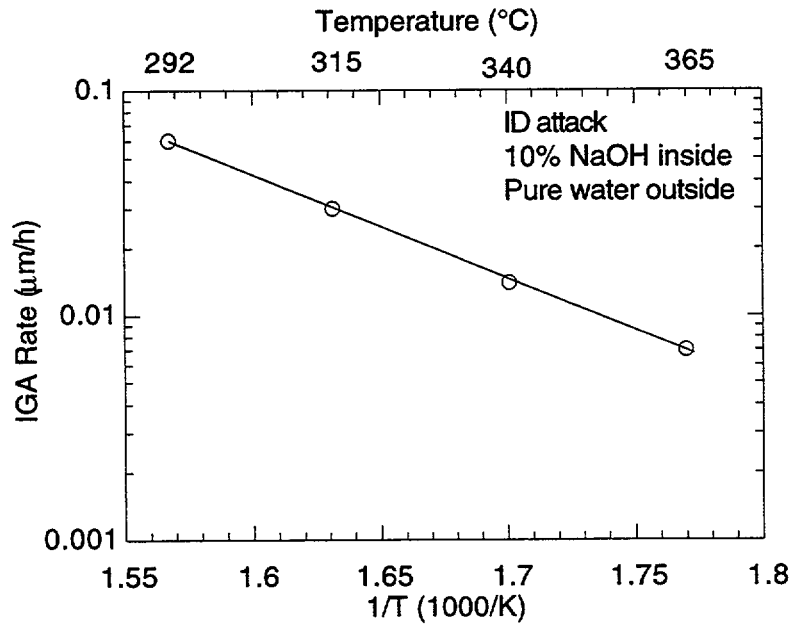


Figure 18. Activation energy for 40-day IGA tests on mill-annealed Alloy 600 (surfaces in compression).<sup>161</sup>

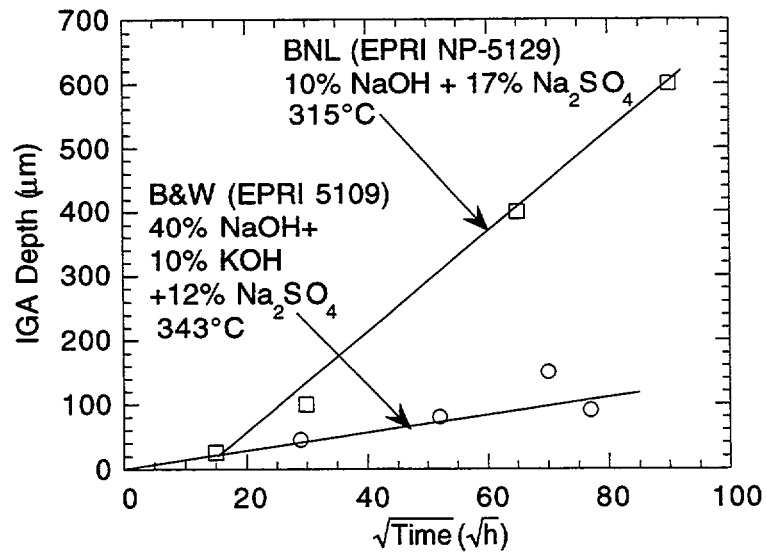


Figure 19. Relationship between square root of time and IGA depth.<sup>163</sup>

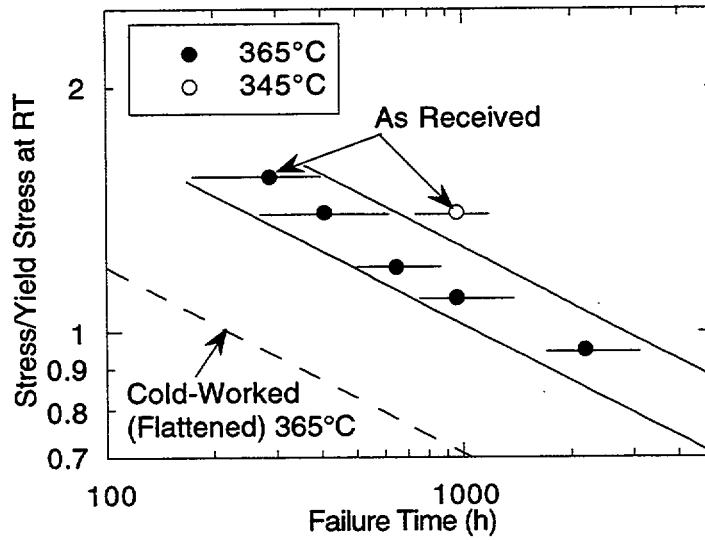


Figure 20. Failure time vs. normalized stress for constant load tests of as-received and cold-worked Alloy 600 tubes in distilled demineralized water at 345 and 365°C.<sup>48</sup> RT = room temperature.

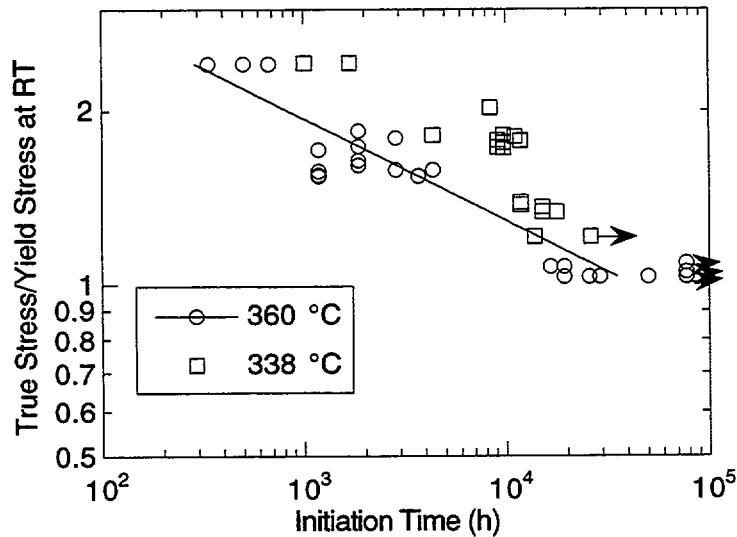


Figure 21. Crack initiation time vs. normalized true stress for split-tube U-bend tests and C-ring tests on LTMA Alloy 600 tubes in deaerated, hydrogenated water at 338 and 360°C.<sup>41</sup> RT = room temperature.

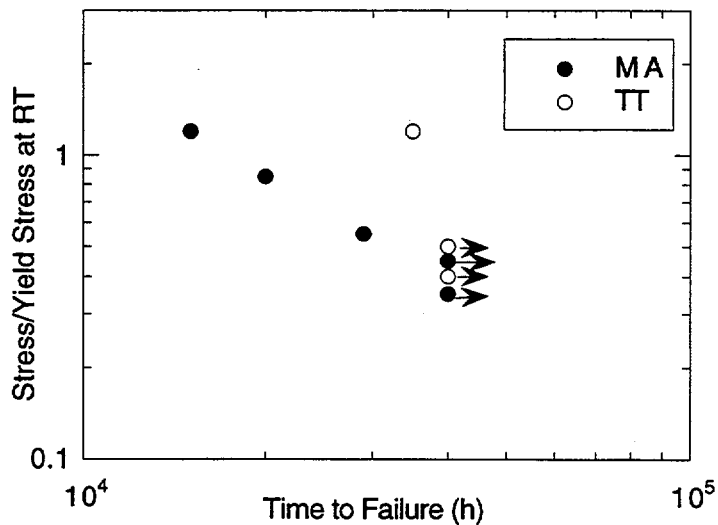


Figure 22. Failure time vs. normalized stress for U-bend tests on mill-annealed (MA) and thermally treated (TT) Alloy 600 tubes in pure water at 343°C.<sup>167</sup> RT = room temperature.

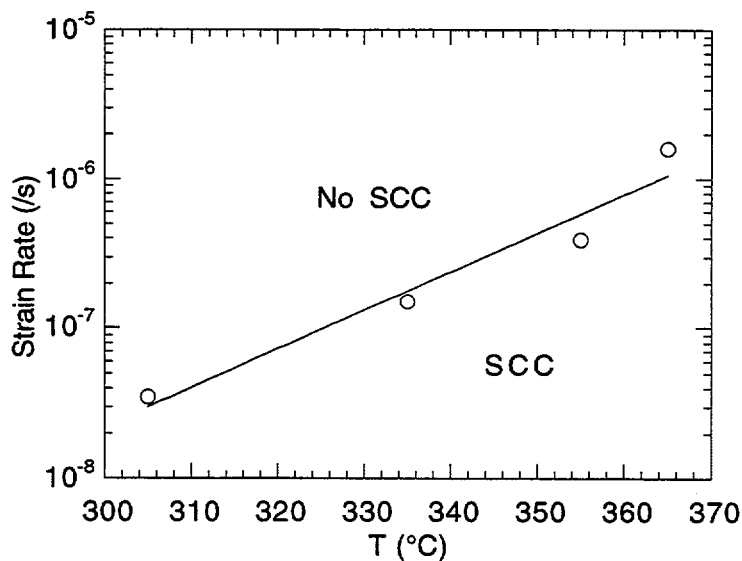


Figure 23. Effect of temperature on limiting strain rate below which SCC is observed in as-received Alloy 600 tested in primary water with hydrogen.<sup>51</sup>

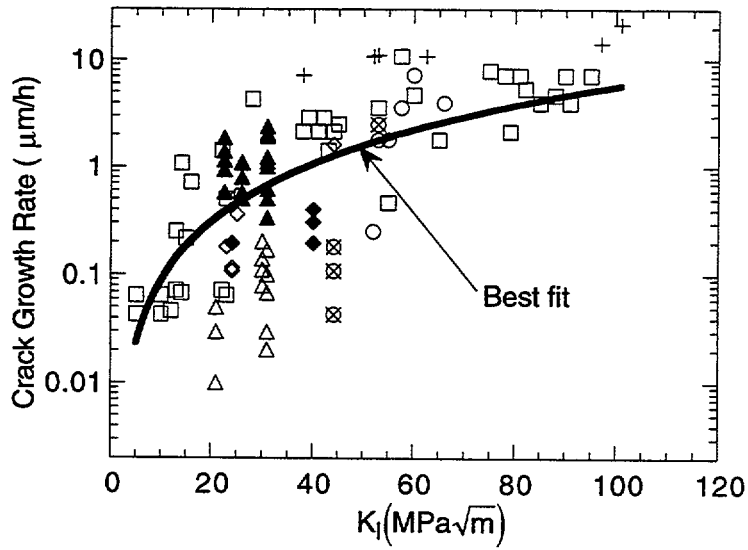
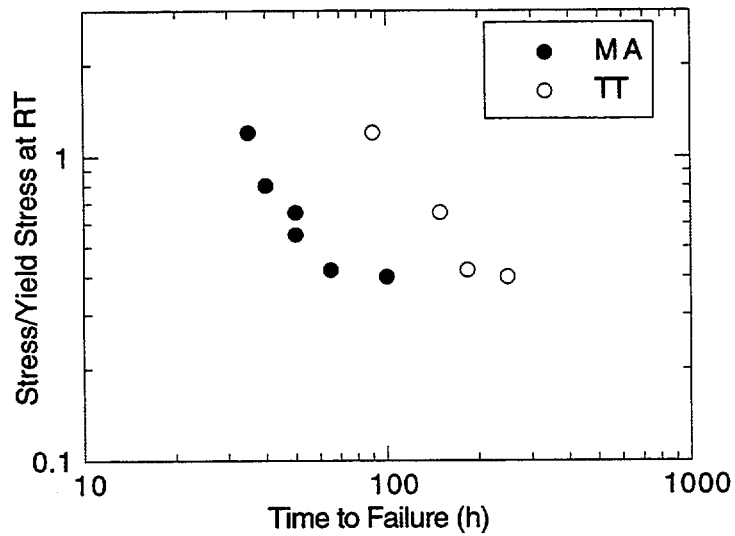
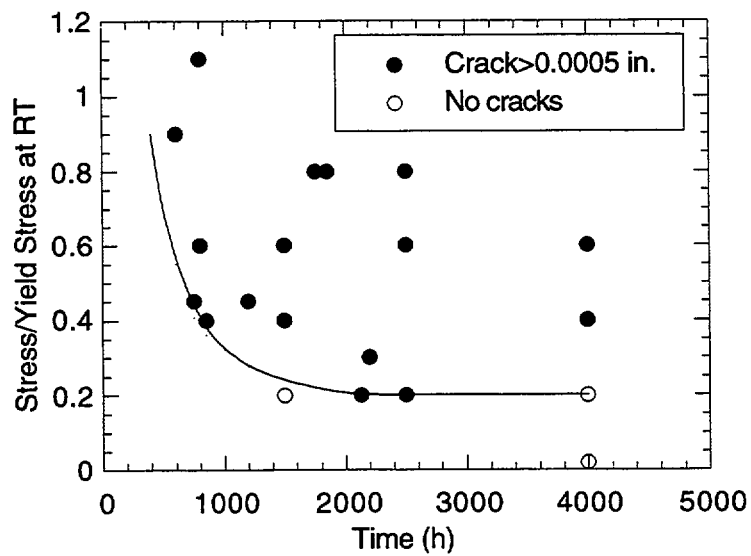


Figure 24. Collected literature data on crack growth rate vs. stress intensity factor for Alloy 600 in simulated primary water.<sup>169</sup>



(a)



(b)

Figure 25. Failure time vs. normalized stress for (a) U-bend tests on mill-annealed (MA) and thermally treated (TT) Alloy 600 tubes in 10% NaOH solution at 289°C,<sup>167</sup> and (b) pressurized tube tests on Alloy 600 tubes in 10% NaOH at 315°C.<sup>171</sup> RT = room temperature.

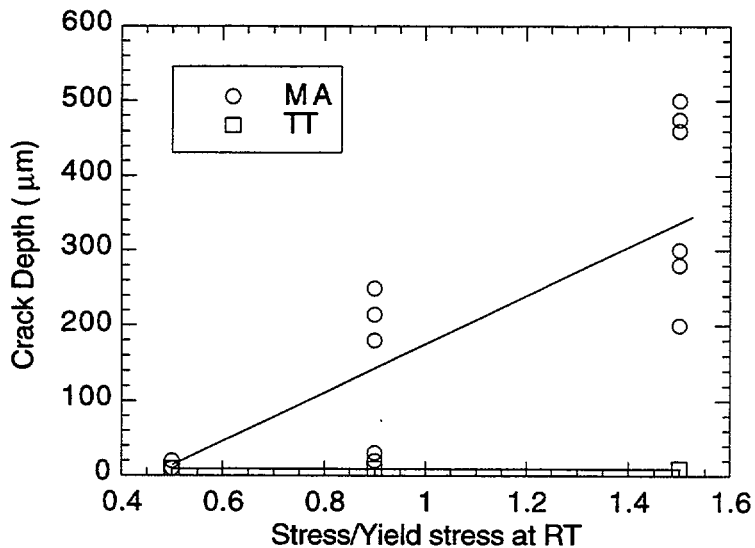


Figure 26. Crack depth vs. normalized stress for C-ring tests on mill-annealed (MA) and thermally treated (TT) Alloy 600 tubes in 10% NaOH solution at 315°C for 2000 h.<sup>36</sup> RT = room temperature.

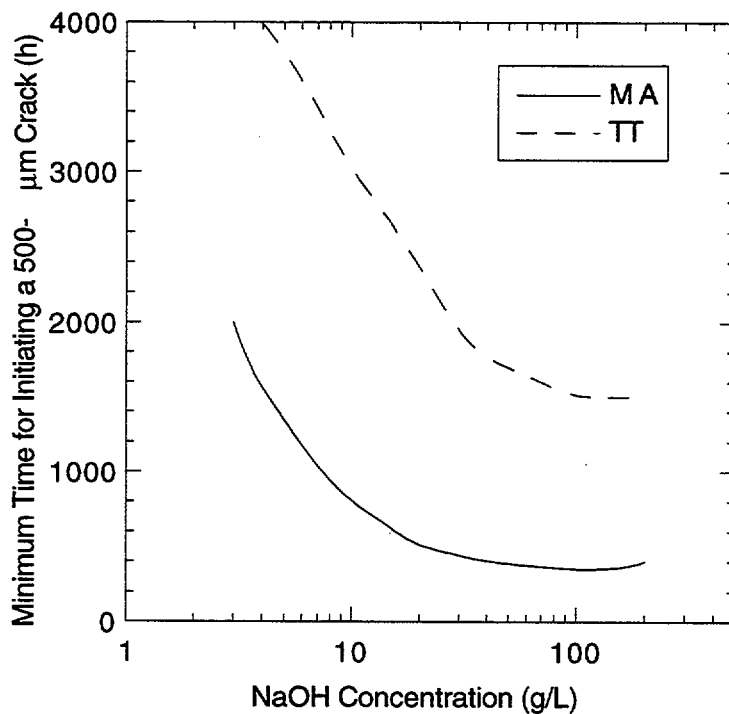
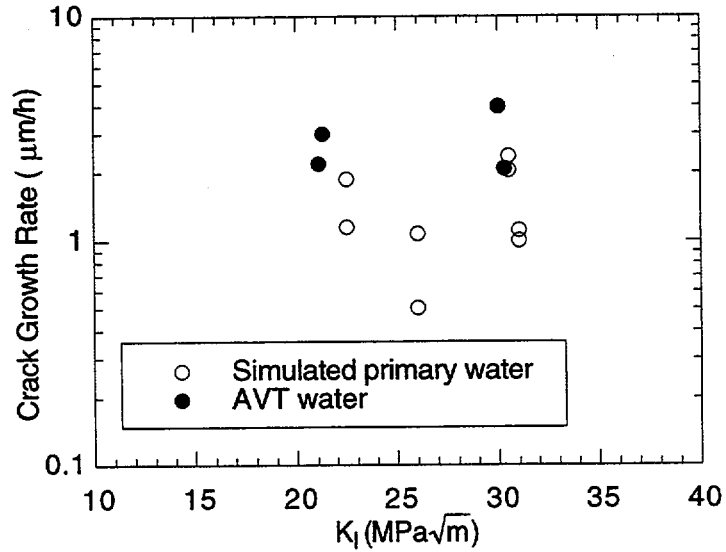
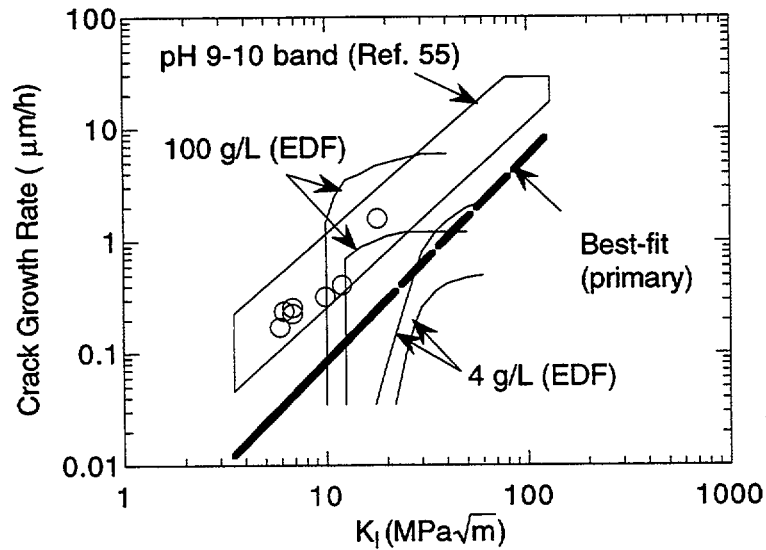


Figure 27. Minimum time to initiate a 500-μm crack at 350°C in C-ring tests of mill-annealed (MA) and thermally treated (TT) tubes at approximately yield stress vs. NaOH concentration.<sup>65</sup>



(a)



(b)

Figure 28. Crack growth rate vs. stress intensity factor for (a) tubular specimen (5% cold worked) in 360°C AVT water with hydrogen<sup>160</sup> and (b) WOL mill-annealed and thermally treated specimens of Alloy 600 (20-mm thick plate, 0.072 carbon, room-temperature yield stress = 360 MPa) in deaerated dilute NaOH solutions at 350°C (EDF)<sup>65</sup>, and precracked mill-annealed tubing (0.04 carbon, room-temperature yield stress = 335 MPa) in 10% caustic at 315°C (Brisson)

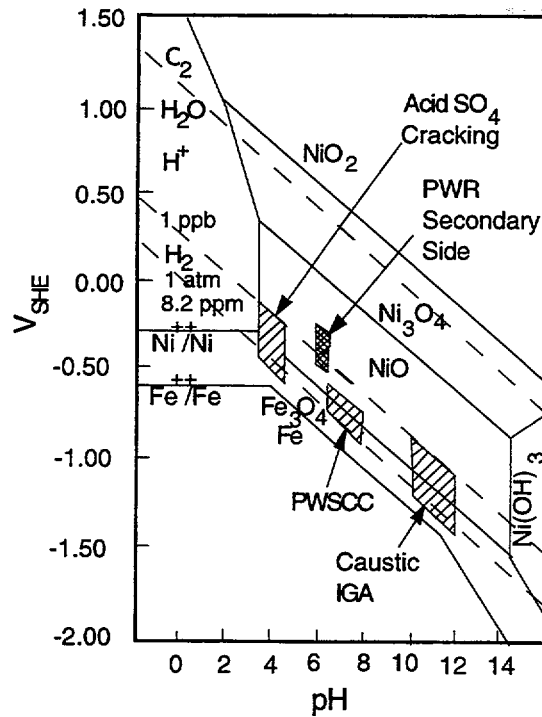


Figure 29. Main domains of IGA and IGSCC of Alloy 600 in aqueous solutions at 290-360°C.<sup>199</sup>

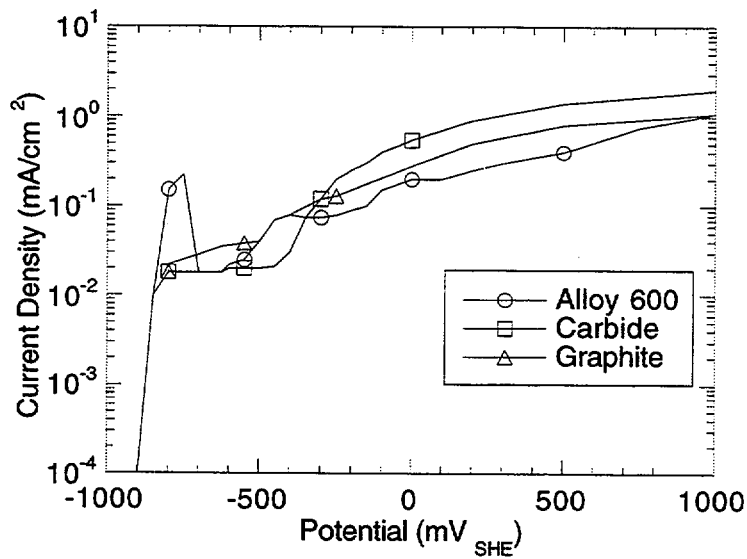


Figure 30. Anodic polarization curve of as-received Alloy 600,  $M_{23}C_6$  carbide, and graphite in 108 ppm B + 7 ppm Li solution at pH = 7, deaerated with hydrogen at 350°C.<sup>121</sup>

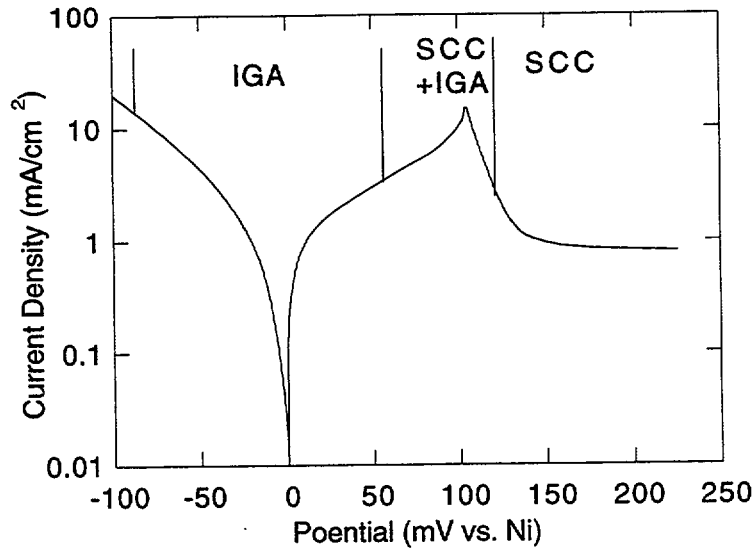


Figure 31. Superimposition of potential areas for IGA and SCC on the polarization curve of Alloy 600 in 10% NaOH + 1% Na<sub>2</sub>CO<sub>3</sub> at 300°C at a scan rate of 20 mV/min.<sup>182</sup>

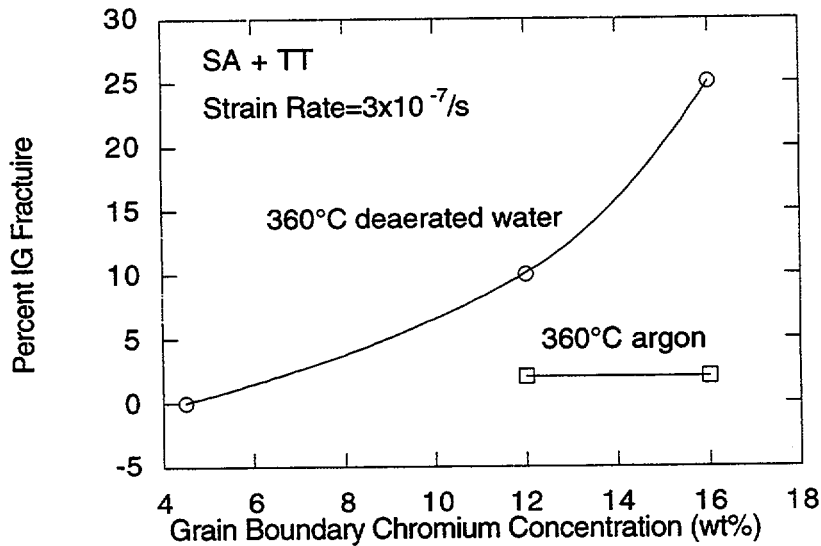


Figure 32. Effect of grain boundary chromium concentration that is a result of chromium carbide precipitation on intergranular cracking of high-purity Alloy 600 in deaerated high-temperature water and in argon.<sup>188</sup> SA = solution annealed, TT = thermally treated.

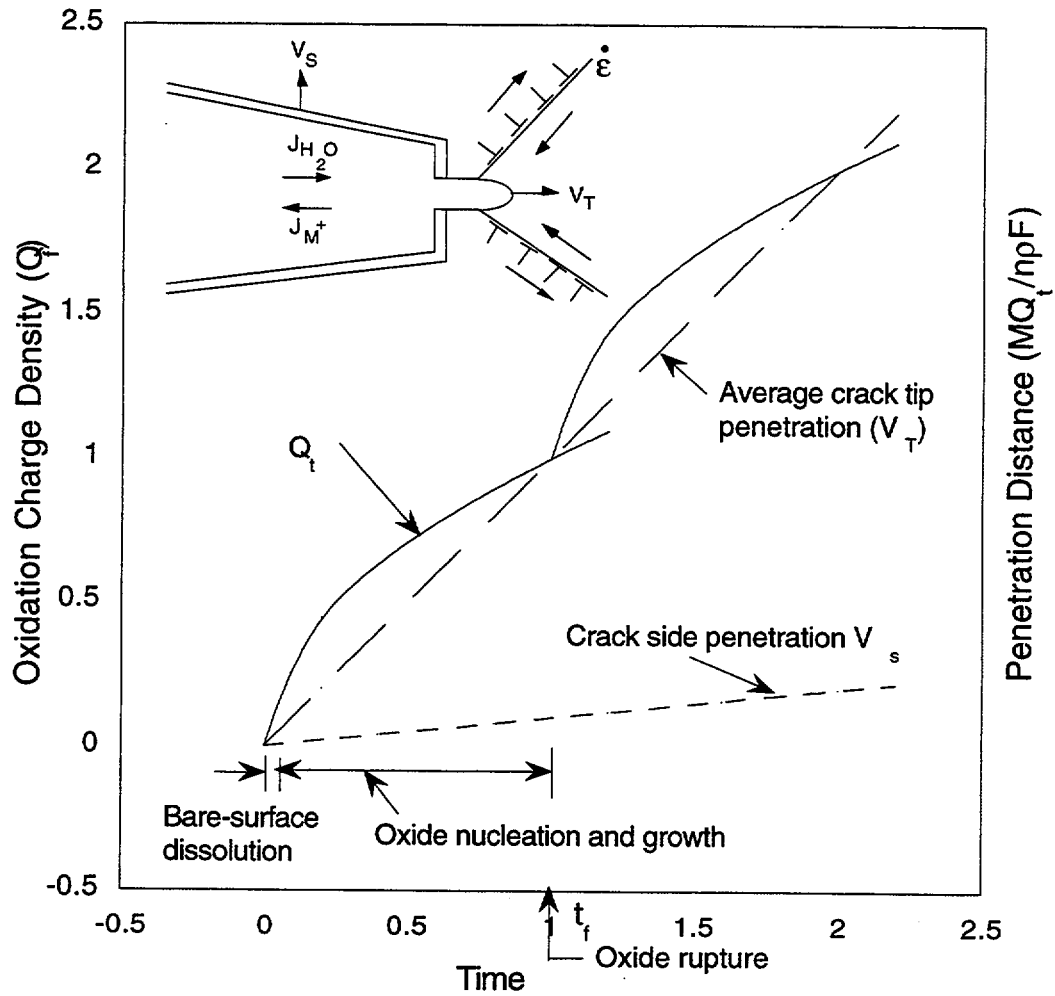


Figure 33. Schematic diagram of oxidation charge density/time relationships of a strained crack tip and unstrained crack sides.<sup>200</sup>

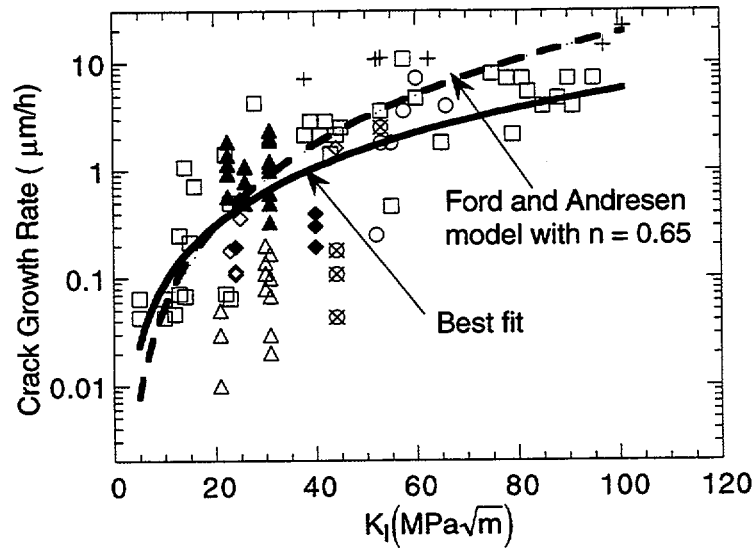


Figure 34. Collected literature data on crack growth rate vs. stress intensity factor for Alloy 600 in simulated primary water together with that predicted by the Ford and Andresen model.<sup>169</sup>

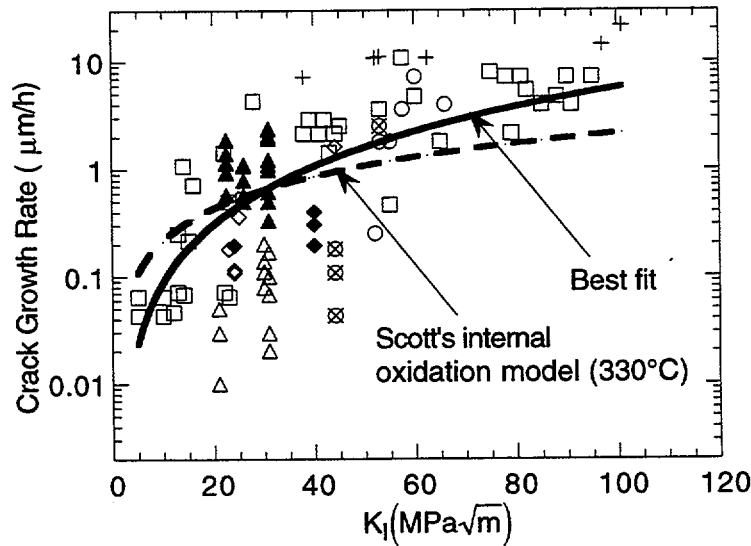


Figure 35. Collected literature data on crack growth rate vs. stress intensity factor for Alloy 600 in simulated primary water together with that predicted by Scott's internal-oxidation model.<sup>213</sup>

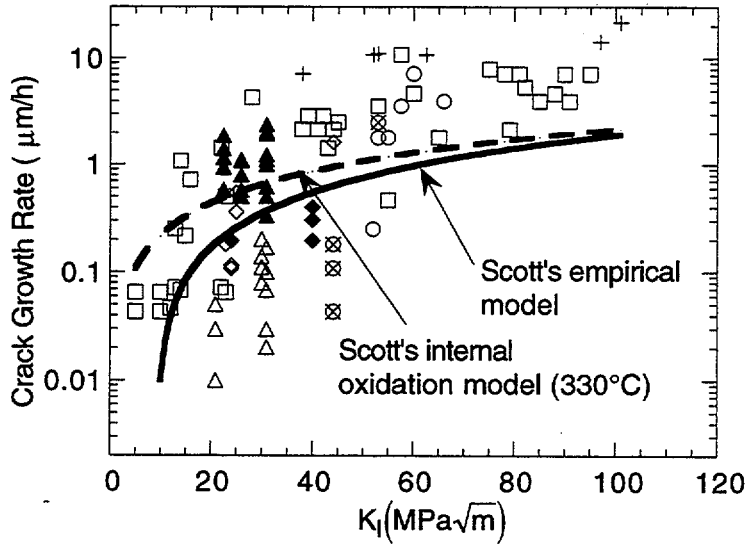


Figure 36. Collected literature data on crack growth rate vs. stress intensity factor for Alloy 600 in simulated primary water together with those predicted by Scott's empirical and internal-oxidation models.<sup>217</sup>

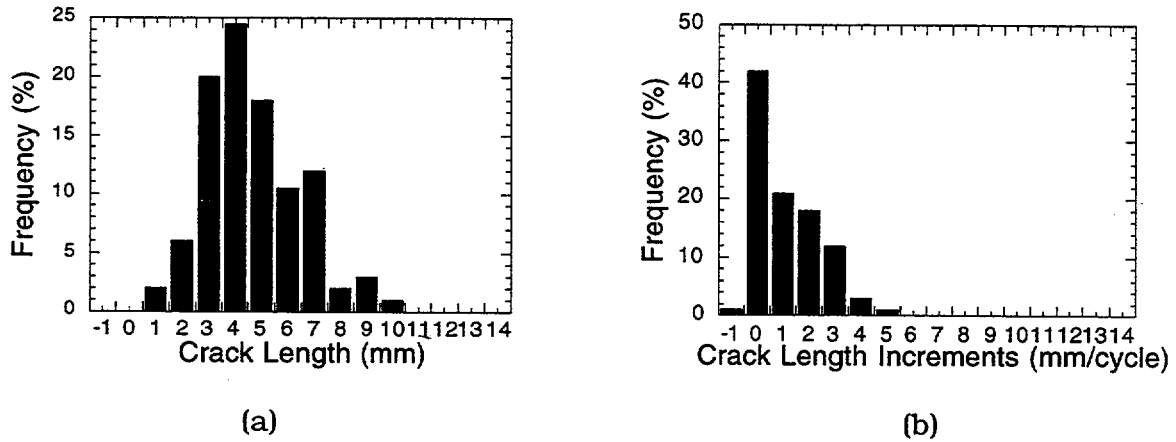


Figure 37. Typical frequency histograms for (a) crack length and (b) crack length increments for 186 cracked tubes from Belgian steam generators during 1986 and 1987.

**BIBLIOGRAPHIC DATA SHEET**

(See instructions on the reverse)

1. REPORT NUMBER  
(Assigned by NRC, Add Vol., Supp., Rev.,  
and Addendum Numbers, if any.)

NUREG/CR-5752  
ANL-99/4

2. TITLE AND SUBTITLE

Assessment of Current Understanding of Mechanisms of Initiation, Arrest, and  
Reinitiation of Stress Corrosion Cracks in PWR Steam Generator Tubing

3. DATE REPORT PUBLISHED

MONTH	YEAR
February	2000

4. FIN OR GRANT NUMBER

W6487

5. AUTHOR(S)

S. Majumdar

6. TYPE OF REPORT

Technical

7. PERIOD COVERED (Inclusive Dates)

8. PERFORMING ORGANIZATION - NAME AND ADDRESS (If NRC, provide Division, Office or Region, U.S. Nuclear Regulatory Commission, and mailing address; if contractor, provide name and mailing address.)

Argonne National Laboratory  
9700 South Cass Avenue  
Argonne, IL 60439

9. SPONSORING ORGANIZATION - NAME AND ADDRESS (If NRC, type "Same as above"; if contractor, provide NRC Division, Office or Region, U.S. Nuclear Regulatory Commission, and mailing address.)

Division of Engineering Technology  
Office of Nuclear Regulatory Research  
U.S. Nuclear Regulatory Commission  
Washington, DC 20555-0001

10. SUPPLEMENTARY NOTES

J. Muscara, NRC Project Manager

11. ABSTRACT (200 words or less)

This report summarizes the status of our current understanding on mechanisms of stress corrosion crack initiation and propagation in Alloy 600 PWR steam generator tubes. More than 200 publications from the literature were reviewed for this purpose. Factors influencing stress corrosion cracking and various mechanistic and empirical models available for predicting stress corrosion cracking behavior are critically reviewed. Tests are recommended for enhancing our understanding and predictive capability on stress corrosion cracking in Alloy 600 steam generator tubes.

12. KEY WORDS/DESCRIPTORS (List words or phrases that will assist researchers in locating the report.)

Steam generator tubing  
Stress corrosion cracking  
Alloy 600, Inconel 600  
Mechanisms of crack initiation  
Crack propagation  
Models for stress corrosion cracking

13. AVAILABILITY STATEMENT

unlimited

14. SECURITY CLASSIFICATION

(This Page)

unclassified

(This Report)

unclassified

15. NUMBER OF PAGES

16. PRICE

**ASSESSMENT OF CURRENT UNDERSTANDING OF MECHANISMS OF  
INITIATION, ARREST, AND REINITIATION OF STRESS CORROSION CRACKS  
IN PWR STEAM GENERATOR TUBING**

**FEBRUARY 2000**

**UNITED STATES  
NUCLEAR REGULATORY COMMISSION  
WASHINGTON, D.C. 20555-0001**

SPECIAL STANDARD MAIL  
POSTAGE AND FEES PAID  
USNRC  
PERMIT NO. G-67

